AD-A048 901 AIR FORCE INST OF TECH WRIGHT-PATTERSON AFB OHIO SCH--ETC F/G 1/3
DESIGN AND EVALUATION OF A SIDE FORCE GENERATOR MODIFICATION FO--ETC(U)
DEC 77 G R LEIMBACH

UNCLASSIFIED AFIT/GAE/AA/77D-7 NL

1 OF 2
ADA048901

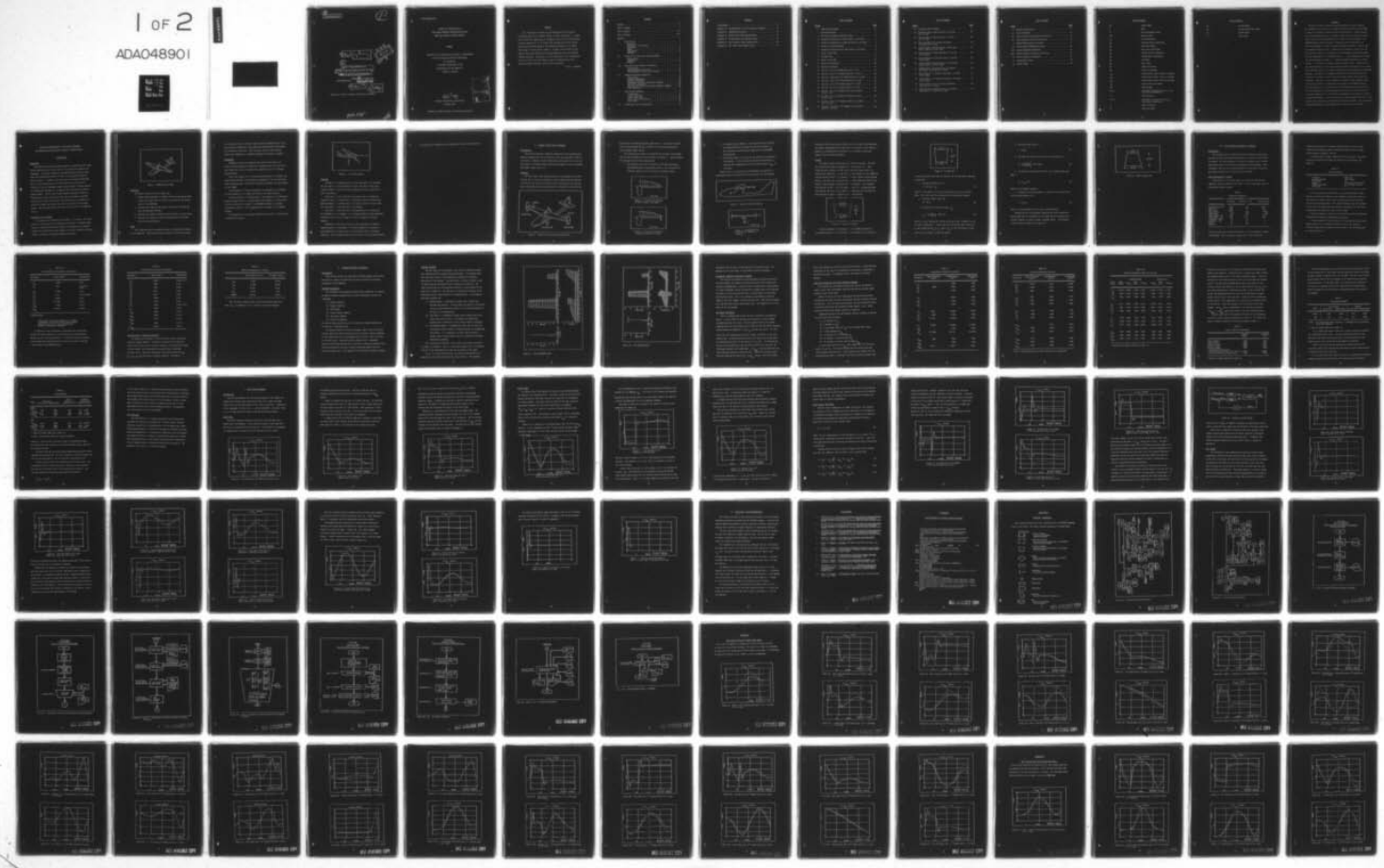

(14) AFIT/GAE/AA/77D-7

(1)

DDC
JAN 23 1978
F

(9) Master's Thesis

(6) DESIGN AND EVALUATION OF A SIDE FORCE GENERATOR MODIFICATION FOR THE XBQM-106, REMOTELY PILOTED VEHICLE

THESIS (10)

AFIT/GAE/AA/77D-7 GLENN R. LEIMBACH
CAPTAIN USAF

(11) Dec 77

(12) 136 p.

Approved for public release; distribution unlimited.

ø12225

4B

AFIT/GAE/AA/77D-7

DESIGN AND EVALUATION OF A SIDE FORCE GENERATOR MODIFICATION FOR THE XBQM-106, REMOTELY PILOTED VEHICLE

THESIS

Presented to the Faculty of the School of Engineering

of the Air Force Institute of Technology

Air University

in Partial Fulfillment of the

Requirements for the Degree of

Master of Science

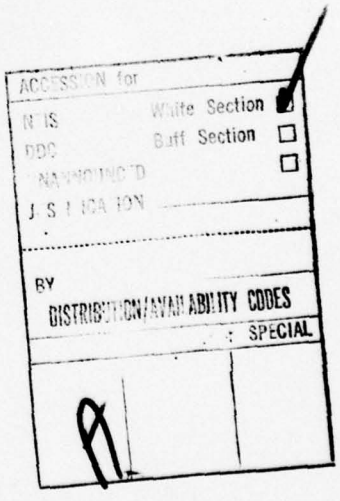

by

Glenn R. Leimbach
Captain USAF

Graduate Aeronautical Engineering

December 1977

Approved for public release; distribution unlimited.

Preface

This study began 10 months ago and during this period several individuals gave me a tremendous amount of advice and support. I would like to take this opportunity to recognize a few of these professionals: My thesis advisor, Dr. D. W. Breuer, who provided me with the initial support and continued guidance and counseling throughout this study. Capt George C. Perley and Mr. Robert C. Schwartz of the AFFDL for the numerous hours they spent with me interpreting and using the FLEXSTAB computer programs. And lastly I wish to recognize Mr. Bill Bustard and Mr. Bill Acton of the AFIT computer center, building 640, for the excellent support they gave me with their facilities.

Glenn R. Leimbach

Contents

Contents

List of Figures

List of Figures

List of Tables

List of Symbols

AR	Aspect Ratio
b	Span
$\bar{c}$	Mean aerodynamic chord
c/4	Quarter chord
C_L	Lift coefficient
C_M	Pitching moment coefficient
C_D	Drag coefficient
C_y	Side force coefficient
C_ℓ	Rolling moment coefficient
C_n	Yawing moment coefficient
C_T	Tip chord
C_R	Root chord
CG	Center of gravity
CP	Center of pressure
I_{xx}	Second moment about X axis (stability)
I_{yy}	Second moment about Y axis (stability)
I_{zz}	Second moment about Z axis (stability)
I_{xz}	Cross product of inertia
LE	Leading edge
p,q,r	Perturbed rotational rates about the X,Y,Z axes respectively
S	Planform area
u,v,w	Perturbed velocities in the X,Y,Z directions respectively
α	Angle of attack
β	Side slip angle

List of Symbols

δA	Aileron angle
δE	Elevator/stabilizer angle
δR	Rudder angle
λ	Taper ratio

Abstract

Wingtip and fuselage mounted side force generating (SFG) surfaces were designed and installed on the XBQM-106 remotely piloted vehicle (RPV) to enhance its lateral terminal response characteristics. These surfaces were sized and positioned in an attempt to keep the net rolling and yawing moments about the CG unchanged when the aircraft was side slipping. The FLEXSTAB digital computer system in conjunction with traditional hand calculated methods were used to evaluate the RPV's stability, control, and time response characteristics. Because of the propeller location and the unconventional shape of the fuselage, three mathematical models were generated for comparing lateral characteristics: a. basic fuselage and vertical tail effectiveness unchanged. b. forward fuselage effectiveness reduced by 50%. c. vertical tail effectiveness increased by 50%. Comparisons of the three data sets with the hand calculated results indicated that the model with increased vertical tail effectiveness more closely modeled the unmodified airplane. In addition the simulation showed that the initial sizing and locations of the SFG produced rolling and yawing moments under side slip conditions. The time history responses to rudder, aileron, rudder/aileron, and wind gust inputs were generated and plotted by the FLEXSTAB program. From these plots it was determined that the SFG modification increased the yaw rate response 10.6% while decreasing the roll rate 10.7% and the side slip angle response 25.1%. The dutch roll damping was increased 4% and the DR period decreased 8%. The roll mode time to half amplitude increased 16.7% and the spiral stability increased for the modified vehicle. The longitudinal stability suffered a slight decrease due to the addition of the SFG.

DESIGN AND EVALUATION OF A SIDE FORCE GENERATOR MODIFICATION FOR THE XBQM-106, REMOTELY PILOTED VEHICLE

I. Introduction

Background

After WWII our military strategies began an increasing shift toward nuclear warfare and as a result the role of conventional weaponry was downgraded. The recent Vietnam war and Middle Eastern conflicts have shown that conventional warfare is still a very important aspect of general warfare. In light of this fact and our increasing technology the Air Force determined in 1971 that there exists a need for an effective, low cost, expendable weapon system capable of being remotely or automatically deployed for use against both stationary and mobile ground targets. The Air Force Flight Dynamics Laboratory (AFFDL) at Wright-Patterson AFB, OH was given the task of providing a Remotely Piloted Vehicle (RPV) to serve as a test bed vehicle to evaluate the electronic seekers and sensors that will be utilized by this weapon system. This study deals with the latest of these RPV's, the XBQM-106 (Fig 1).

Statement of the Problem

The problem can be defined in this manner: To design a side force generator modification for the XBQM-106 and evaluate its effect on the vehicle's response and stability. Side force generators were studied because this modification should improve the lateral response characteristics, in specific, the yawing response capability.

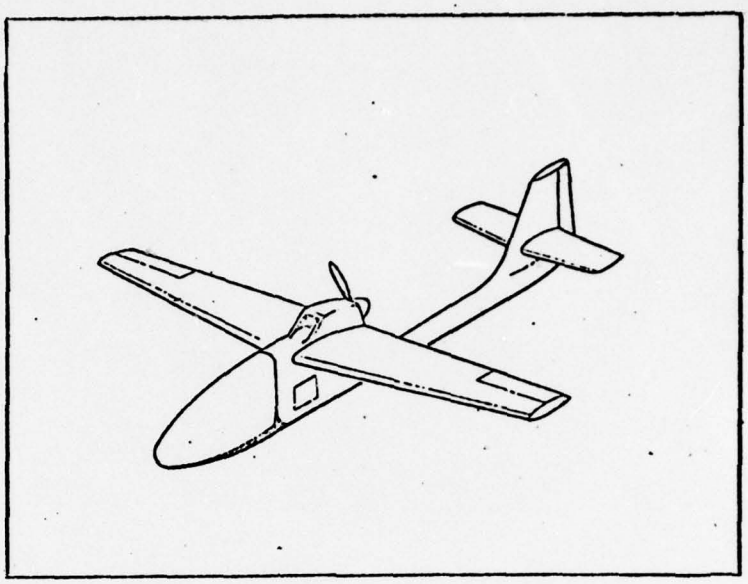

Figure 1. XBQM-106 Basic Model

Objectives

The primary objectives of this report are:

1. Prepare design drawings of suitable side force generating (SFG) surfaces and submit them to AFFDL for construction and installation on the XBQM-106.
2. Calculate the stability and control derivatives for both the basic and modified vehicles.
3. Calculate the dynamic response of both vehicles to given inputs.
4. Determine the change in stability characteristics resulting from the SFG modification.

Scope

This study describes the stepwise process of sizing the SFG system for the XBQM-106. Stability and control derivatives for both vehicles

are calculated using the digital computer program FLEXSTAB (Refs 1,2,3) and partially validated by using traditional geometrically based parameter estimation techniques. With this data the basic and modified models were compared using computer generated time history responses.

Assumptions

FLEXSTAB, the primary analytical tool used in this thesis, is based on linear aerodynamic theory and consequently the user must avoid such conditions that would produce flow seperation and its resulting nonlinearities.

Due to the complexity of the flow associated with the propeller and other similar problems with modeling the propeller, a torque free environment excluding power effects and "corkscrew" propeller wash was assumed in this study.

All aeroelastic effects are assumed to be negligible and therefore all the analyses in this report are based on the rigid airplane.

In hand calculating the derivatives it was assumed that interference effects between different aircraft bodies (for example, horizontal tail/vertical tail) were negligible. The FLEXSTAB programs do calculate interference effects so this assumption does not apply in the computer studies.

The assumed coordinate system centered at the center of gravity (CG) is depicted in figure 2.

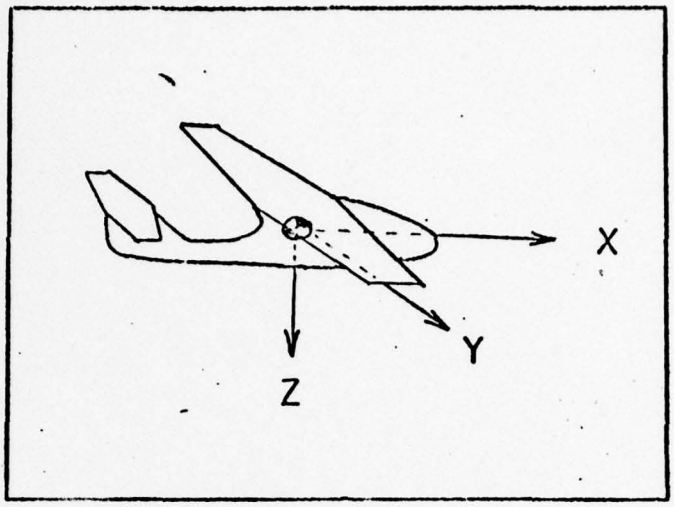

Figure 2. Coordinate System

Approach

To begin this evaluation the side force generators were designed for the lower wingtips and fuselage bottom. The upper SFG was then sized to counter balance the rolling moment due to yaw caused by the first two surfaces.

After the geometry of the modified vehicle was established the problem of parameter estimation was confronted. Hand calculated estimation methods from several sources were used to determine some of the more important stability and control derivatives.

Next both vehicles were defined mathematically and evaluated by the FLEXSTAB computer program. The previously mentioned hand calculated derivatives were used as a comparison with the computer generated numbers.

FLEXSTAB was then used to generate static and dynamic stability characteristics for each model. From these analyses time histories were produced using various control and wind gust inputs as forcing functions. The conclusions concerning the effect of the SFG modification

were drawn after consideration and comparison of these time histories.

II. Design of Side Force Generators

Introduction

This section contains a detailed explanation of the placement and design/sizing process used to locate the side force generators (SFG) on the vehicle. Symmetric airfoils (NACA 0015) were chosen for use as the SFG because of strength reasons and good performance in the low subsonic mach number range, .04 to .3.

Placement

The first step in the design process was the placement of the SFG. The goal was to locate the surfaces in such a manner that horizontally (x direction) the centers of pressure would coincide with the fore/aft center of gravity location and vertically (z direction) so that the SFG

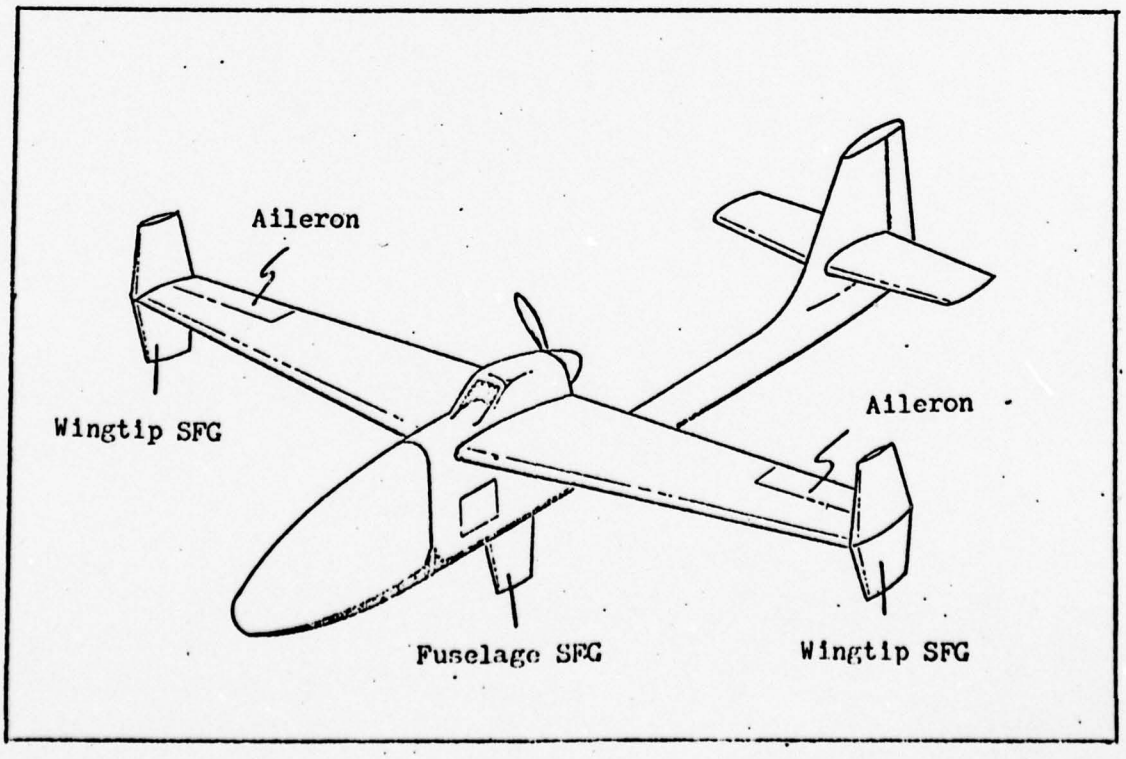

Figure 3. Side Force Generator Modified Vehicle

would create no unbalanced moments about the CG. In essence this modification was designed to have no effect on the existing yawing and rolling moments about the CG.

Two locations were chosen to accomodate the surfaces, the wingtips and the lower fuselage below the mainwing, see Figure 3. Further reasons for placing the SFG on the wingtips were:

1. The surfaces would act as end plates, therefore producing a more uniform pressure distribution which in turn increases the effective aspect ratio of the wing, see Figures 4 and 5.

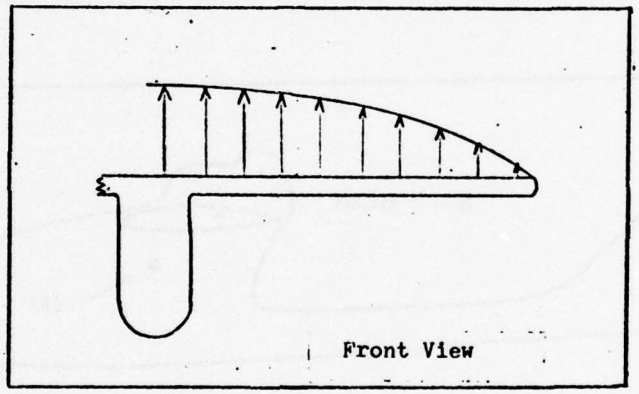

Figure 4. Pressure Distribution on Basic Vehicle, Left Wing

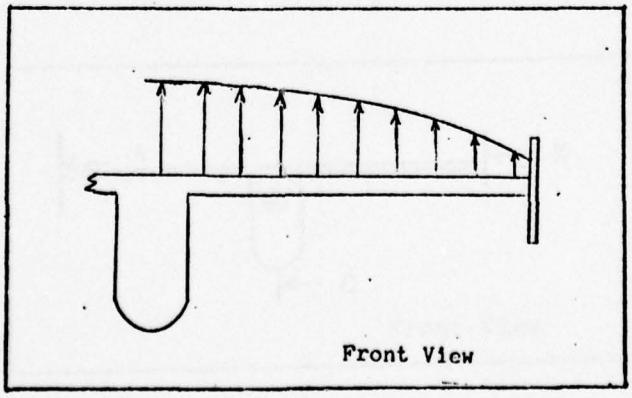

Figure 5. Pressure Distribution on Modified Vehicle, Left Wing

2. In conjunction with number 1, the end plate effect decreases the induced drag and increases the lift-curve slope, C_{L_α}. These benefits are particularly important for performance considerations.

3. Referencing Figure 3, one can see the ailerons lie adjacent to the wingtips. In this region the pressure distribution is improved and consequently the aileron control power, $C_{\ell_{\delta A}}$, is increased.

Because the CG is located below the mainwing (see Figure 6) a balancing SFG had to be placed on the lower section of the fuselage.

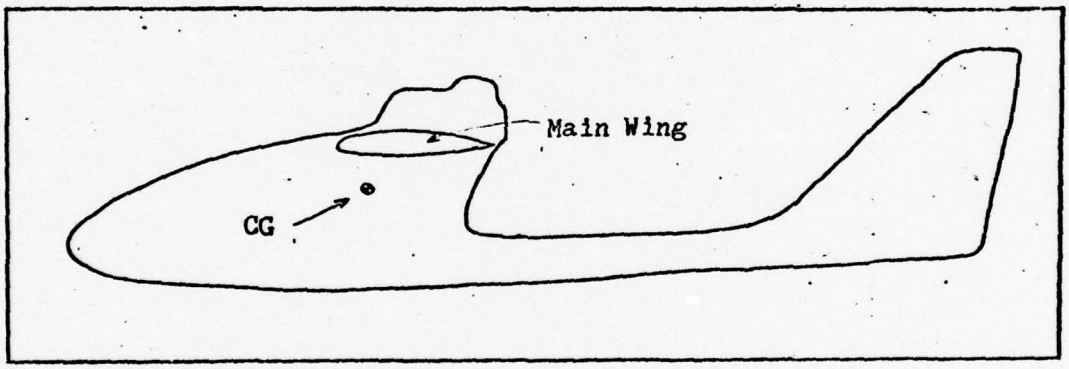

Figure 6. Center of Gravity Location

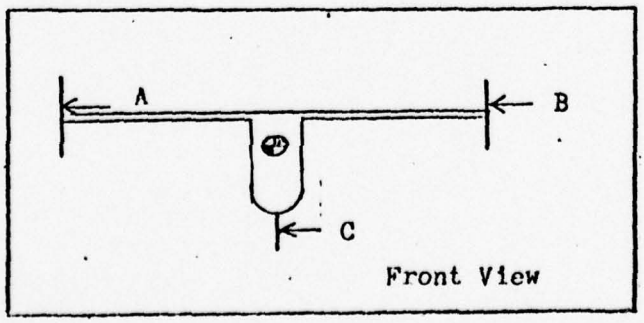

Figure 7. Aerodynamic Side Forces on SFG caused by Sideslip

Placing the SFG here provides a force below the CG which counterbalances the forces acting above the CG (see Figure 7). Forces A and B create a moment in a counterclockwise direction and C provides a balancing moment in the clockwise direction.

Sizing

The actual sizing process was constrained in two ways. The maximum vertical span under the wingtip was restricted to 7.3". This allows the RPV a maximum of ±10° of bank when the center skid is in contact with the ground. It was felt that this amount of roll capability would be needed to assist in lateral directional control during landing phases. The other constraint was that the lower fuselage SFG had to be stowed in the fuselage during the launching sequence. This required that the span of this surface be approximately 12". Considering these restrictions, the planforms of the lower wingtip SFG and fuselage SFG were designed as shown in Figures 8 and 9, respectively.

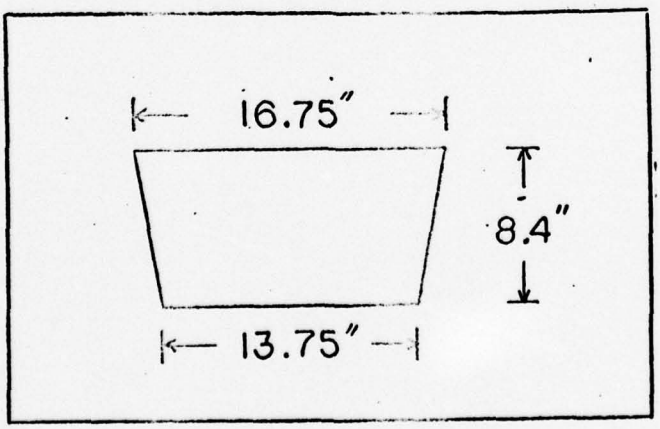

Figure 8. Lower Wingtip SFG

With the placement and sizing of these two SFGs complete the rolling moment due to side slip produced by them had to be calculated.

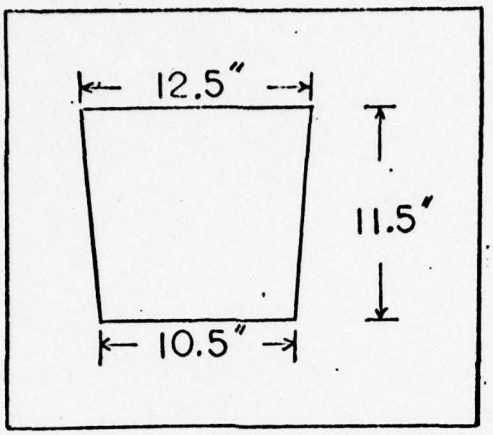

Figure 9. Fuselage SFG

A seven step process was used to evaluate the rolling moment component of each SFG.

1. Compute planform area, S:

$$S = \tfrac{1}{2}\, b\, (C_T + C_R) \quad (1)$$

where b is the span, C_T is the tip chord and C_R is the root chord.

Note: All of the side force generators were trapezoidal shapes.

2. Calculate aspect ratio, AR:

$$AR = b^2 / S \quad (2)$$

3. Calculate the lift-curve slope, C_{L_α}:

$$C_{L_\alpha} = \frac{a_o}{1 + a_o / AR} \quad \text{(Ref 4:4)} \quad (3)$$

where a_o is the theoretical section lift-curve slope (assumed to be 2π in these calculations). Since side force was needed rather than lift, it was assumed that $C_{y_\beta} \approx C_{L_\alpha}$, where C_{y_β} is the coefficient of side force due to a change in side slip angle, .

4. Calculate taper ratio, λ:

$$\lambda = C_T/C_R \tag{4}$$

5. Determine the location of the center of pressure, CP:

$$CP = \frac{b}{2}\left[\frac{1+2\lambda}{3(1+\lambda)}\right] \quad \text{(Ref 5:502)} \tag{5}$$

6. Calculate the resulting side force, F_y, caused by side slip angle:

$$F_y = C_{y_\beta}\ \beta\ \bar{q}\ S \tag{6}$$

where $\bar{q}$ is the dynamic pressure.

7. Determine the rolling moment, L, about the CG created by the force acting through its CP.

$$L = F_y \times \ell \tag{7}$$

where ℓ is the distance the CP is above or below the CG.

Knowing the net rolling moment caused by the lower wingtip SFG and fuselage SFG, the dimensions of the upper SFG were changed in an iterative manner to create an equal, opposing moment. The planform of this surface is depicted in Figure 10.

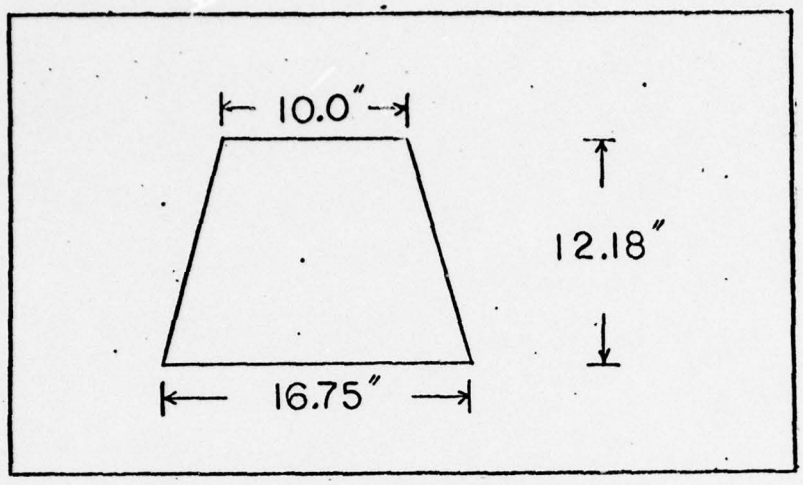

Figure 10. Upper Wingtip SFG

III. Hand Calculated Parameter Estimation

Introduction

This section lists in tabular form various stability and control derivatives that were hand calculated and the reference used to obtain the method. The express purpose for these calculations was to obtain approximate values to be used in validating the FLEXSTAB model. Also included in this section is the method by which the center of gravity and moments/crossproduct of inertia were calculated.

Hand Calculated Derivatives

Since there exists no wind tunnel or flight test data for the XBQM-106, the basic geometry (see Table I) was the only input used for determining the derivatives.

Table I

Geometry Information

	Mainwing	Horizontal Tail	Vertical Tail
Planform Area $(in)^2$	2714	528	470.4
Span (in)	139	48	24
Mac $\bar{c}$ (in)	19.52	11	19.6
Aspect Ratio	7.12	4.364	1.224
Taper Ratio	.751	.692	.352
Sweep Angle - LE	2.5°	4.5°	44°
Sweep Angle - C/4	1.0°	2.5°	39.5°
Incidence - Root	4°	0°	-
Incidence - Tip	1°	0°	-
Twist	3°	0°	-
Dihedral	0°	0°	-

Several sources were consulted during the search for parameter estimation methods. The two primary sources used in this study were:

"Stability and Control of Airplanes and Helicopters," (Ref 4), and "Methods for Estimating Stability and Control Derivatives of Conventional Subsonic Airplanes," (Ref 6).

A standard cruise flight condition within the vehicle's operating envelope was arbitrarily chosen and used in the calculations, see Table II.

Table II

Flight Condition

Altitude	2000' MSL
Forward Velocity	110.9 ft/sec
Mach Number	0.1
Weight	140 lb Basic/145 lb SFG
Flight Path Angle	0° (Straight & Level)
Bank Angle	0°

All the calculations were based on a power-off situation consequently no account was taken for such unknowns as gyroscopic force of the propeller, torque of the engine, and "corkscrew" prop wash that the tail section experienced. This assumed condition was not intended to infer that the above mentioned items are negligible, but that their incorporation was beyond the scope of this study.

Listed in Tables III and IV are the derivatives and the references from which the methods of calculation were taken.

A certain amount of caution needs to be exercised when using these numbers because it is extremely difficult to arrive at accurate solutions using only the geometry of the vehicle. The following quote was taken from Ref 6.

Table III

Hand Calculated Longitudinal Derivatives

Derivative	Value (rad^{-1})	Reference(s)
C_{D_o}	.0162*	4:165
C_{L_α}	4.933	4:5, 6:3.2, 7:460
C_{D_α}	.2939	6:3.1
C_{m_α}	-1.115	6:3.3,8:3.40
C_{L_q}	6.4916	6:5.1
C_{m_q}	-17.1028	6:5.2
$C_{L_{\delta E}}$	.7448	6:10.3
$C_{m_{\delta E}}$	-2.5153	6:10.4

* Dimensionless

> "When better accuracy is desired, it is always recommended to use (wind) tunnel data and/or a combination of (wind) tunnel data and the methods of Reference 1 (Datcom)."

In addition to the uncertainties associated with a particular method, the values obtained for a given derivative using different methods can also vary significantly. As stated previously the purpose of generating these hand calculated derivatives was only to provide a basic check on the FLEXSTAB model.

Table IV

Hand Calculated Lateral Derivatives

Derivative	Value (rad^{-1})	Reference(s)
C_{y_β}	-.4333	4:223, 6:7.1
C_{ℓ_β}	-.0621	6:7.3
C_{n_β}	.068	4:239
C_{y_p}	-.011	6:8.1
C_{ℓ_p}	-.452	4:231
C_{n_p}	.0052	6:8.3
C_{y_r}	.3713	6:9.2
C_{ℓ_r}	.1608	4:222, 6:9.3
C_{n_r}	-.2177	6:9.3
$C_{\ell_{\delta A}}$	.2458	6:11.1
$C_{n_{\delta A}}$	-.0252	6:11.2
$C_{y_{\delta R}}$	.1971	6:12.1
$C_{\ell_{\delta R}}$	.0017	6:12.1
$C_{n_{\delta R}}$	-.1203	6:12.1

Inertia/Center of Gravity Calculation

The moments/cross product of inertia and the CG were calculated using the digital computer. The process consisted of dividing the vehicle into several finite volumetric elements, calculating the weight of each element, and calculating its distance from an arbitrary reference point. Using this information the program solved for I_{xx}, I_{yy}, I_{zz}, I_{xz} and the center of gravity location. See Table V.

Table V

Moments/Crossproduct of Inertia

	Basic Model (sl-ft)	SFG Model (sl-ft)
I_{xx}	9.167	13.125
I_{yy}	25.486	25.625
I_{zz}	32.431	36.25
I_{xz}	-1.528	-1.59
Weight	140 lb	145 lb

Note the large increase (43%) in the second moment about the x axis, I_{xx}. See Appendix A for a listing of Inertia/CG Program.

IV. FLEXSTAB Parameter Estimation

Introduction

This section explains the applicable FLEXSTAB programs and how they were used to predict the stability and control derivatives and model information of the XBQM-106.

FLEXSTAB Explanation

The FLEXSTAB 2.01.00 Computer Program system (FLEXSTAB) is a system of digital computer programs based on linear aerodynamic theories for evaluating:

(1) Static stability

(2) Dynamic stability

(3) Trim states

(4) Linear systems analysis

(5) Structural loading

(6) Elastic deformation

The vehicle being analyzed can be of an arbitrary shape/configuration in subsonic or supersonic flow.

The system consists of fourteen programs, eight of which deal with airplane definition and the remaining six are airplane analysis programs. In this study only five of the programs were utilized. They are listed in the order used: Geometry Definition program (GD), Aerodynamic Influence Coefficient program (AIC), AIC Matrix Correction program (CAIC), Stability Derivatives and Static Stability program (SD&SS) and Time Histories program (TH). See Appendix B for the general FLEXSTAB overview.

Geometry Overivew

The sole input to this program is the vehicle's dimensions which were obtained from the original design blueprints. The program takes this input and creates a three-dimensional mathematical geometry definition of the airplane. The basic model is shown in Figure 11 and the model with the SFG modification is depicted in Figure 12. The reader should note the increased panel density in the proximity of the wing tips of Figure 12. This was done to increase the accuracy of the modeling process in these regions of changing pressure. This geometry definition consists of:

(1) Slender bodies - A mathematical model used to define the fuselage and nacelles. Slender bodies are bodies of revolution with an area distribution similar to the area distribution of the part it is representing.

(2) Thin bodies - A mathematical model used to define wing, horizontal and vertical tails. Thin bodies are defined by a planform that is identical to the actual airplane's planform.

(3) Interference bodies - A mathematical model used to model the interference effects between a slender body and its neighboring thin bodies. It is composed of a shell that surrounds a slender body in regions where there are significant wing/body interference effects.

Due to the type of analysis in this study, thin bodies were given no camber or thickness. This is a reasonable approach since incremental effects of the modification were the main interests in the study.

Due to its unconventional shape, the forward fuselage had to be modeled as a thin body connecting two slender bodies. The problems

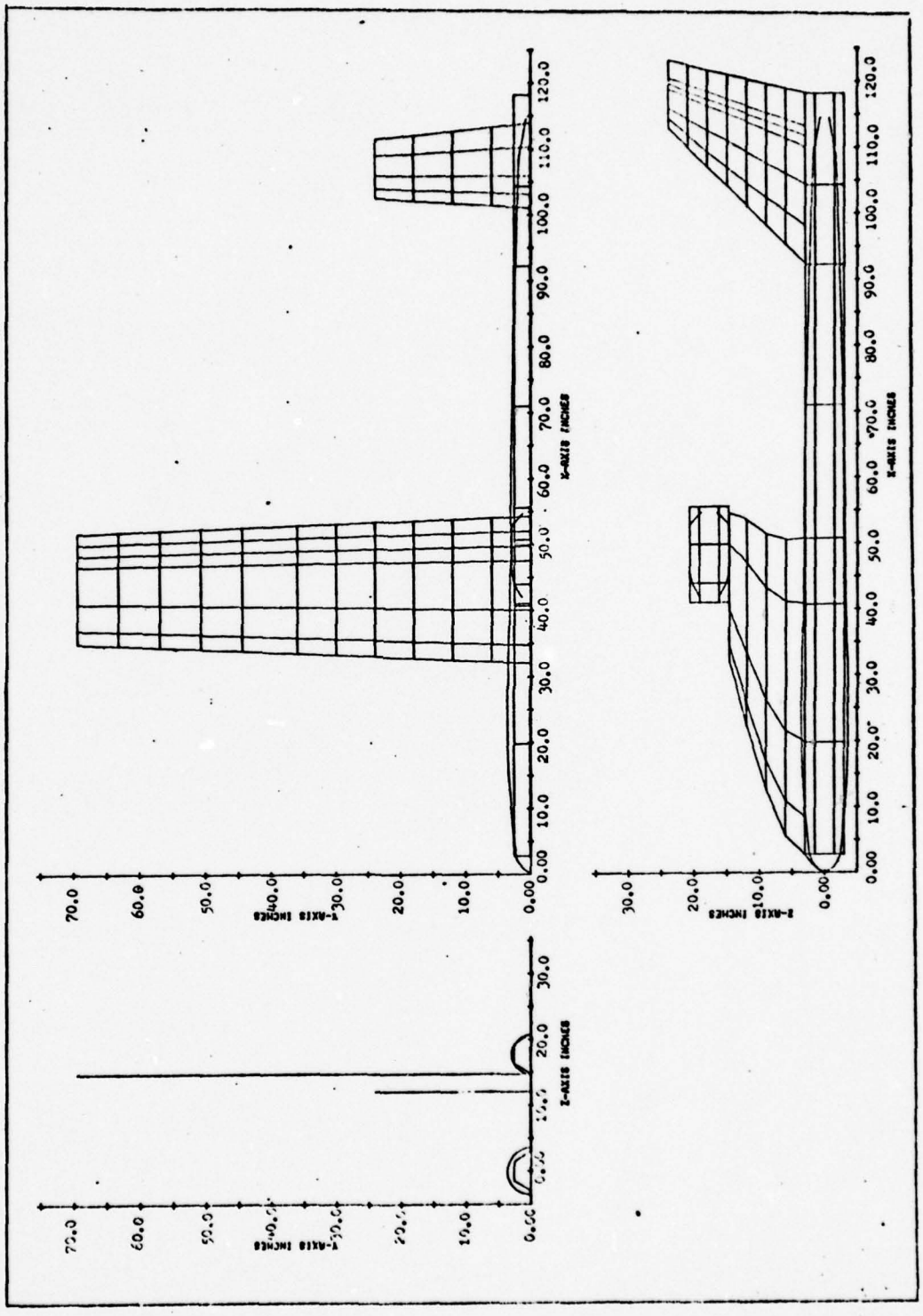

Figure 11. Basic FLEXSTAB Model

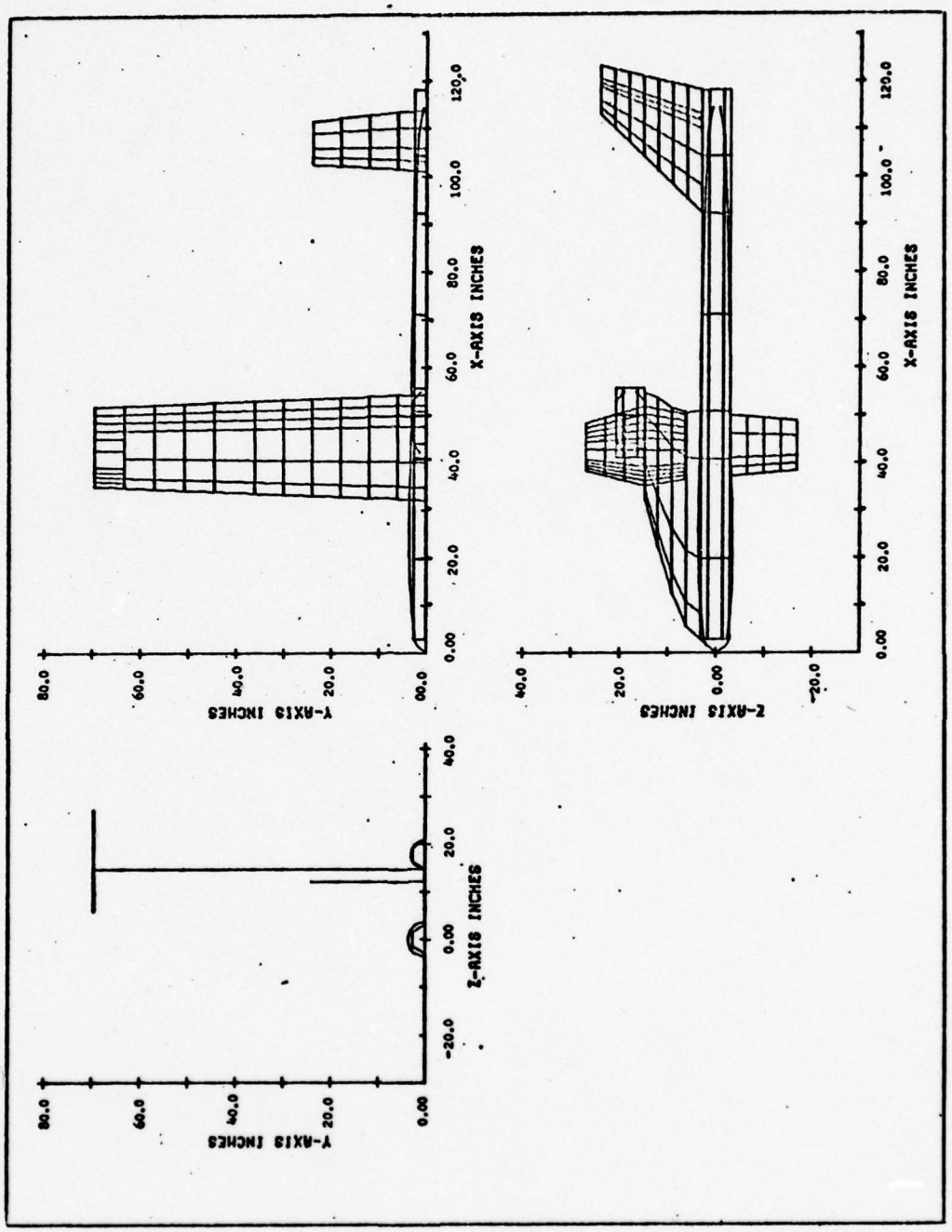

Figure 12. SFG FLEXSTAB Model

associated with this type of modeling will be discussed later. See Appendix B for a flow chart of the Geometry Definition program.

Aerodynamic Influence Coefficient Program

This portion of FLEXSTAB uses the mathematical geometry definition (GD) and computes the steady and unsteady matrices used to define the airplane aerodynamically. Basically the AIC program uses a modification of linear aerodynamic theory introduced by Woodward (Ref 9) to determine the effect of each panel/control point in the geometry on every other panel/control point. This is an extremely long program in terms of computer time. For example, typical durations are: 3000 seconds compilation time and 2500 seconds input/output time. See Appendix B for a flow chart of the AIC program.

AIC Matrix Correction

CAIC is a program that allows the user to modify an existing AIC matrix. In this study the forward vertical portion of the fuselage was modeled using a thin body. The data gathered using this scheme suggested that this thin body was more effective than the actual fuselage mainly because the magnitude of the C_{n_β} term was very small. For this reason the CAIC program was utilized to reduce the effect of this Thin body by 50%. A second modification of the AIC matrix was accomplished by increasing the effect of the vertical tail by 50%. To differentiate between the data gathered using the three different AIC matrices, the following convention was established. ".5 $C_{y_{FUS}}$ " denotes data where the front fuselage effect was reduced by 50%. "Baseline" represents data from the unaltered AIC matrix and "1.5 $C_{y_{VT}}$ " denotes data from a model

with a 50% increase in the effect of the vertical tail. A more detailed explanation of the reason for modifying the AIC matrix is presented in the SD & SS section. See Appendix B for a flow chart of the CAIC program.

Stability Derivatives and Static Stability Program

This program uses the geometry definition and the AIC matrix to compute rigid static and dynamic stability derivatives and mode shape characteristics of the model.

Tables VI and VII list the longitudinal and lateral derivatives respectively for both the basic and modified vehicles using the baseline AIC matrices. Also for comparison purposes, the hand calculated values of selected derivatives are included in these tables. Note: These values are based on the flight condition in Table II.

Comparing the basic with the modified vehicle in Tables VI and VII one will notice the following:

(1) An increase in C_{L_α}

(2) A decrease in C_{D_o}

(3) A very small value for C_{n_β} of the FLEXSTAB basic model

(4) A large change in C_{y_β}

(5) An increase in roll damping, C_{ℓ_p}

(6) An increase in yaw stiffness, C_{n_r}

(7) An increase in aileron control power $C_{\ell_{\delta A}}$

As was stated earlier, the C_{n_β} term (.0006 rad^{-1}) for the basic model is very low. This would indicate that the vehicle had very little weather cock stability. After comparing this number with the hand calculated value of .068 rad^{-1} and consulting the personnel that

Table VI

Longitudinal FLEXSTAB Derivatives

Derivative	Hand Calculated (rad^{-1})	FLEXSTAB Basic (rad^{-1})	FLEXSTAB SFG (rad^{-1})
C_{L_o}	-	.2095	.2152
C_{D_o}	.0162	.0165	.0143
C_{m_o}	-	.1188	.0726
C_{L_u}	-	1.0772	1.1158
C_{D_u}	-	.1346	.1371
C_{m_u}	-	.0736	.0740
C_{L_α}	4.933	5.0585	5.4472
C_{D_α}	.2939	.5744	.5445
C_{m_α}	-1.115	-1.6566	-1.7219
C_{L_q}	6.4916	10.4086	10.6842
C_{D_q}	-	.6344	.6559
C_{m_q}	-17.1028	-19.119	-19.1128
$C_{L_{\delta E}}$	.7448	.8525	.8555
$C_{D_{\delta E}}$	-	.0696	.0762
$C_{m_{\delta E}}$	-2.513	-2.696	-2.682

Table VII

Lateral FLEXSTAB Derivatives

Derivative	Hand Calculated (rad^{-1})	FLEXSTAB Basic (rad^{-1})	FLEXSTAB SFG (rad^{-1})
C_{y_β}	-.4122	-.4136	-1.3428
C_{ℓ_β}	-.0418	-.0434	- .0723
C_{n_β}	.068	.0006	.0158
C_{y_p}	-.011	-.1002	- .1546
C_{ℓ_p}	-.452	-.5225	- .6412
C_{n_p}	.0052	.0227	.0082
C_{y_r}	.3713	.4105	.5225
C_{ℓ_r}	.1608	.1495	.1784
C_{n_r}	-.2177	-.1899	- .1968
$C_{y_{\delta A}}$	-	.0111	.0237
$C_{\ell_{\delta A}}$	.2458	-.2376*	- .2824*
$C_{n_{\delta A}}$	-.0252	-.0167	- .0155
$C_{y_{\delta R}}$	.1971	.2584	.2600
$C_{\ell_{\delta R}}$	.0017	.0006	.0003
$C_{n_{\delta R}}$	-.1203	-.1355	- .1355

* Note: FLEXSTAB defines its control derivatives as negatives.

Table VIII

Modified FLEXSTAB LATERAL Derivatives*

Derivative	Hand Calc'd	FLEXSTAB BASIC			FLEXSTAB SFG		
		$.5C_{y_{FUS}}$	Baseline	$1.5C_{y_{VT}}$	$.5C_{y_{FUS}}$	Baseline	$1.5C_{y_{VT}}$
C_{y_β}	-.4122	-.3784	-.4136	-.5875	-1.2887	-1.3428	-1.5179
C_{ℓ_β}	-.0418	-.0272	-.0434	-.0446	- .0556	- .0723	- .0734
C_{n_β}	.068	.0576	.0006	.0837	.0707	.0158	.0987
C_{y_p}	-.011	-.0994	-.1002	-.1122	-.1532	-.1546	- .1665
C_{ℓ_p}	-.452	-.5222	-.5225	-.5226	-.640	-.6412	- .6414
C_{n_p}	.0052	.0238	.0227	.0288	.0092	.0082	.0142
C_{y_r}	.3713	.4053	.4105	.6062	.5141	.5225	.7194
C_{ℓ_r}	.1608	.1482	.1495	.1508	.1771	.1784	.1795
C_{n_r}	-.2177	-.1942	-.1899	-.2846	-.2008	-.1968	-.2912
$C_{y_{\delta R}}$	.1971	.2584	.2584	.3876	.2600	.2600	.3900
$C_{\ell_{\delta R}}$	.0017	.0006	.0006	.0009	.0003	.0003	.0006
$C_{n_{\delta R}}$	-.1203	-.1355	-.1355	-.1891	-.1353	-.1353	-.2031

* Based on the flight condition in Table II.

flight test the vehicle it was theorized that the RPV does have good weather cock stability. Considering this, attempts were made to match the FLEXSTAB values closer to the hand calculated figures. First the influence of the forward vertical portion of the fuselage was reduced by 50%. This alteration mathematically states that there is less vertical surface area forward of the CG which increases the C_{n_β} term. The second modification, increasing the effect of the vertical tail by 50%, was prompted because the tail section experiences a higher dynamic pressure due to the prop wash. Neither of these alterations had any effect on the longitudinal or aileron control characteristics of the vehicle. Table VIII displays the 12 derivatives that were changed. The C_{n_β} terms corresponding to the altered AIC matrices ($.5C_{y_{FUS}} + 1.5C_{y_{VT}}$) agree much closer to the hand calculated data.

Another useful set of data obtained from the SD & SS program is the list of static stability parameters in Table IX. The values are given in decimal fractions of the mean aerodynamic chord, $\bar{c}$.

Table IX

Static Stability Parameters*

	FLEXSTAB BASIC	FLEXSTAB SFG
Static Margin	.3161	.3275
Neutral Point	.6122	.6175
Load Factor (g)	1.0022	1.0021
Maneuver Point	.6887	.6997
Maneuver Margin	.3926	.4098
Longitudinal Control per G Steady Pullup (Deg/unit load factor)	-4.9901	-4.9953
Stick Speed Stability (Deg/in/sec)	.0064	.0064

* Based on flight condition in Table I-I.

From these parameters one can see that the fore/aft position of the CG can be moved aft to some degree without making the vehicle statically unstable (CG aft of Neutral Point) (Ref 10:209). The last area of information gained from the SD & SS program is the characteristic equation rooting analysis. As the name infers, the characteristic equation of the vehicle is analyzed both for the longitudinal and lateral modes. Table X displays the two oscillatory longitudinal modes, short period and phugoid.

Table X

Longitudinal Modes*,**

Model	Short Period		Phugoid	
	Period (sec)	Damping Ratio	Period (sec)	Damping Ratio
Basic	1.28	.5228	15.2	.0515
SFG	1.25	.517	15.2	.0499

* Note: The longitudinal model analysis is unchanged by the alteration of the AIC matrices.

** Base of flight condition in Table II.

It is evident from Table X that only a slight variance was noted in the longitudinal model values. The SFG modification caused a 2.3% decrease in the short period period and a 1% and 3% decrease in the damping ratios of the short period and phugoid respectively.

Table XI lists the lateral characteristic modes which are the oscillatory dutch roll mode and the remaining two non-oscillatory modes, rolling mode and spiral stability.

It is evident from this table that there is a significant difference between the data from the Baseline AIC matrix and the two altered

Table XI

Lateral Modes*

Model	Dutch Roll Period (sec)	Dutch Roll Damping Ratio	Roll Time to ½ Amplitude (sec)	Spiral Time to ½/2 Amplitude (sec)
Basic				
$.5C_{y_{FUS}}$	2.88	.3834	.078	(2A) 14.86*
Baseline	12.6	.1578	.078	(½A) .427
$1.5C_{y_{VT}}$	2.41	.4144	.078	(2A) 42.13**
SFG				
$.5C_{y_{FUS}}$	2.63	.4004	.091	(2A) 29.29**
Baseline	5.92	.6680	.091	(½A) 3.499
$1.5C_{y_{VT}}$	2.25	.4238	.091	(2A) 397**

* Based on flight condition in Table II.

** Note: These spiral modes are slightly unstable.

matrices. Since the last two sets of data were obtained by using derivatives that were closest to the hand calculated values, they will be discussed further.

The dutch roll (DR) period decreased approximately 8% while the DR damping increased about 4%. The roll response was decreased because the time to half amplitude for the roll mode was increased by 16.7%.

The last lateral mode to be considered was the spiral mode. The predominant factor in determining spiral stability is the magnitude and sign of the constant term in the characteristic equation. This constant contains the following combination of derivatives:

$$C_{\ell_\beta} C_{n_r} - C_{n_\beta} C_{\ell_r}$$

If its sign is positive the vehicle usually possesses spiral stability, but if the value is negative the vehicle will display spiral instability. The Baseline model has spiral stability while the other models did not. This slight spiral instability is of little concern, in fact, several general aviation aircraft exhibit an unstable spiral mode of this magnitude and still remain easy to manually control See Appendix B for a flow chart of the SD & SS program.

Time Histories

The Time Histories (TH) program calculates the nonlinear time responses for coupled perturbations due to control inputs, discrete wind gusts, and/or initial perturbations. The TH program uses information generated by the GD and SD & SS programs to calculate nonlinear coupled perturbations about steady state conditions in the time domain. The program uses this information to generate the equations of motion which include gust and control surface forcing function coefficients. The next chapter provides the detailed time histories analysis. See Appendix B for a flow chart of the TH program.

V. Time History Response

Introduction

This section presents the time history response of the models to a rudder step, aileron step, cross control step (left rudder and right aileron) and two wind gust inputs in the v and w directions. Comparisons of the perturbed velocities (u, v, w) and perturbed rotational rates (p, q, r) along with Euler angles, alpha and beta are presented.

Rudder Step

The first sequence studied was a positive (trailing edge left) rudder step of two degrees. This control was input at time equal zero, held for five seconds and then neutralized. The computer was programmed to integrate over a twenty second time interval with all initial

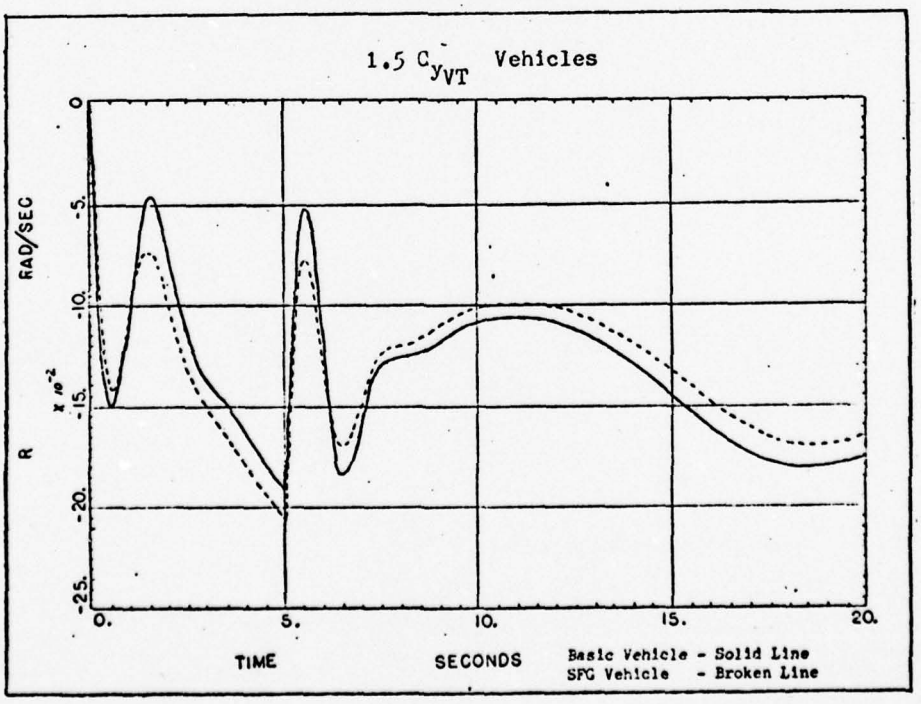

Figure 13. Yaw Rate Due to 2° Rudder Step (0 to 5 sec)

perturbation quantities being zero. From this input yaw rate (r), roll/yaw coupling and side slip were investigated using the $1.5C_{y_{VT}}$ models.

Figure 13 compares the yaw rate (r) of both vehicles. The modified vehicle reached a yaw rate of -.2061 rad/sec at five seconds compared to the basic model's yaw rate of -.1864 rad/sec. That represents a 10.6% increase in yaw rate due to the SFG. It is also evident that the basic vehicle has more overshoot (less dutch roll damping).

A comparison of the roll (Euler) angle phi in Figure 14 shows that the basic model rolled through -35.68° while the SFG model achieved a bank angle of -37.03°, a 1.4% increase in roll angle due to yaw.

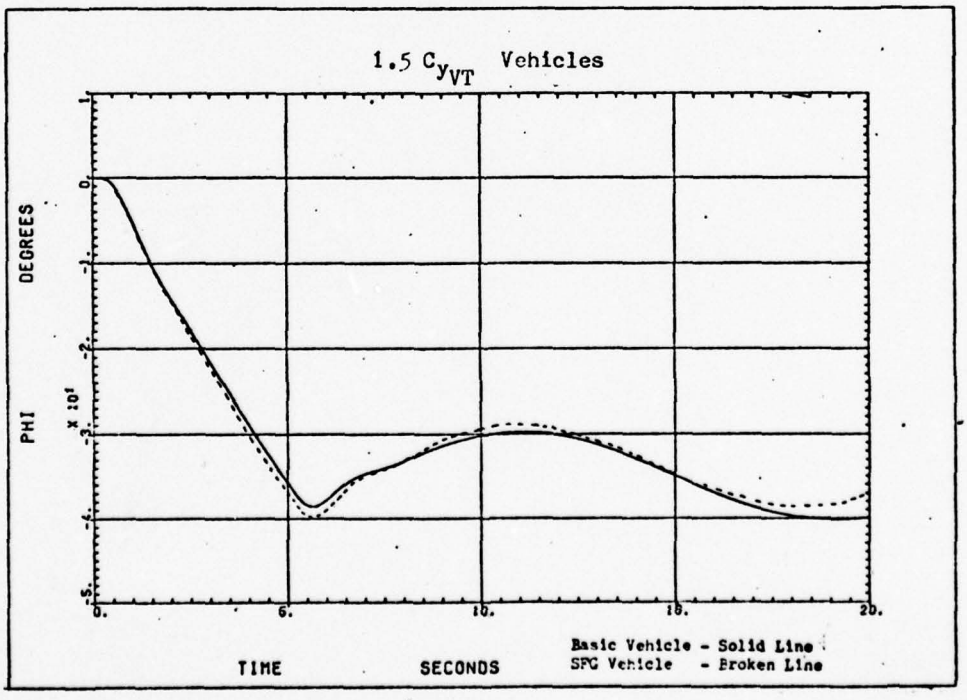

Figure 14. Roll Angle of 2 Rudder Step (0 to 5 sec)

This roll due to yaw, caused by the increased C_{ℓ_r} term, is usually considered an adverse effect and a possible solution to the problem would be to lower the centers of pressure of the SFG by increasing their respective spans. Although this violates an earlier restriction from Chapter II, the AFFDL is considering placing small wheels on the extended SFG and evaluating this option in the wind tunnel.

Figure 15 is a representation of the side slip angles beta. The unmodified vehicle developed a side slip angle of 2.75° in five seconds while beta of the SFG model was 2.06°, a 25.1% decrease. The SFG vehicle possesses more yaw stiffness, mainly due to the increase in C_{n_β}, and this accounts for the smaller side slip angle. The comp time history response caused by the rudder step is located in Appendix C.

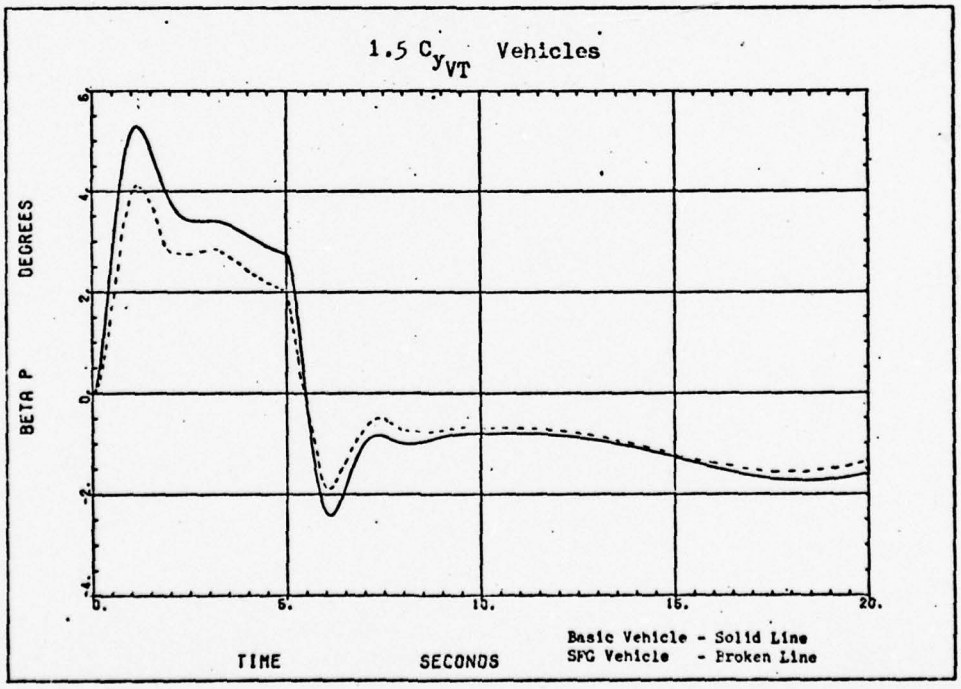

Figure 15. Side Slip Angle Due to 2° Rudder Step (0 to 5 sec)

Aileron Step

An aileron step of two degrees was applied to gain knowledge about the vehicles' roll characteristics. The control input was held for five seconds starting at time equal zero and the equations were integrated for twenty seconds. The reader should be aware of the sign convention employed by FLEXSTAB; all the control derivatives are negative ($C\ell_{\delta A}$, $C_{n_{\delta R}}$, $C_{m_{\delta E}}$ < 0). That is, a positive aileron deflection will cause a negative roll. Some authors, such as Seckel (Ref 4) and Roskam (Ref 6), do not follow this convention and define $C_{\ell_{\delta A}}$ as a positive quantity.

Figure 16 is a comparison of the bank angles, phi, for the 1.5 $C_{y_{VT}}$ vehicles. At the termination of the 2° aileron step, the basic model achieved a bank angle of -73.3° while the SFG vehicle rolled through a -68.4° angle.

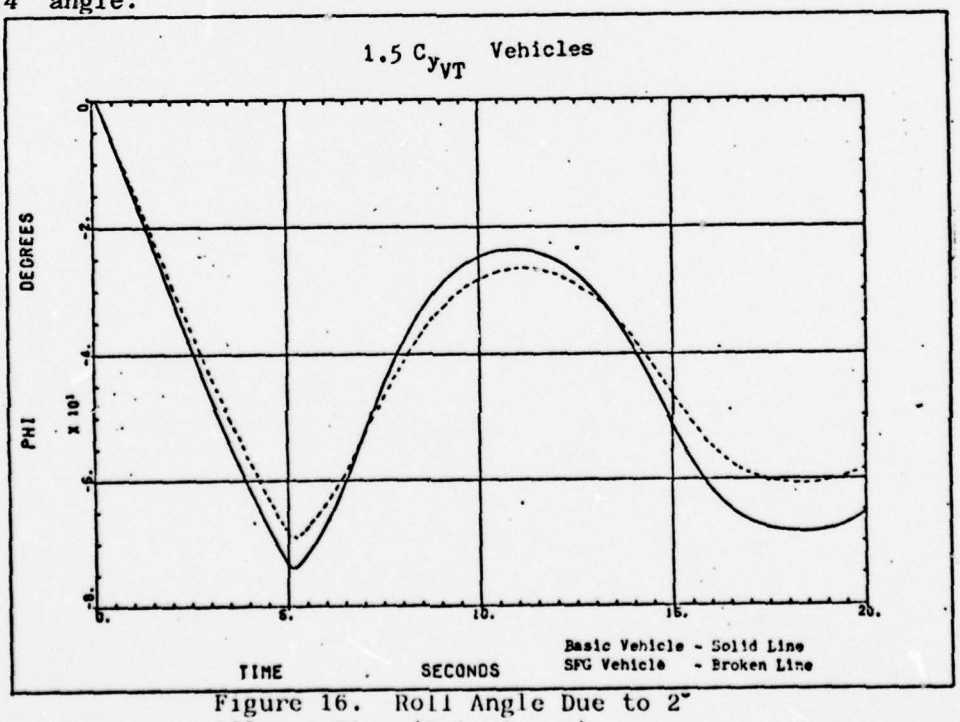

Figure 16. Roll Angle Due to 2° Aileron Step (0 to 5 sec)

The 7.2% decrease in roll response can be mainly attributed to the increase in roll damping, C_{ℓ_p}. This loss of roll response was expected because when any lifting (vertical or horizontal) surfaces are added to a vehicle the magnitude of the roll damping increases.

The effect of this roll damping is also evident in the roll rate comparisons of Figure 17.

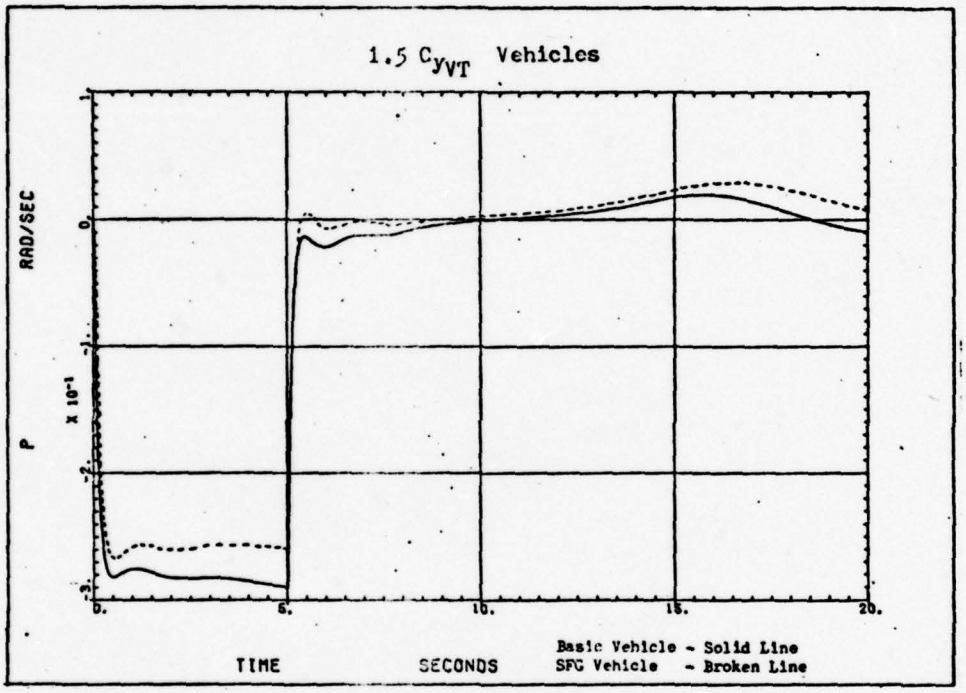

Figure 17. Roll Rate Due to 2° Aileron Step (0 to 5 sec)

The basic vehicle reaches a value of -.290 rad/sec and the SFG model achieved -.259 rad/sec at 5 seconds. This is a decrease of 10.7% in roll rate response.

Another factor that effects roll response is the rolling moment of inertia, I_{xx}. The SFG modification increased the I_{xx} value by 43% which means theoretically that the modified vehicle should have a lower roll acceleration. There is no visible change in the slopes of the roll

rate curves of Figure 17 in the acceleration periods from 0 to 0.5 sec and 5.0 to 5.5 sec. A conclusion drawn from Figure 17 is that the increased I_{xx} term has little effect on the roll response.

It should also be noted that both airplanes have excellent transient characteristics in that they have little overshoot and reach their steady state roll rate (± .01 rad/sec) in approximately a half second.

The last area considered in the aileron step situation was adverse yaw which is primarily influenced by the $C_{n_{\delta A}}$ term. Figure 18, yaw rate due to an aileron step, shows the adverse yaw in the first second after control application.

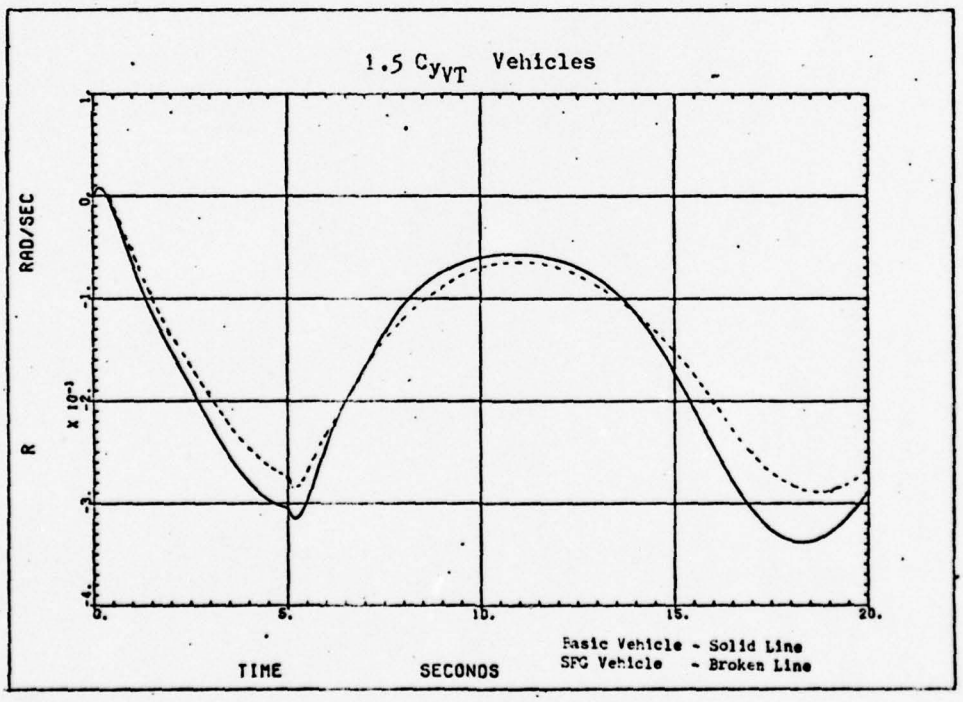

Figure 18. Yaw Rate Due to 2° Aileron Step (0 to 5 sec)

The yaw rates generated at t = .3 sec are .0074 rad/sec and .0068 rad/sec for the basic and SFG models respectively. The basic vehicle has

about 8.1% more adverse yaw rate than the SFG model, but considering the very small magnitude of both values, adverse yaw should not be a problem with either vehicle. The complete time history response caused by the aileron step is located in Appendix D.

Cross Control Step Input

With the correct combination of rudder and aileron the airplane will execute a flat or skidding turn with a bank angle of zero degrees. To determine the proper control deflections to accomplish this maneuver the steady state problem was analyzed by representing the lateral equations of motion in state variable form:

$$\dot{\bar{x}} = A\,\bar{x} + B\,\bar{u} \tag{8}$$

where $\bar{x}$ is a column matrix of state variables β, p, r, and ϕ. $\bar{u}$ is a column matrix containing the control variables, δA and δR. A and B are the coefficient matrices containing the stability and control derivatives respectively.

Assuming that p, ϕ and the rates of change of the state variables are zero, the equations can be written in the following form:

$$0 = C_{y_\beta}\,\beta + C_{y_r}\frac{rb}{2u_1} + C_{y_{\delta A}}\,\delta A + C_{y_{\delta R}}\,\delta R \tag{9}$$

$$0 = C_{\ell_\beta}\,\beta + C_{\ell_r}\frac{rb}{2u_1} + C_{\ell_{\delta A}}\,A + C_{\ell_{\delta R}}\,\delta R \tag{10}$$

$$0 = C_{n_\beta}\,\beta + C_{n_r}\frac{rb}{2u_1} + C_{n_{\delta A}}\,\delta A + C_{n_{\delta R}}\,\delta R \tag{11}$$

Using a given δR of .1 radians, equations (9), (10), and (11) were solved simultaneously for the remaining 3 unknown variables. From this analysis an aileron input of -.042 radians would re required to maintain a flat turn of zero degrees bank with a rudder input of .1 radians for the basic 1.5 $C_{y_{VT}}$ model. A ratio of this combination of rudder and aileron was then used to analyze both 1.5 $C_{y_{VT}}$ vehicles.

Figures 19, 20, 21, and 22 display the respective comparisons of roll rate, yaw rate, roll angle and side slip angle.

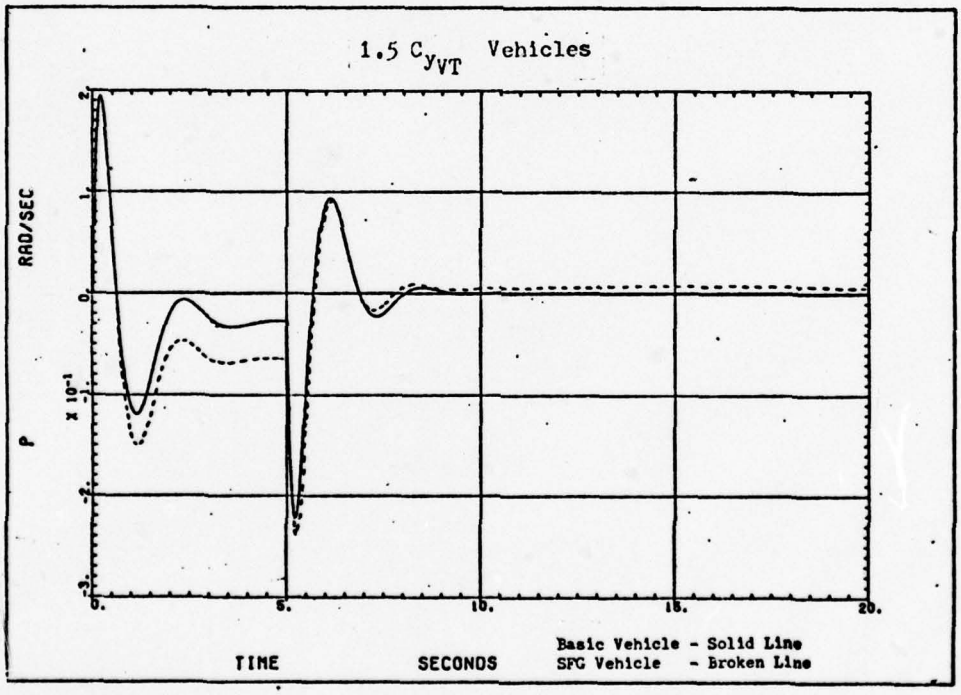

Figure 19. Roll Rate due to 4° Rudder/ -1.68° Aileron Step (0 to 5 sec)

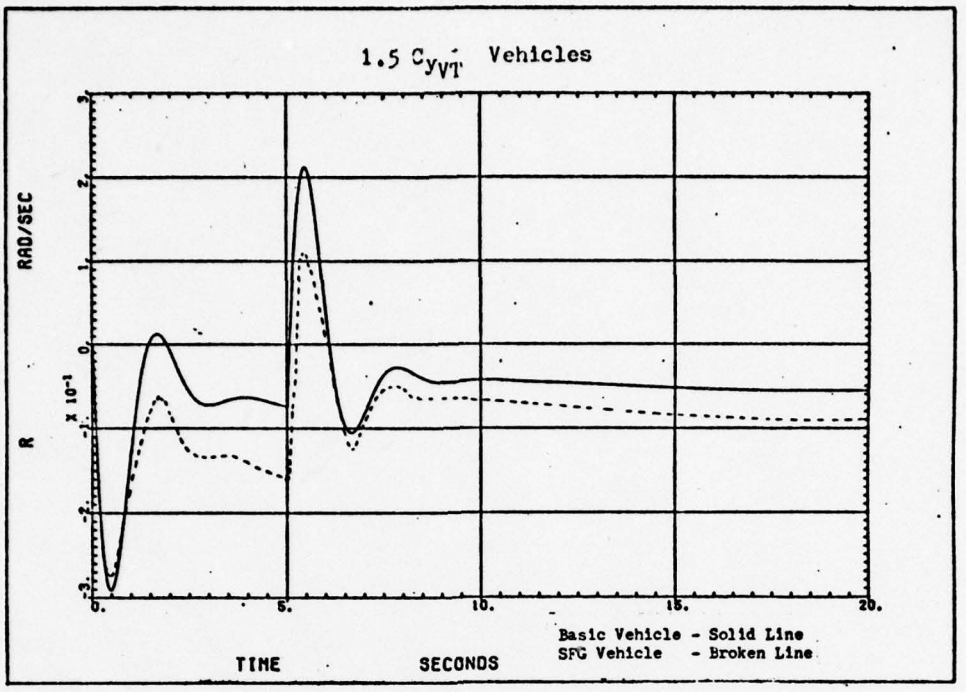

Figure 20. Yaw Rate Due to 4° Rudder/ -1.68° Aileron Step (0 to 5 sec)

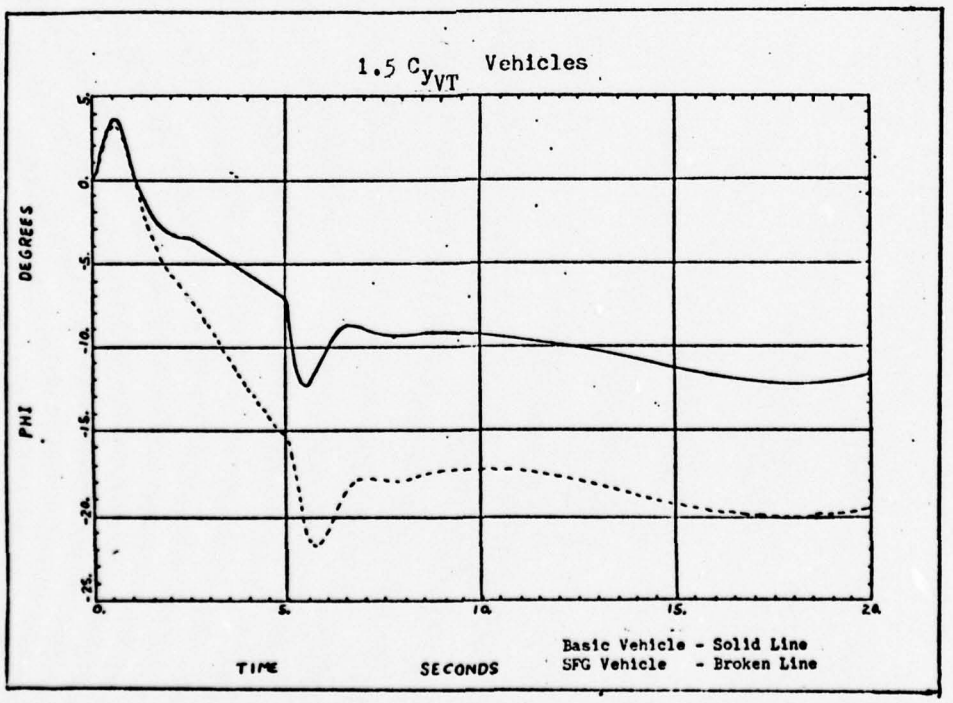

Figure 21. Roll Angle Due to 4° Rudder/-1.68° Aileron Step (0 to 5 sec)

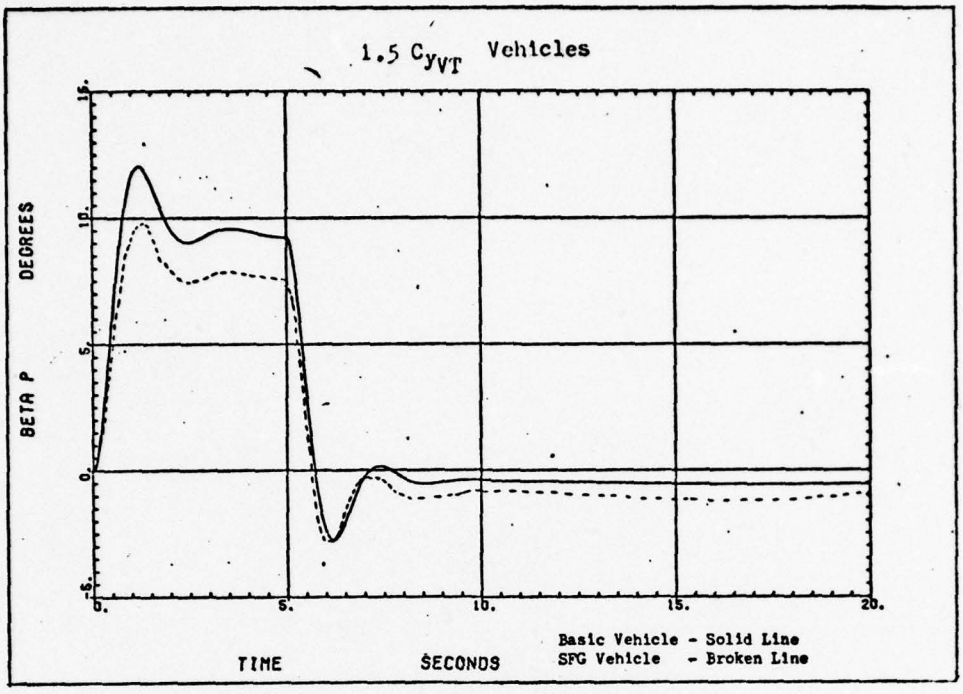

Figure 22. Side Slip Angle Due to 4° Rudder/-1.68° Aileron Step (0 to 5 sec)

From these figures one can see that the steady state control input prediction for the basic 1.5 $C_{y_{VT}}$ vehicle was in error. The basic model rolled through an angle of -7.13° during the control application. The reason the steady state solution differs from the FLEXSTAB solution is because FLEXSTAB solves the entire set of non-linear differential equations (Ref 6:2.24) while the steady state method uses only the uncoupled linearized lateral equations of motion, consequently some small but significant terms are neglected.

One method of overcoming the problem of proper control inputs would be to use an automatic control system similar to the one depicted in Figure 23. With this controller the bank angle is maintained at the specified value by electronically comparing the actual bank angle, as sensed by the gyro system, to the angle desired. The autopilot then

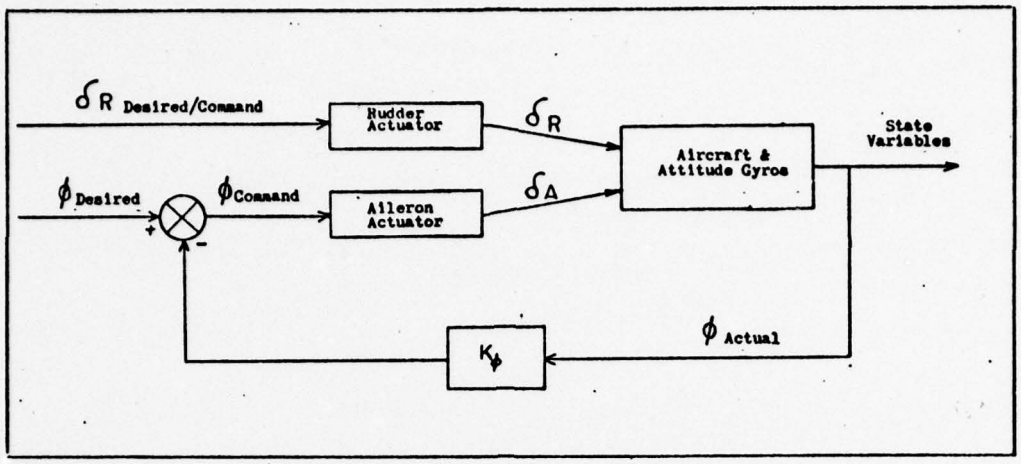

Figure 23. Automatic Control System

uses this error signal, ϕ command, to generate an appropriate aileron input to keep the error signal zero and the bank at the amount specified.

Notice also in Figures 19 through 22 that small changes in the stability derivatives between the two models produced a substantial change in the rolling and yawing characteristics. A complete time history response caused by the cross control input is located in Appendix E.

Gust Inputs

Two wind gusts of equal magnitude but different direction were programmed to disturb the model from the steady state flight condition. In the first case a gust of 11.09 ft/sec from the positive "y" direction was applied to the model for one second starting at time equal zero. Refer to Figures 24, 25 and 26 for roll rate, yaw rate, and side slip angle histories, respectively. From these figures it is easy to recognize the oscillatory dutch roll period of approximately 2.4 seconds in the two to five second intervals. Figure 26 also shows that the SFG

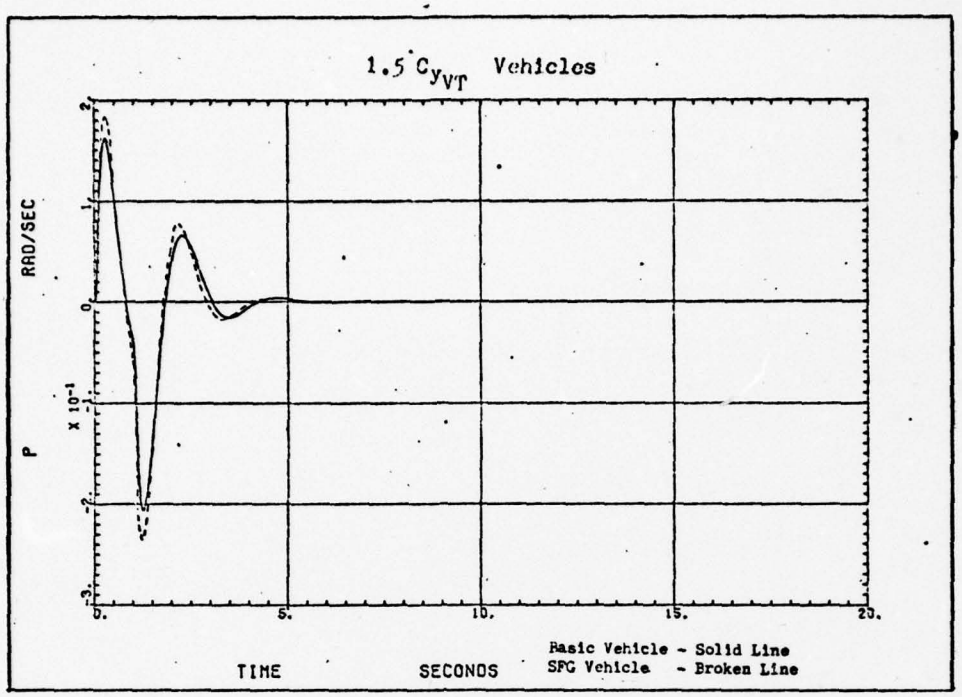

Figure 24. Roll Rate Due to Side Wind Gust, 11.09 fps (0 to 1 sec)

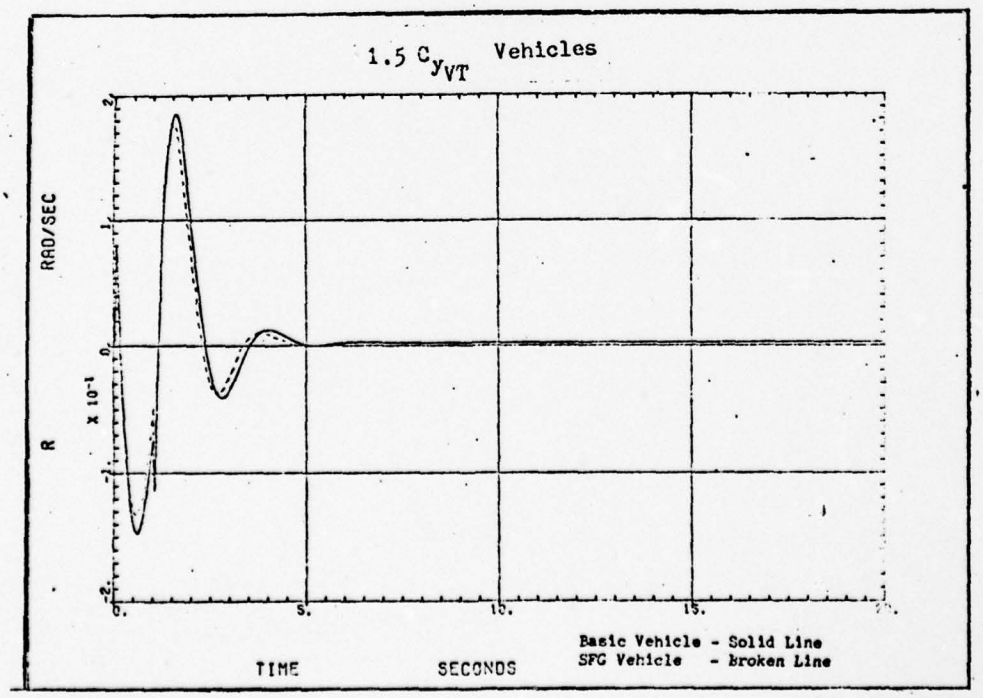

Figure 25. Yaw Rate Due to Side Wind Gust, 11.09 fps (0 to 1 sec)

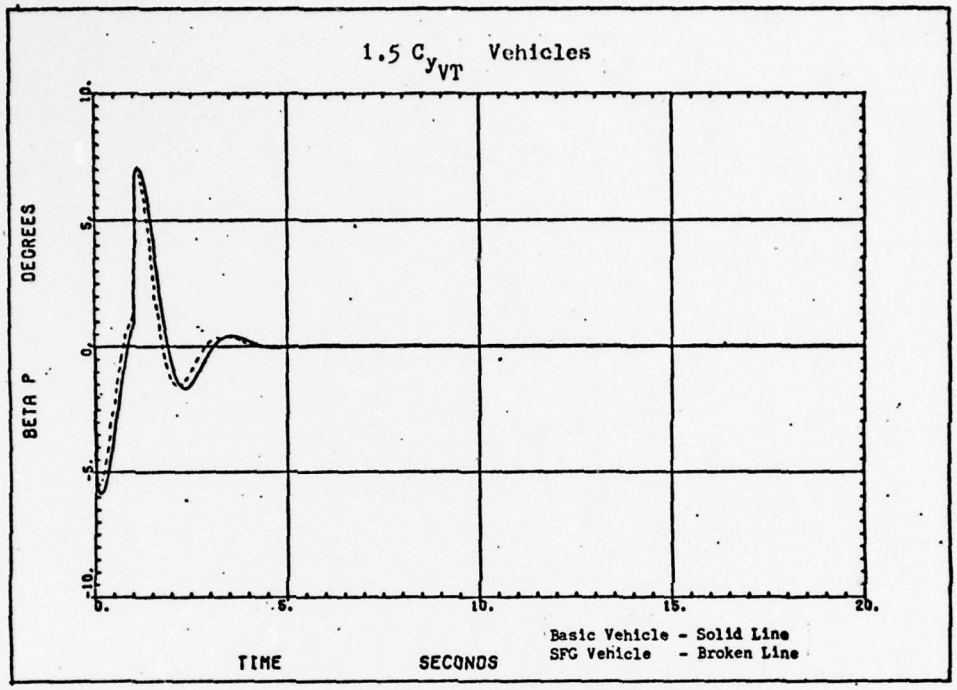

Figure 26. Side Slip Angle Due to Side Wind Gust, 11.09 fps (0 to 1 sec)

vehicle has slightly more dutch roll damping (amplitude of the oscillations are lower) and a lower natural frequency.

Because the six equations of motion are coupled, this particular gust also excited the two oscillatory longitudinal modes, phugoid and short period. The phugoid, characterized by a changing forward speed u (Figure 27), pitch rate q (Figure 28), and pitch angle θ (Figure 29), has a period of approximately fifteen seconds and is visible after five seconds in all three figures. The oscillatory short period, as seen in the 1.5 to 4.0 second time interval of Figures 28, 29, and 30, is well damped and has a period of approximately 1.25 seconds.

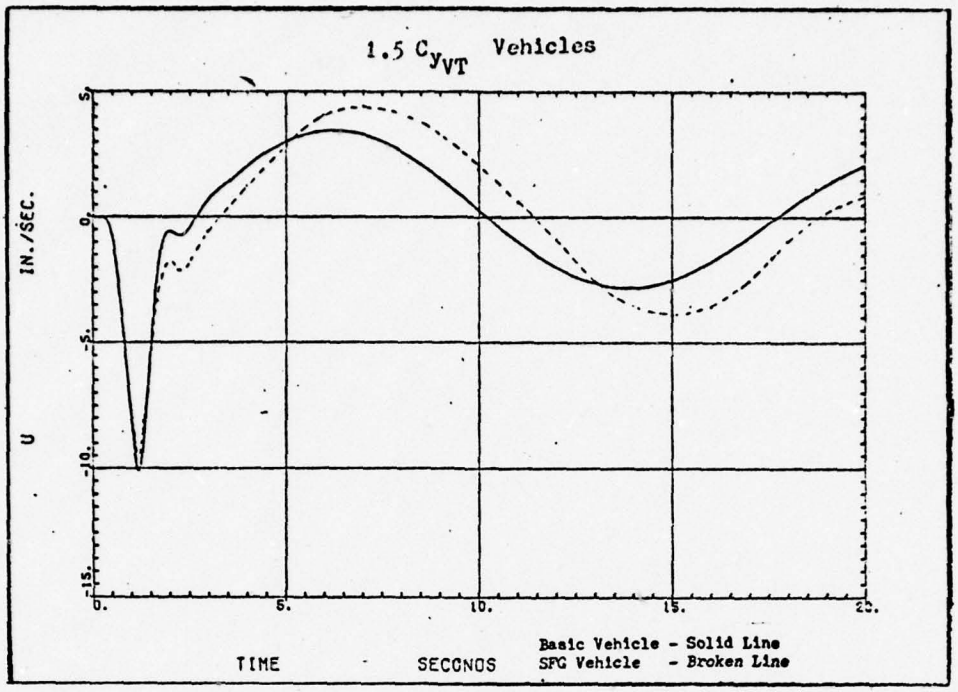

Figure 27. Forward Speed Perturbation Due to Side Wind Gust, 11.09 fps (0 to 1 sec)

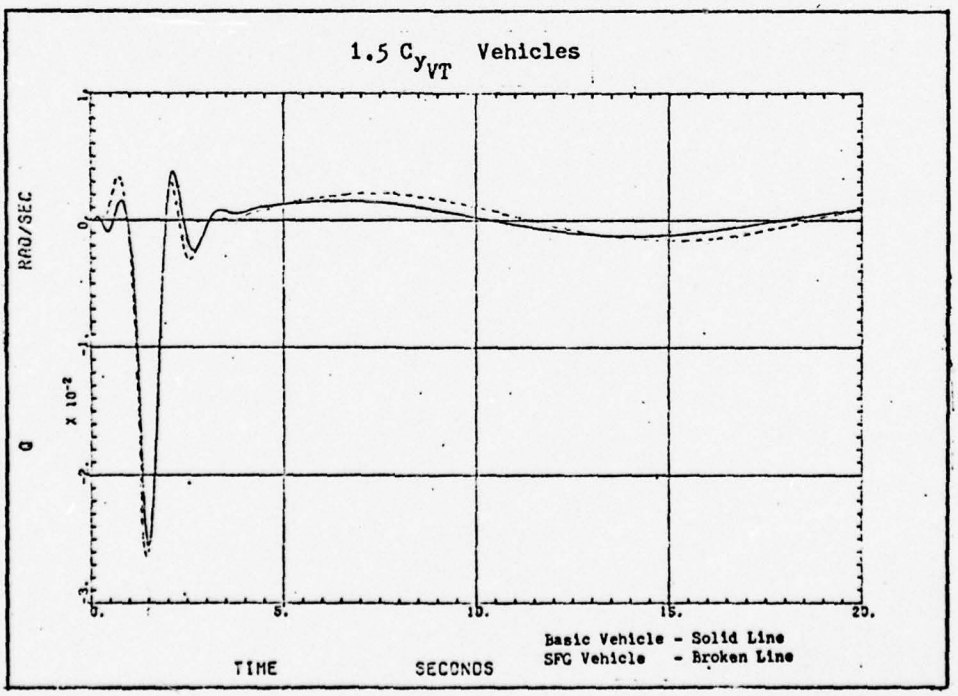

Figure 28. Pitch Rate Change Due to Side Gust, 11.09 fps (0 to 1 sec)

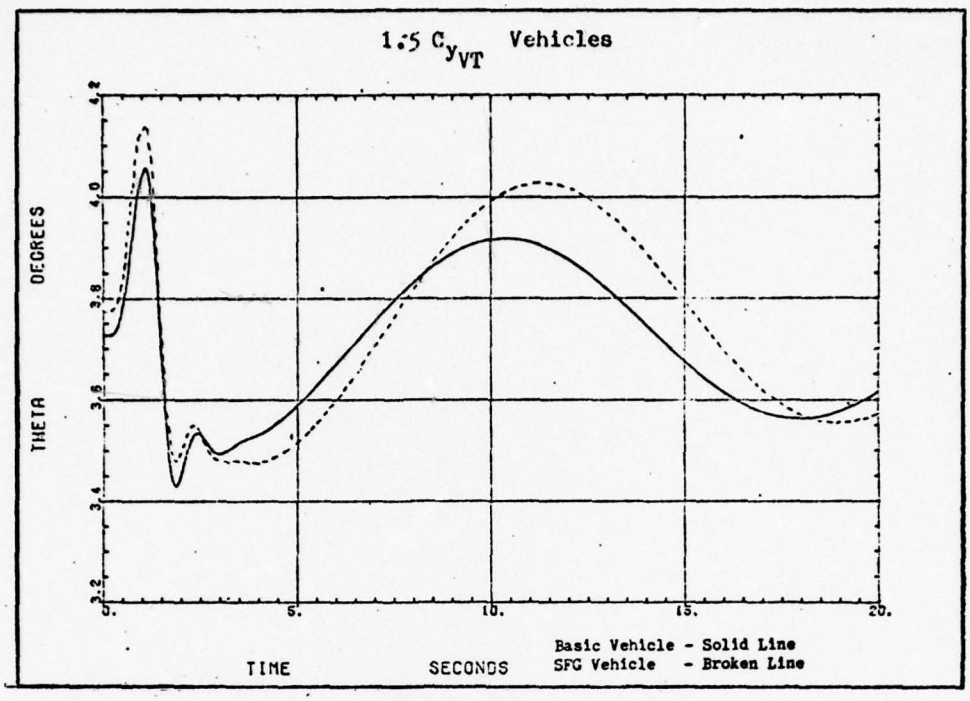

Figure 29. Pitch Angle Change Due to Side Gust, 11.09 fps (0 to 1 sec)

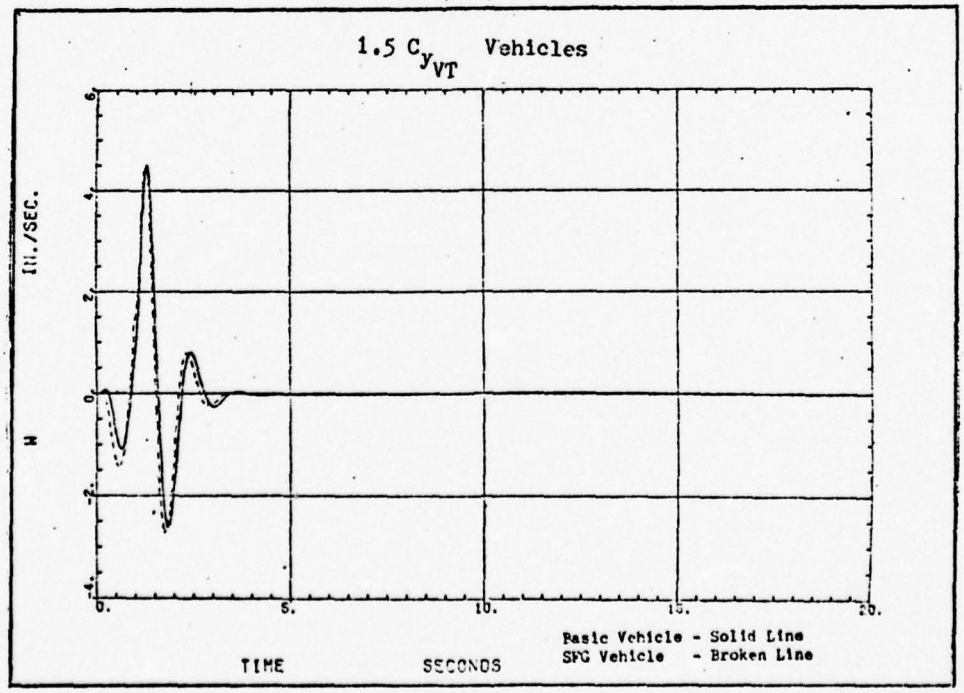

Figure 30. Vertical Speed Perturbation Due to Side Gust, 11.09 fps (0 to 1 sec)

The last situation that was analyzed was the vertical gust condition of 11.09 ft/sec for one second starting at zero time. Since this gust had no "v" component, only the longitudinal modes were excited.

The phugoid mode was analyzed in a similar manner as before by observing the forward speed perturbation u (Figure 31), pitch rate q (Figure 32), and pitch angle (Figure 33). The lightly damped oscillatory phugoid mode is present after five seconds in the three figures. Another characteristic of the phugoid mode is that the angle of attack, alpha, remains almost constant (Figure 34).

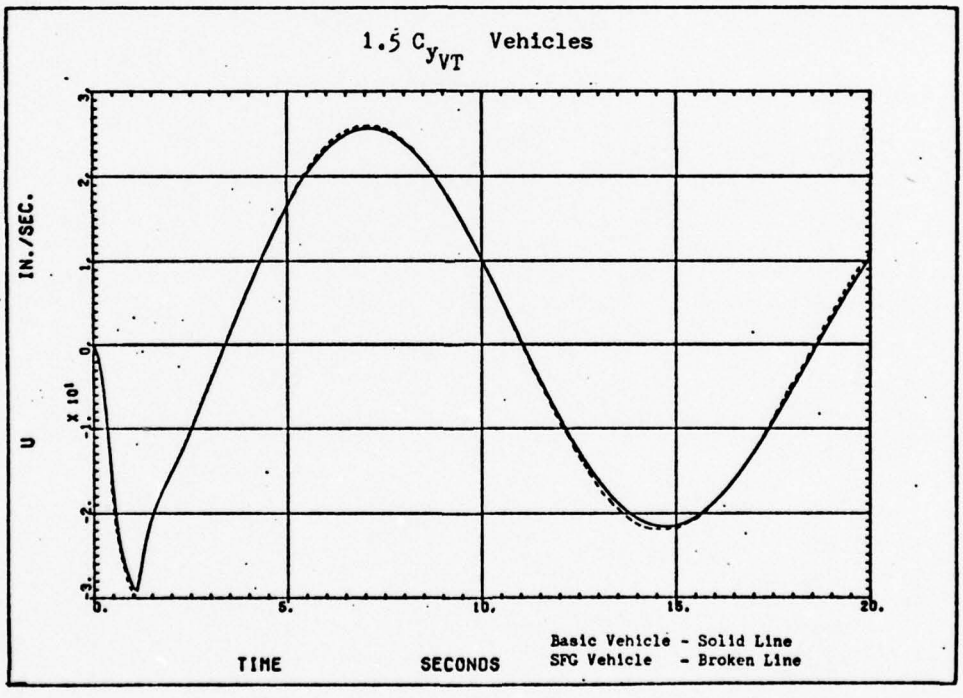

Figure 31. Forward Speed Perturbation Due to a Vertical Gust, 11.09 fps (0 to 1 sec)

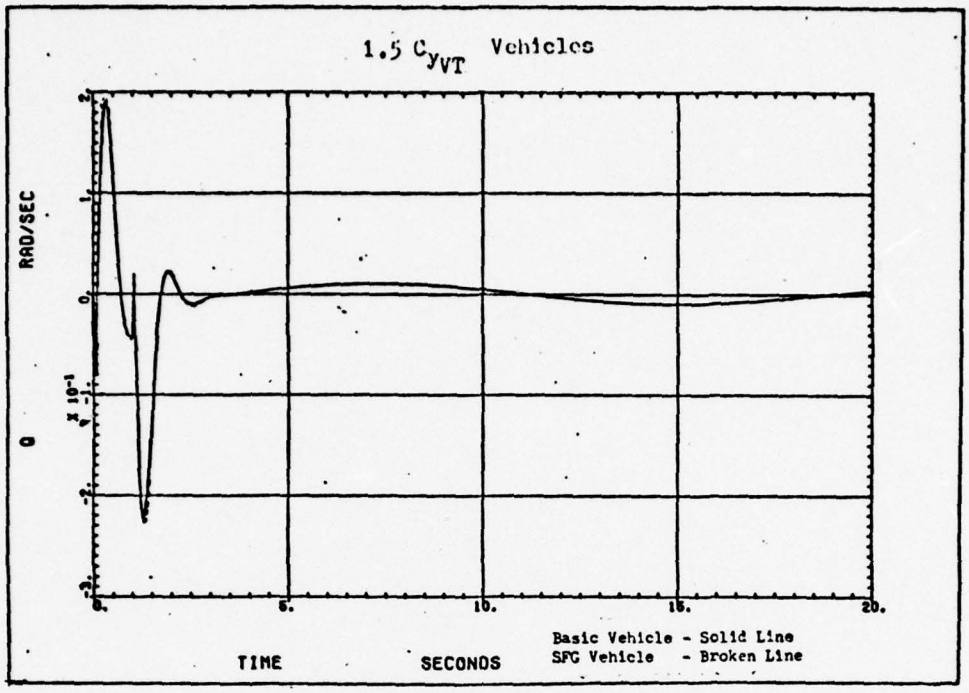

Figure 32. Pitch Rate Due to Vertical Gust, 11.09 fps (0 to 1 sec)

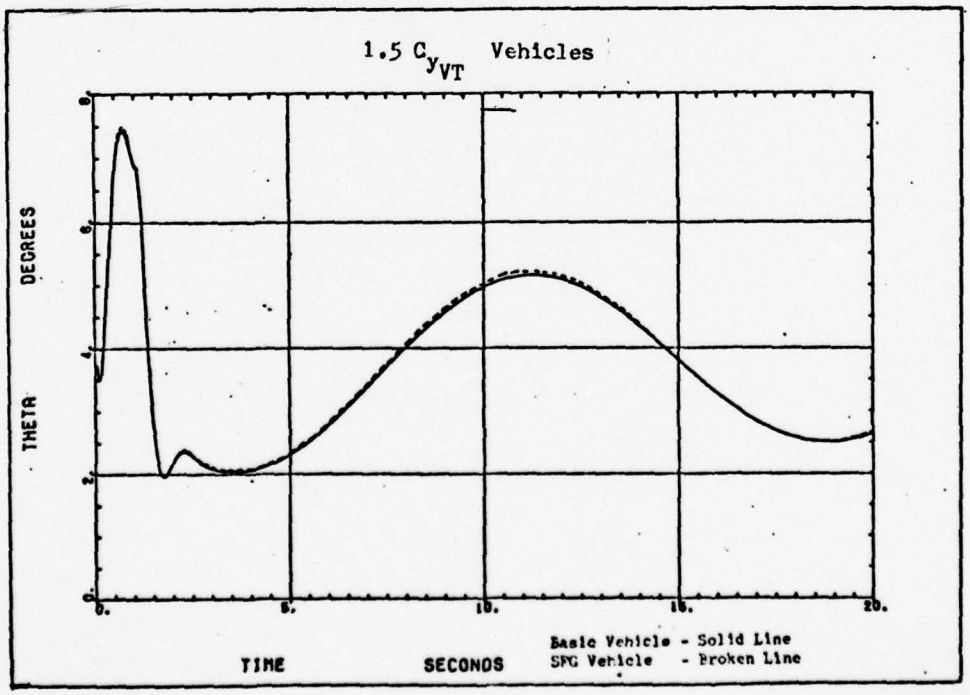

Figure 33. Pitch Angle Due to Vertical Gust, 11.09 fps (0 to 1 sec)

The short period mode is again observable in the 1.5 to 4.0 second intervals of Figures 32, 33, and 35. A complete time history response due to the gust inputs is located in Appendix F.

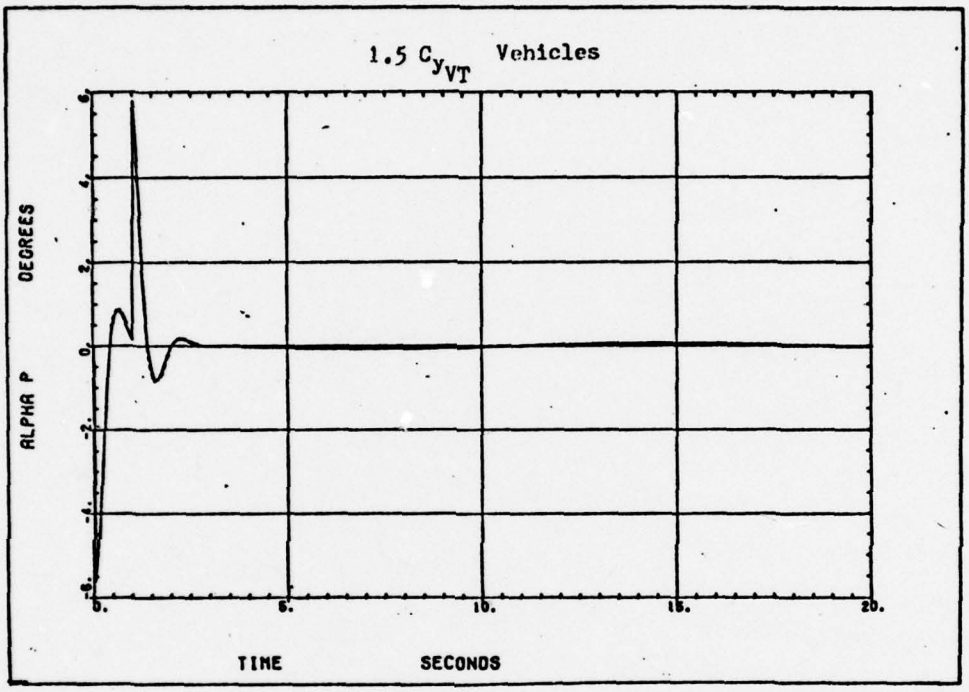

Figure 34. Angle of Attack Due to Vertical Gust, 11.09 fps (0 to 1 sec)

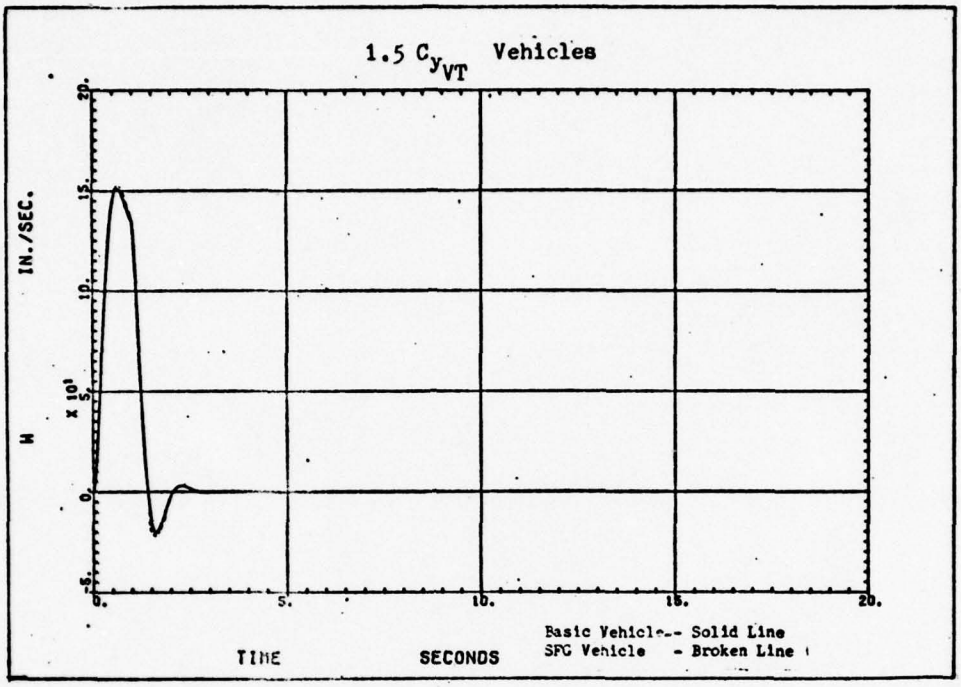

Figure 35. Vertical Speed Perturbation Due to Vertical Gust, 11.09 fps (0 to 1 sec)

VI. Conclusions and Recommendations

The conclusions drawn in this section were based on the time history calculations and plots generated by the FLEXSTAB program. In general the modified XBQM-106 displayed an overall increase in lateral stability and response while suffering a slight reduction of longitudinal stability.

The most significant effect of the SFG modification was to increase the yaw rate induced by a rudder step by 10.6%. The roll due to yaw, an adverse condition, was increased by 1.4%, but this problem could easily be overcome by a simple autopilot.

The response due to an aileron step indicated that the modification decreased the vehicle's roll rate by 10.7%, mainly caused by the increased C_{ℓ_p} term. The aileron input also showed the vehicle's adverse yaw. Although these yaw rates were small (a maximum of less than 0.4 deg/sec) the basic model had a 8.1% higher adverse yaw rate when compared to the SFG vehicle.

The damping ratios of both longitudinal modes, short period and phugoid, were decreased from 1% to 3% by the SFG modification. Examining the lateral modes, the dutch roll period decreased 8% while the DR damping ratio increased by 4%. The roll mode time to half amplitude increased by 16.7% and the spiral stability increased for all the models.

The reader should bear in mind that this study is theoretical in nature and a judicious use of this data along with future wind tunnel and flight test data will allow the AFFDL to make a thorough evaluation of the XBQM-106.

Bibliography

1. AFFDL-TR-74-91. A Method for Predicting the Stability Characteristics of Control Configured Vehicles. Vol. I. FLEXSTAB 2.01.00 User's Manual. Seattle, Washington: The Boeing Airplane Comp, November 1974.

2. AFFDL-TR-74-91. A Method for Predicting the Stability Characteristics of Control Configured Vehicles. Vol. II. FLEXSTAB 2.01.00 User's Manual. Seattle, Washington: The Boeing Airplane Comp, November 1974.

3. AFFDL-TR-74-91. A Method for Predicting the Stability Characteristics of Control Configured Vehicles. Vol. III. FLEXSTAB 2.01.00 User's Manual. Seattle, Washington: The Boeing Airplane Comp, November 1974.

4. Seckel, E. Stability and Control of Airplanes and Helicopters. New York: Academic Press Inc., 1964.

5. Etkin, B. Dynamics of Flight. New York: John Wiley and Sons, Inc., 1959.

6. Roskam, J. Methods For Estimating Stability and Control Derivatives of Conventional Subsonic Airplanes. Lawrence, Kansas: Roskam Aviation and Engineering Corp., 1973.

7. NACA-TR-460. The Characteristics of 78 Related Airfoil Sections from Tests in the Variable Density Wind Tunnel. 1933.

8. Roskam, J. Flight Dynamics of Rigid and Elastic Airplanes. Vol. 1. Lawrence, Kansas: Roskam Avaition and Engineering Corp., 1972.

9. Woodward, F., Tinoco, E., and Larsen, J. Analysis and Design of Supersonic Wing-Body Combinations, Including Flow Properties in the Near Field. Part I. Theory and Application. NASA-CR-73106, August 1967.

10. Etkin, B. Dynamics of Atmospheric Flight. New York: John Wiley and Sons, Inc., 1972.

BEST AVAILABLE COPY

Appendix A

Inertia/Center of Gravity Location Program

```
      PROGRAM TEST(INPUT,OUTPUT,TAPE1=INPUT,TAPE2=OUTPUT)
      REAL MOMX,MOMY,MOMZ,MASS,IX,IY,IZ,IXZ
      DIMENSION X(170),Y(170),Z(170),A(170),B(170),WT(170)
      CALL CENGRAV(170,TOTWT,A,B,WT,X,Y,Z,XCG,YCG,ZCG)
      STOP
      END
      SUBROUTINE CENGRAV(INM,TOTWT,A,B,WT,X,Y,Z,XCG,YCG,ZCG)
      REAL MOMX,MOMY,MOMZ,MASS,IX,IY,IZ,IXZ
      DIMENSION X(INM),Y(INM),Z(INM),A(INM),B(INM),WT(INM)
      TOTWT=MOMX=MOMY=MOMZ=0.0
      WRITE(2,9007)
 9007 FORMAT("-         ITEM          WEIGHT       X          Y          Z")
      DO 9008 I=1,INM
      READ(1,9005) A(I),B(I),WT(I),X(I),Y(I),Z(I)
 9005 FORMAT (2A10,4G10.3)
 9008 WRITE (2,9006) A(I),B(I),WT(I),X(I),Y(I),Z(I)
 9006 FORMAT (" ",2A10,4G10.3)
      DO 9009 I=1,INM
      MOMX=MOMX + WT(I)*X(I)
      MOMY=MOMY + WT(I)*Y(I)
      MOMZ=MOMZ + WT(I)*Z(I)
 9009 TOTWT=TOTWT + WT(I)
      WRITE (2,9003) TOTWT
 9003 FORMAT ("/AIRCRAFT WEIGHT IS",G10.3,"OUNCES.")
      XCG=MOMX/TOTWT
      YCG=MOMY/TOTWT
      ZCG=MOMZ/TOTWT
      WRITE (2,9004) XCG,YCG,ZCG
 9004 FORMAT("/AIRCRAFT CG IS LOCATED AT X=",G10.3,",Y=",G10.3,",Z=",
     1G10.3,".")
      IX=IY=IZ=IXZ=0.0
      DO 9001 I=1,INM
      MASS=(WT(I)/16.0)/32.174
      IXZ=IXZ-MASS*(X(I)-XCG)*(Z(I)-ZCG)
      IX=IX + MASS*((Y(I)-YCG)*(Y(I)-YCG))+((Z(I)-ZCG)*(Z(I)-ZCG)))
      IY=IY + MASS*((X(I)-XCG)*(X(I)-XCG))+((Z(I)-ZCG)*(Z(I)-ZCG)))
 9001 IZ=IZ + MASS*((X(I)-XCG)*(X(I)-XCG))+((Y(I)-YCG)*(Y(I)-YCG)))
      WRITE (2,9002) IX,IY,IZ,IXZ
 9002 FORMAT ("/MOMENTS OF INERTIA IN SLUG-INCHES SQUARED ARE  I-XX=",
     1G10.3,",I-YY=",G10.3,"I-ZZ=",G10.3,"I-XZ=",G10.3)
      RETURN
      END
```

BEST AVAILABLE COPY

Appendix B

FLEXSTAB Flowcharts

This section contains the basic flowcharts for the FLEXSTAB programs used in this study. The common computer symbols are defined below.

Flowchart symbols:

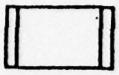

Precompiler statements
a set of statements producing FORTRAN source code.

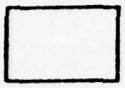

Computational processing
a block or portion of a program or subprogram that processes a set of instructions or equations.

Input/output processing
a block or portion of a program or subprogram that processes input/output requests.

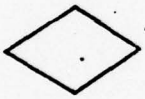

Decision
a point in the program where a branch to alternate paths is possible depending upon variable conditions.

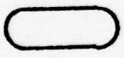

Terminal
the beginning or end of a program or subprogram.

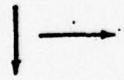

Flow direction
the direction of processing or data flow.

Offpage connector

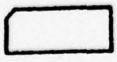

Punched cards

Output listings

Magnetic tape
used for permanent storage of data and programs.

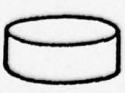

Disk
used for temporary storage of data and programs.

BEST AVAILABLE COPY

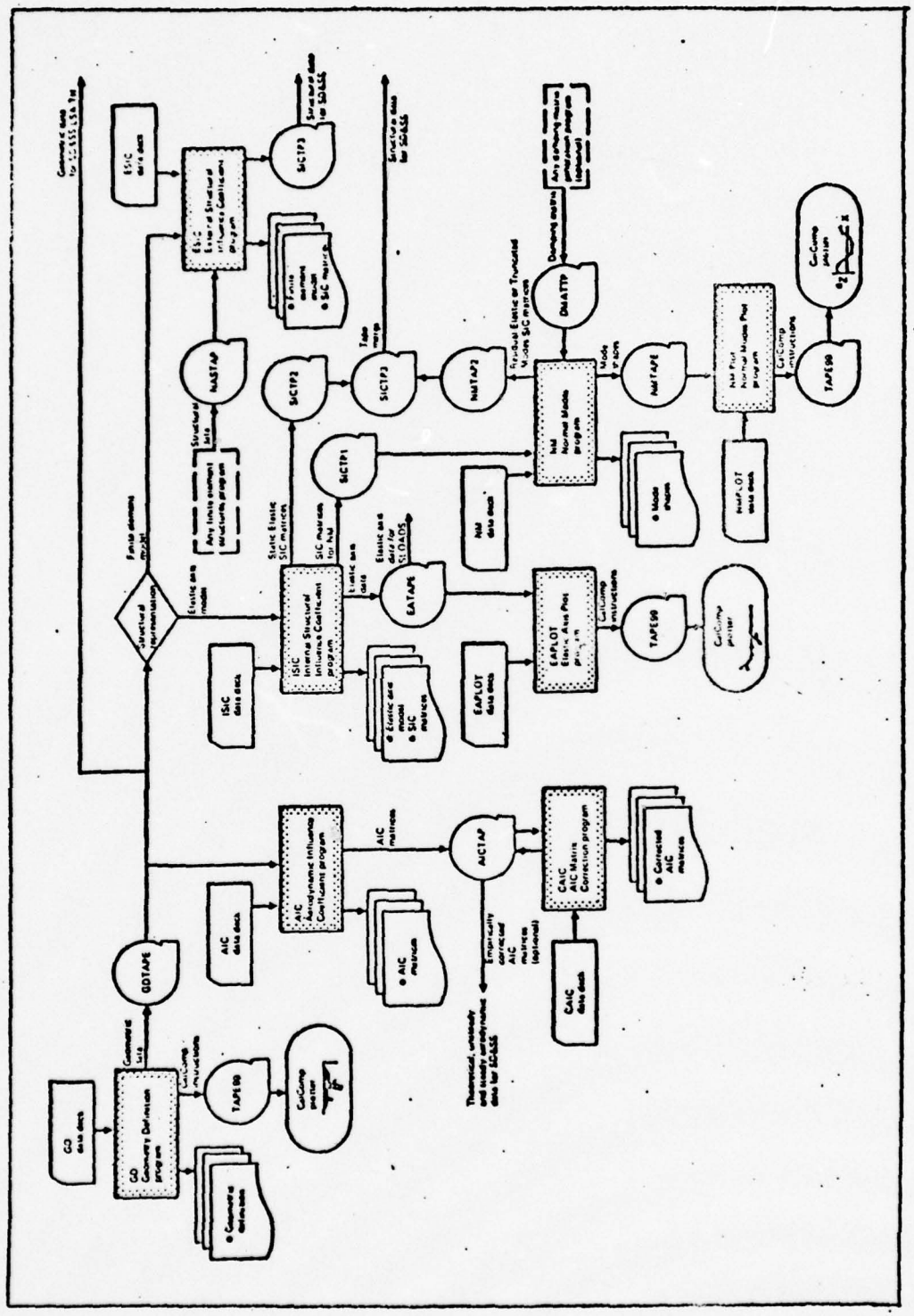

Figure B1. Airplane Definition Section

BEST AVAILABLE COPY

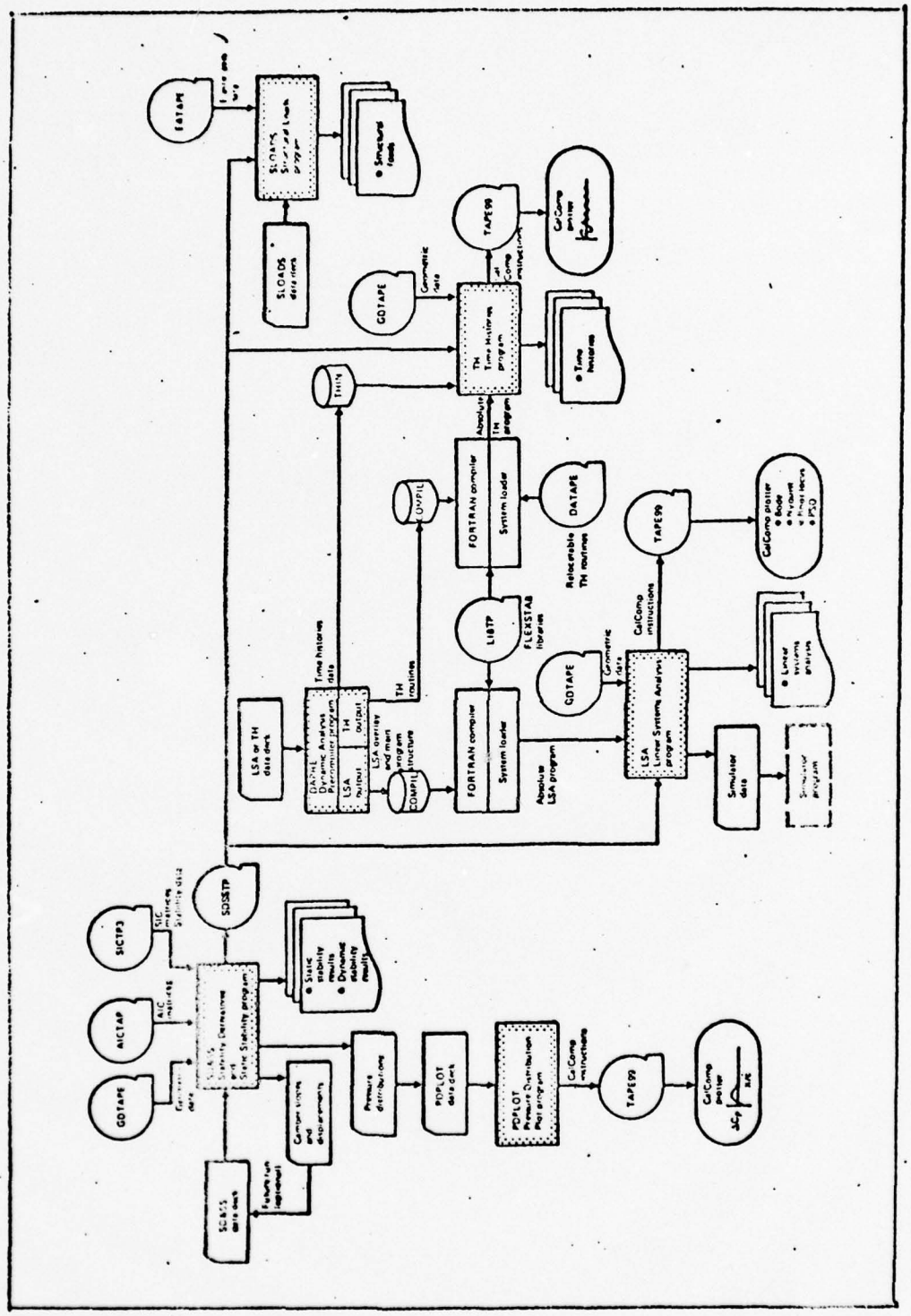

Figure B2. Airplane Analysis Section

BEST AVAILABLE COPY

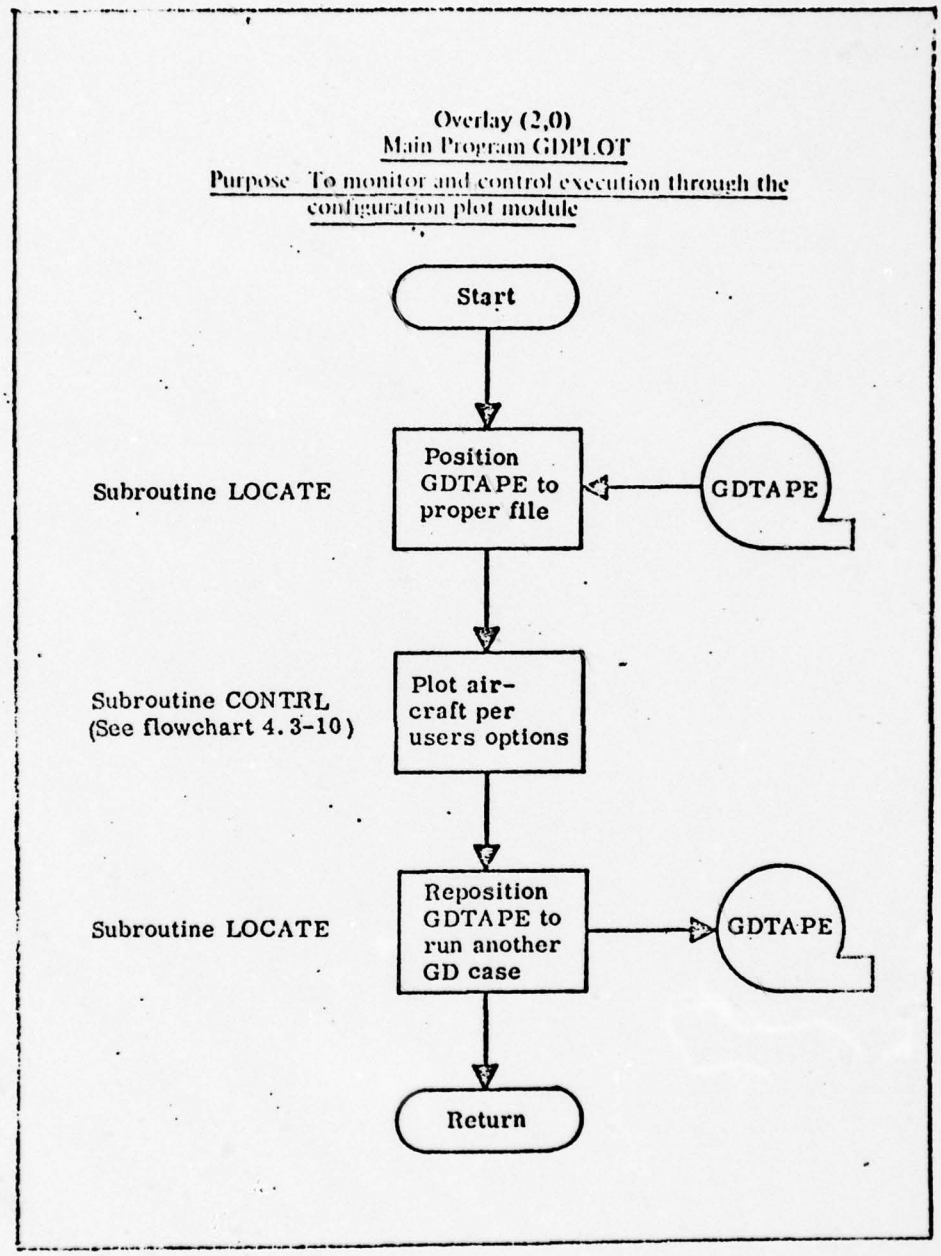

Figure B3. Geometry Definition Program Flowchart

BEST AVAILABLE COPY

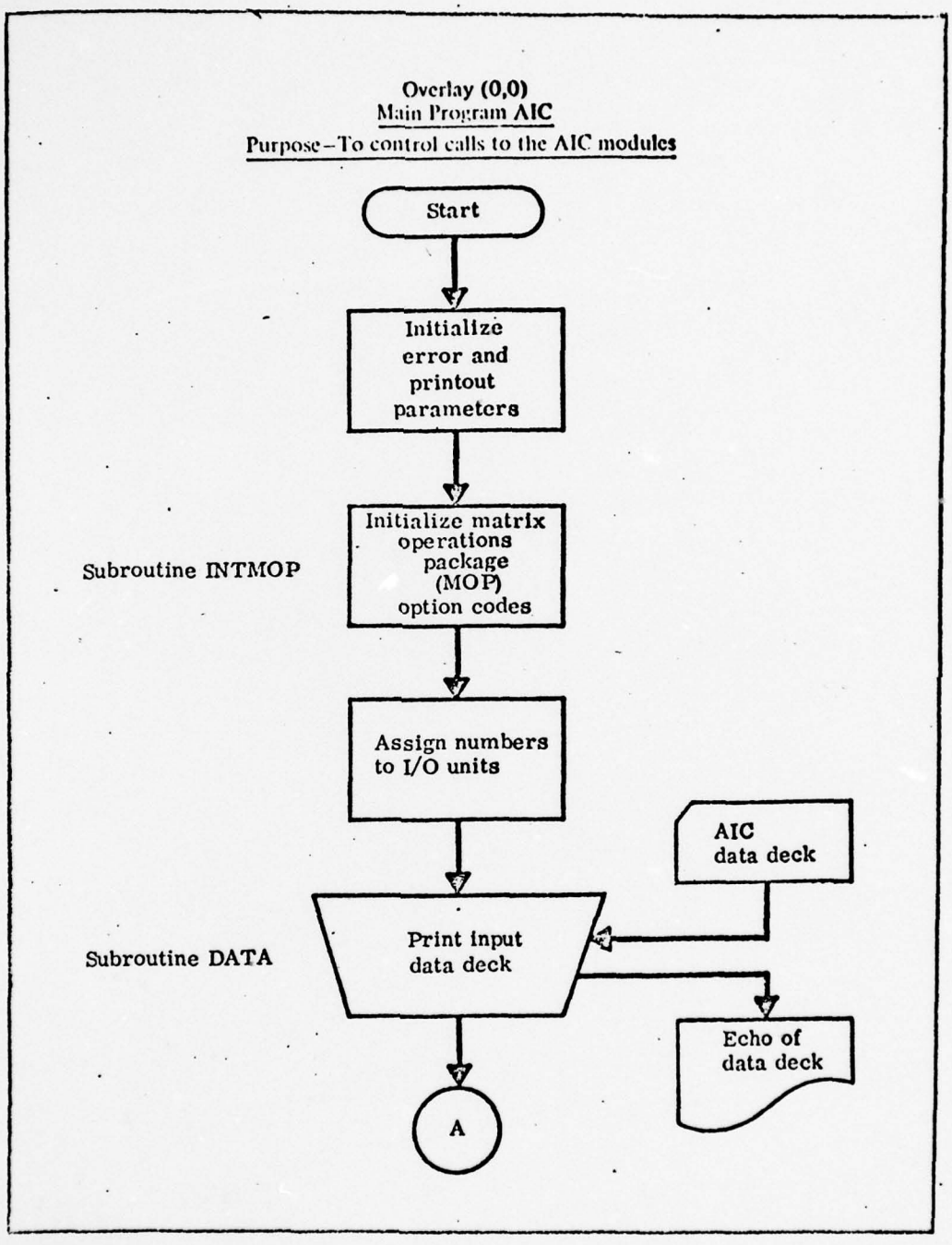

Figure B4. Aerodynamic Influence Coefficient Program Flowchart

BEST AVAILABLE COPY

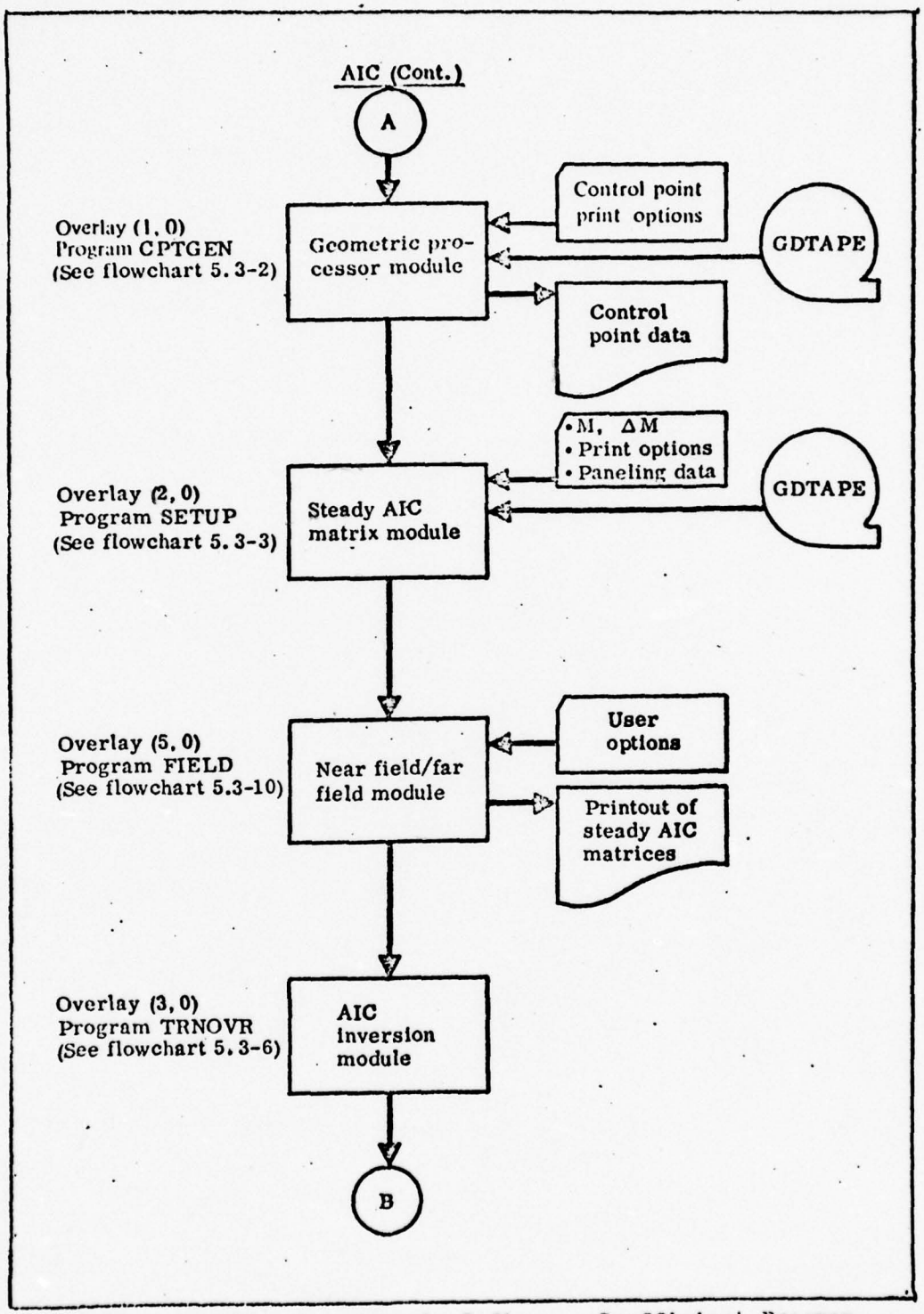

Figure B4 - Cont'd. Aerodynamic Influence Coefficient Program Flowchart

BEST AVAILABLE COPY

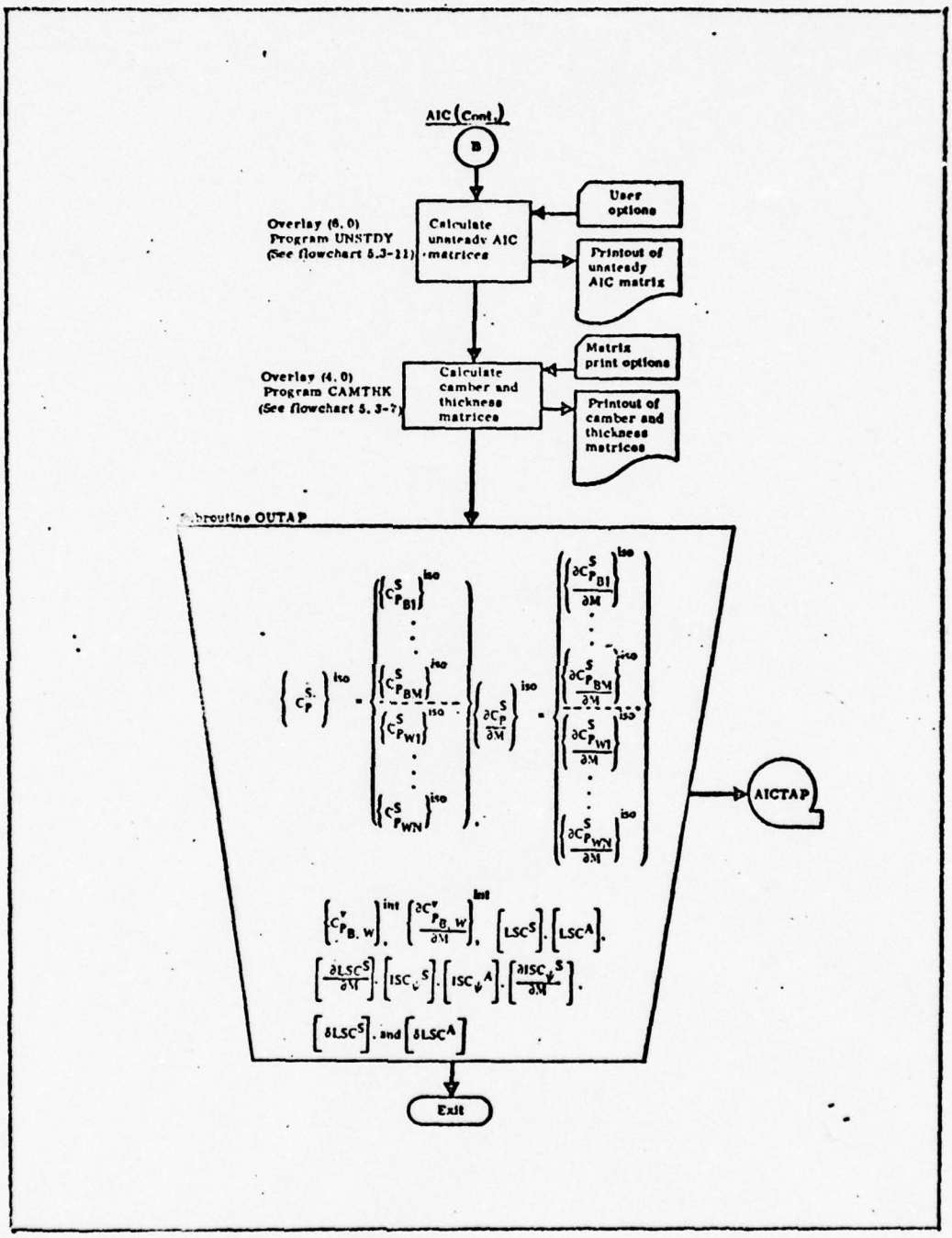

Figure B4 - Cont'd. Aerodynamic Influence Coefficient Program Flowchart

BEST AVAILABLE COPY

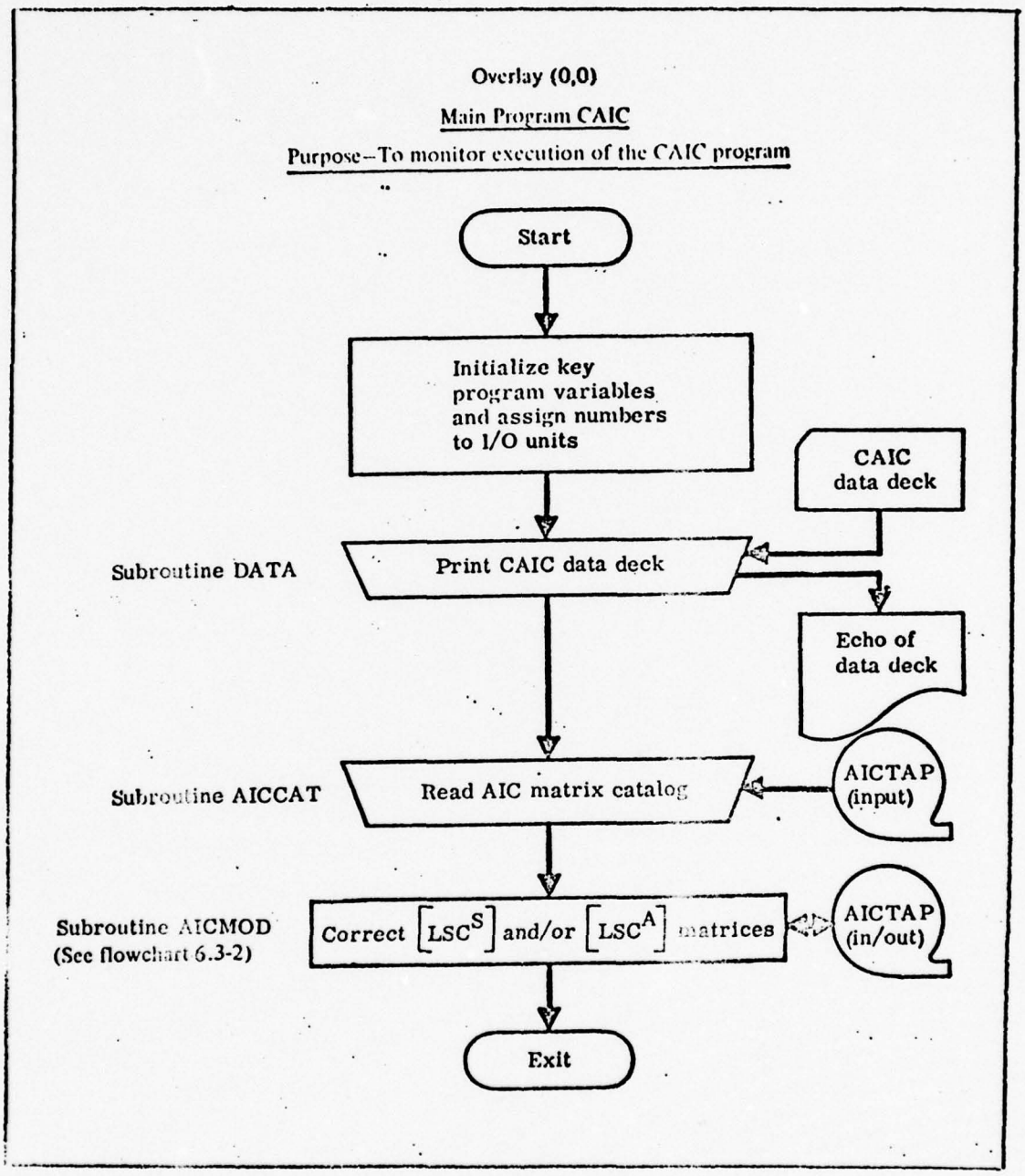

Figure B5. AIC Correction Matrix Program Flowchart

BEST AVAILABLE COPY

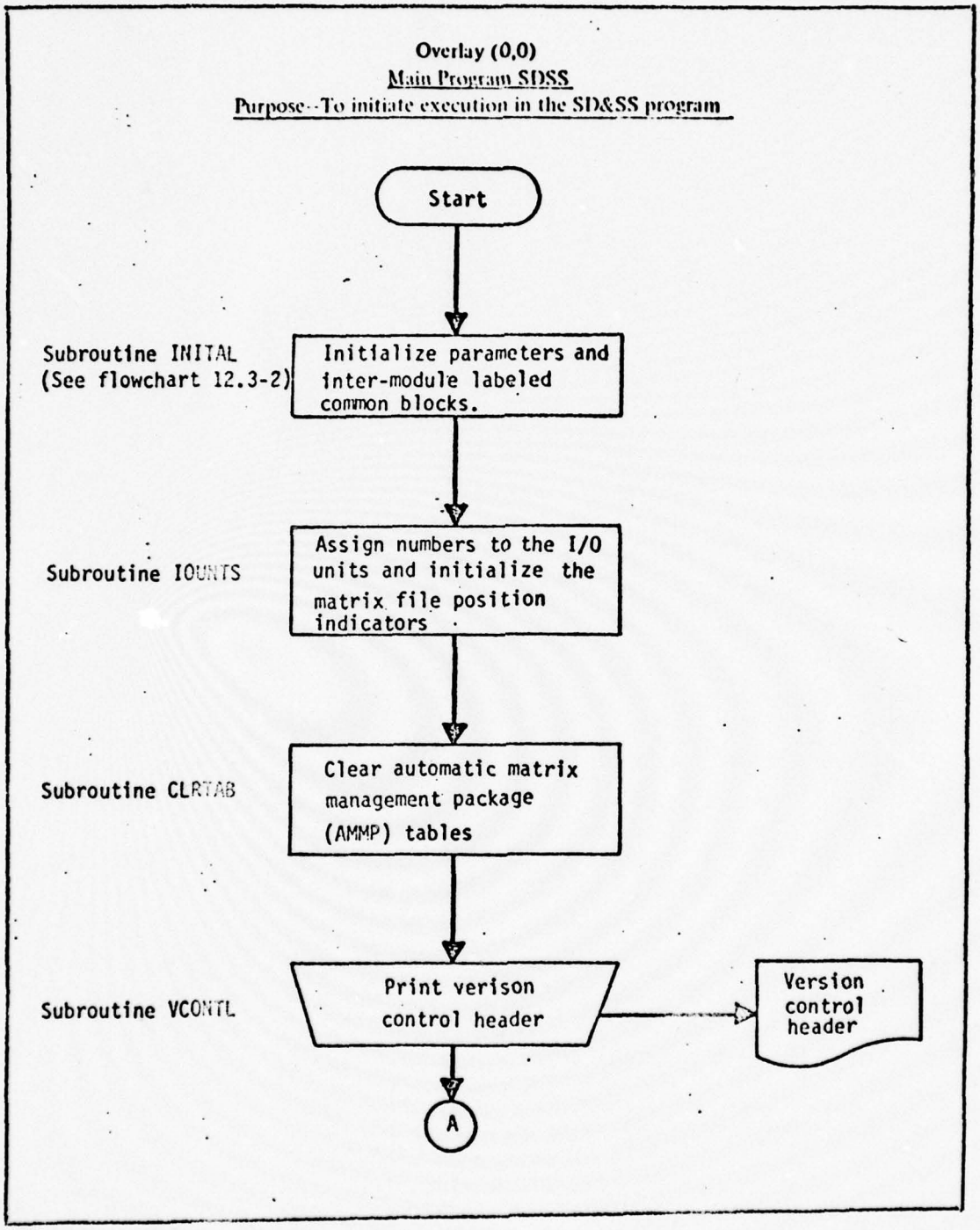

Figure B6. SD & SS Program Flowchart

BEST AVAILABLE COPY

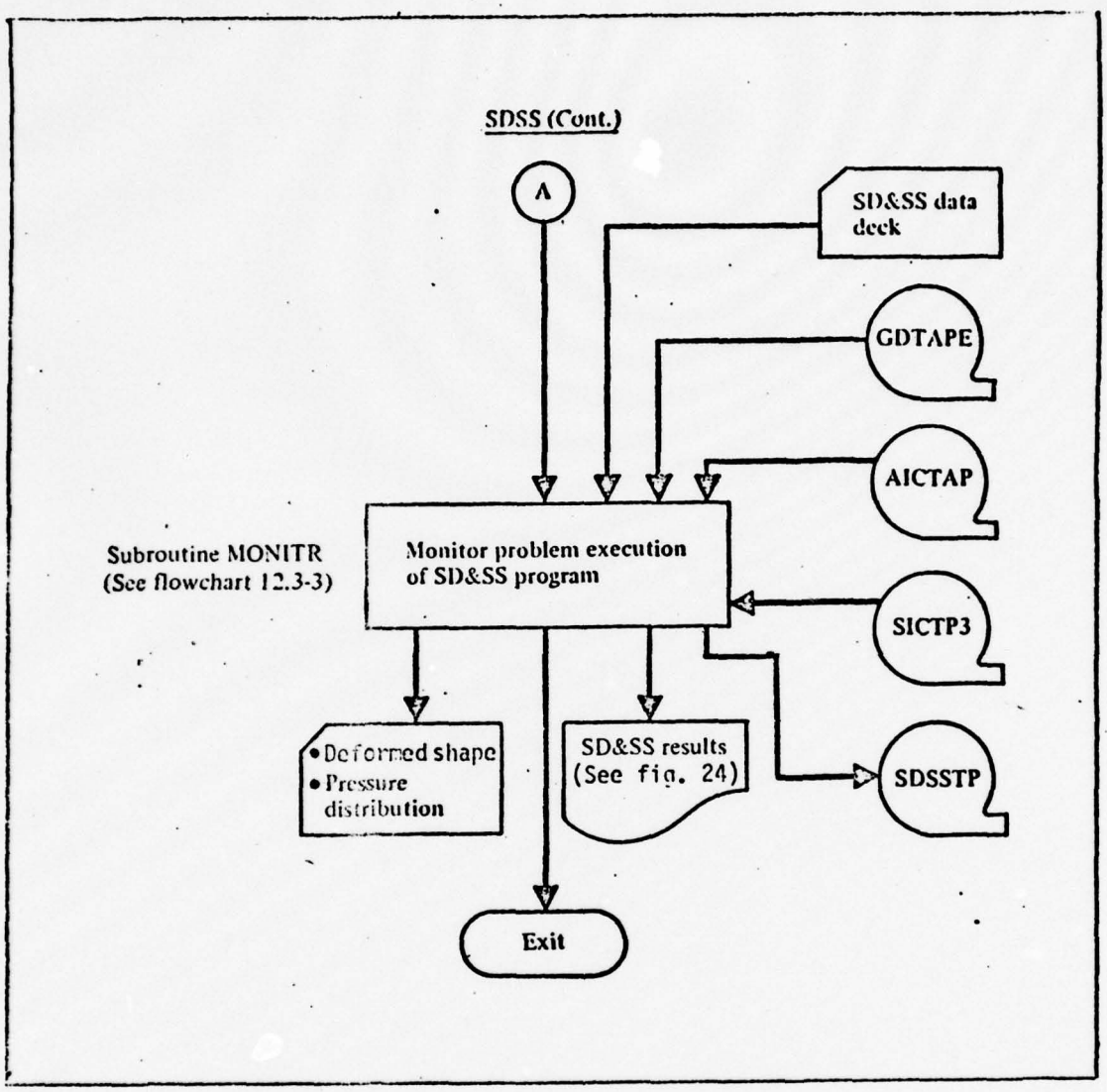

Figure B6 - Cont'd. SD & SS Program Flowchart

BEST AVAILABLE COPY

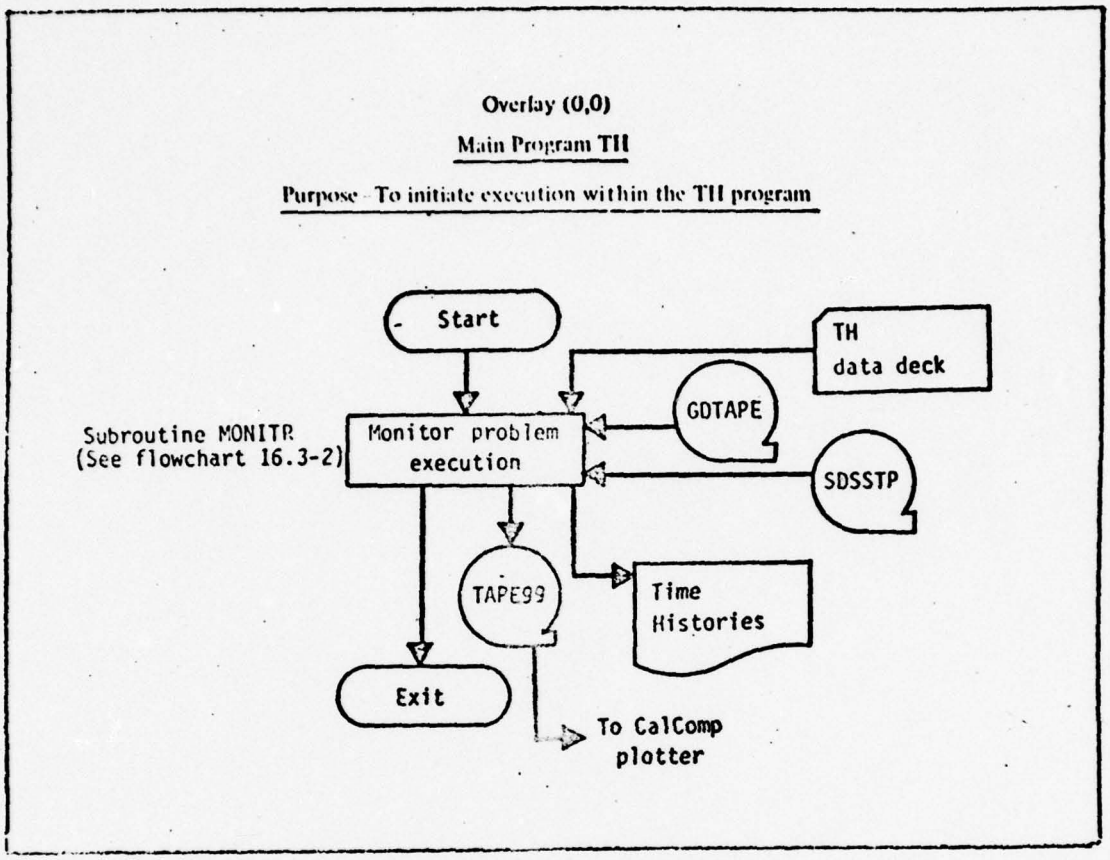

Figure B7. Time Histories Program Flowchart

BEST AVAILABLE COPY

Appendix C

Time History Plots for Rudder Step Input

This section contains the complete set of time history plots for the baseline and modified vehicles. The rudder step input was initiated at time zero with a magnitude of 2° and held for 5 seconds. The following variables are plotted in this order: u, v, w, p, q, r, θ, ϕ, ψ, α, β.

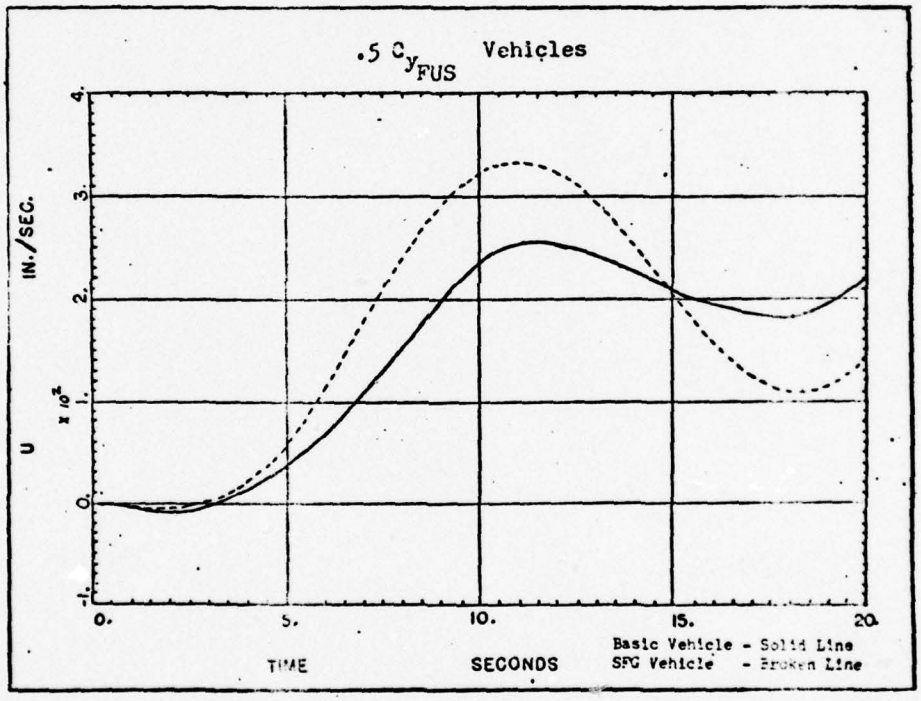

Figure C1. Forward Speed Perturbation Due to 2° Rudder Step (0 to 5 sec)

BEST AVAILABLE COPY

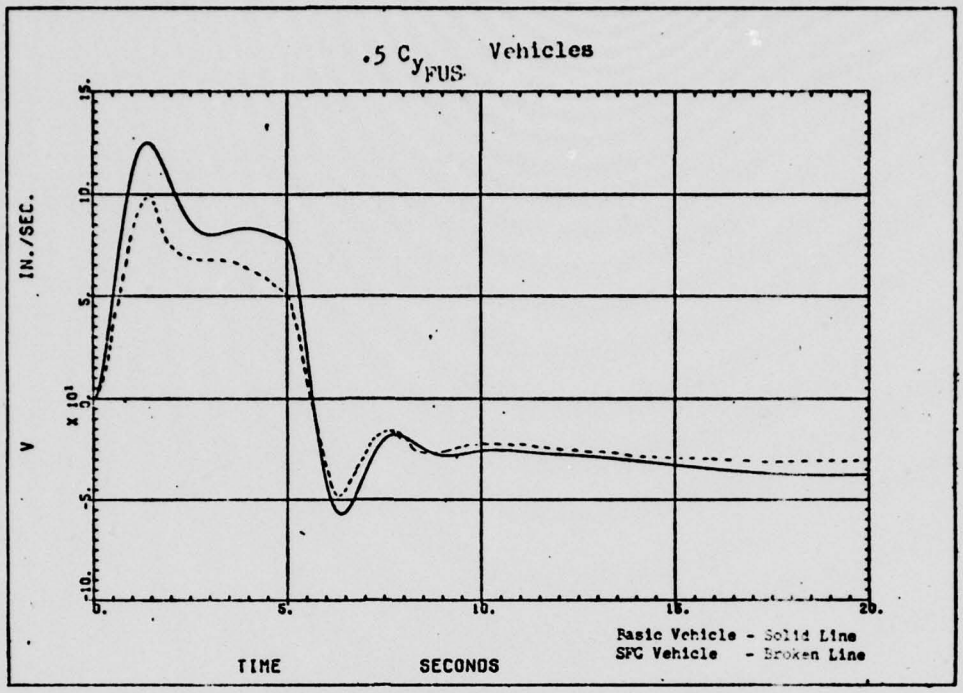

Figure C2. Side Speed Perturbation Due to 2° Rudder Step (0 to 5 sec)

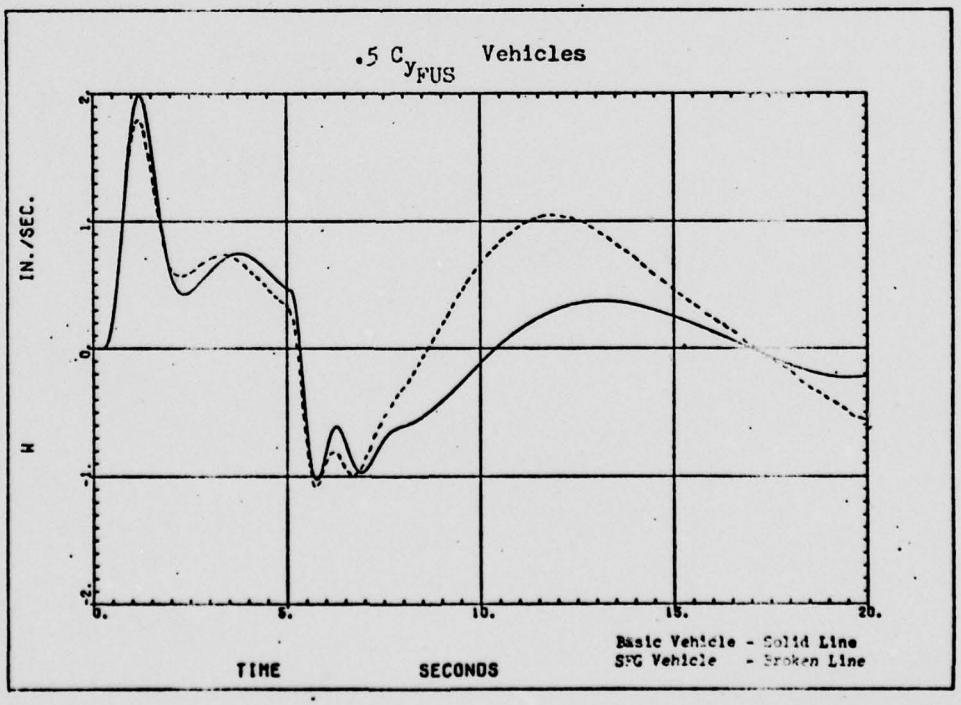

Figure C3. Downward Speed Perturbation Due to 2° Rudder Step (0 to 5 sec)

BEST AVAILABLE COPY

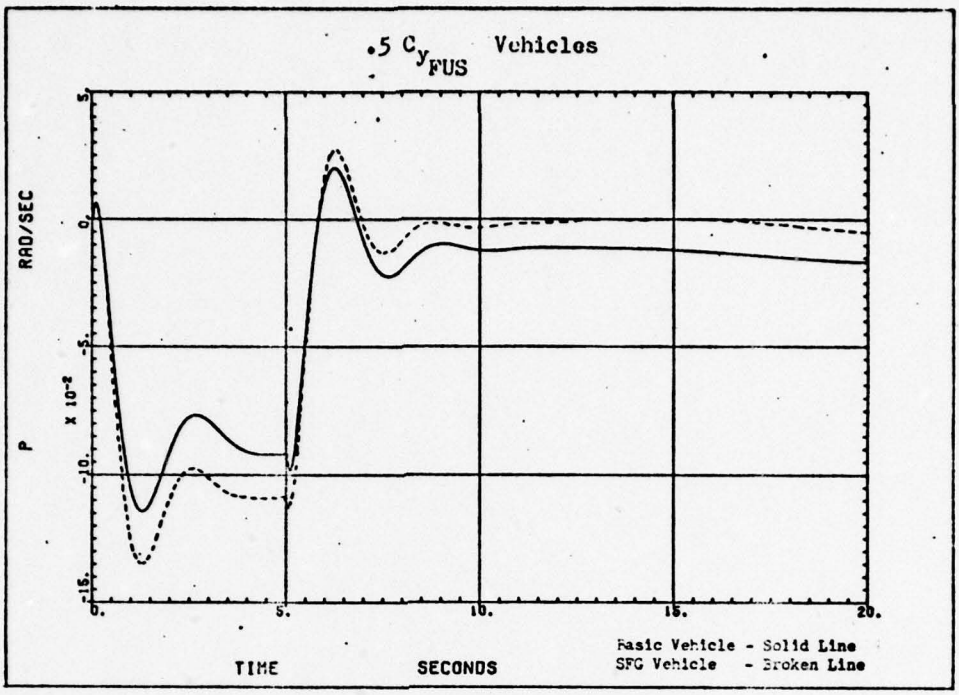

Figure C4. Roll Rate Due to 2° Rudder Step (0 to 5 sec)

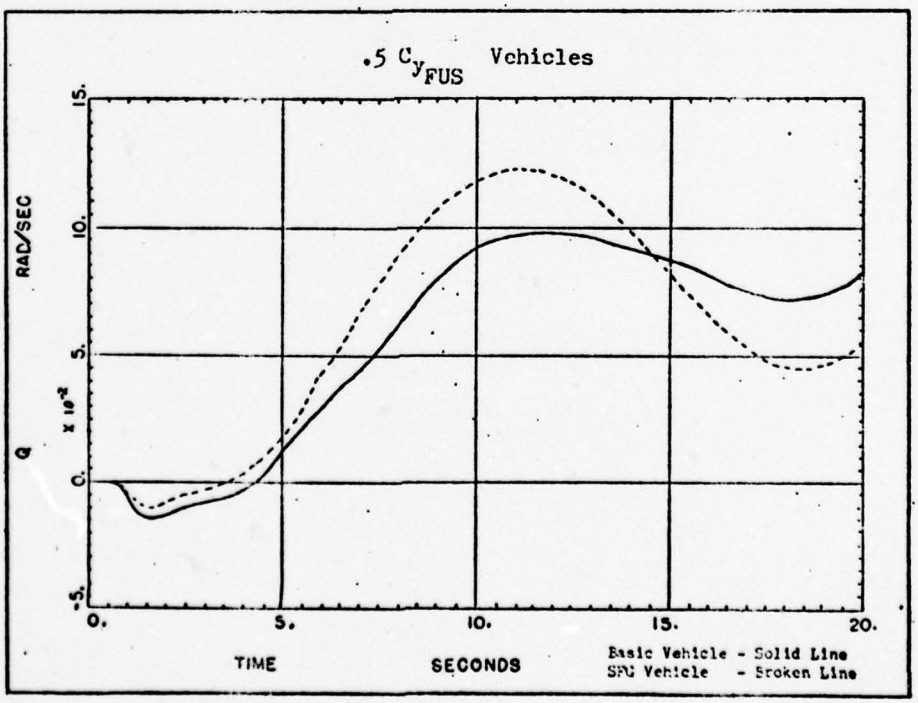

Figure C5. Pitch Rate Due to 2° Rudder Step (0 to 5 sec)

BEST AVAILABLE COPY

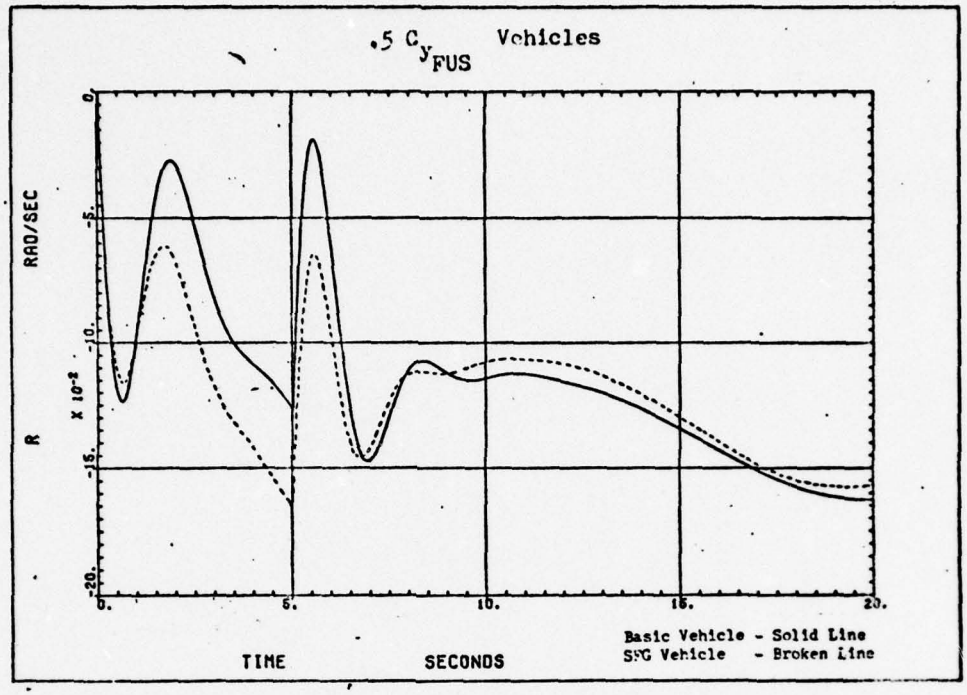

Figure C6. Yaw Rate Due to 2° Rudder Step (0 to 5sec)

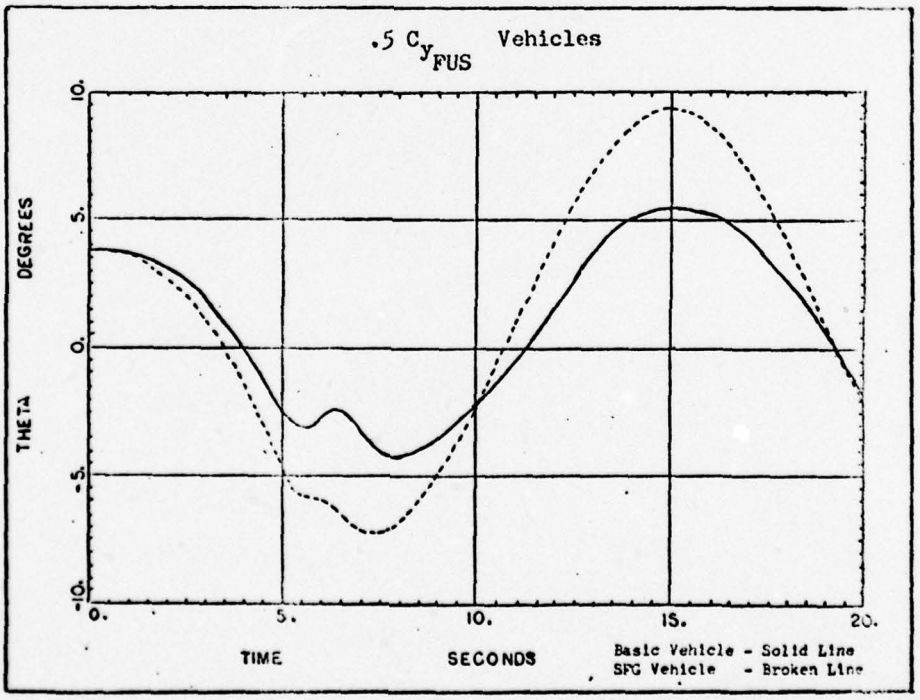

Figure C7. Pitch Angle Due to 2° Rudder Step (0 to 5 sec)

BEST AVAILABLE COPY

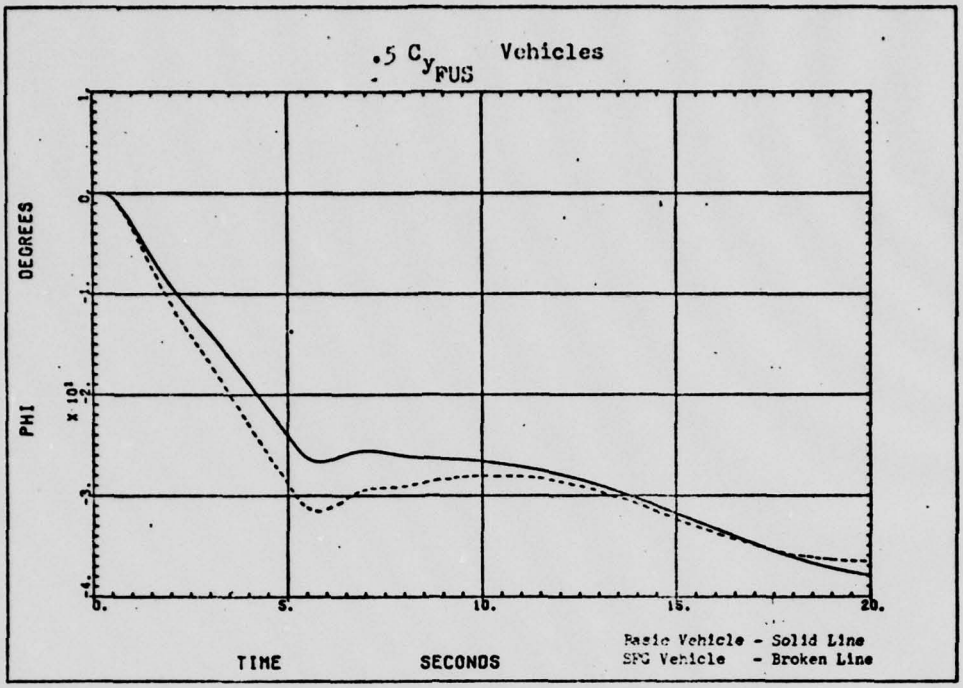

Figure C8. Roll Angle Due to 2° Rudder Step (0 to 5 sec)

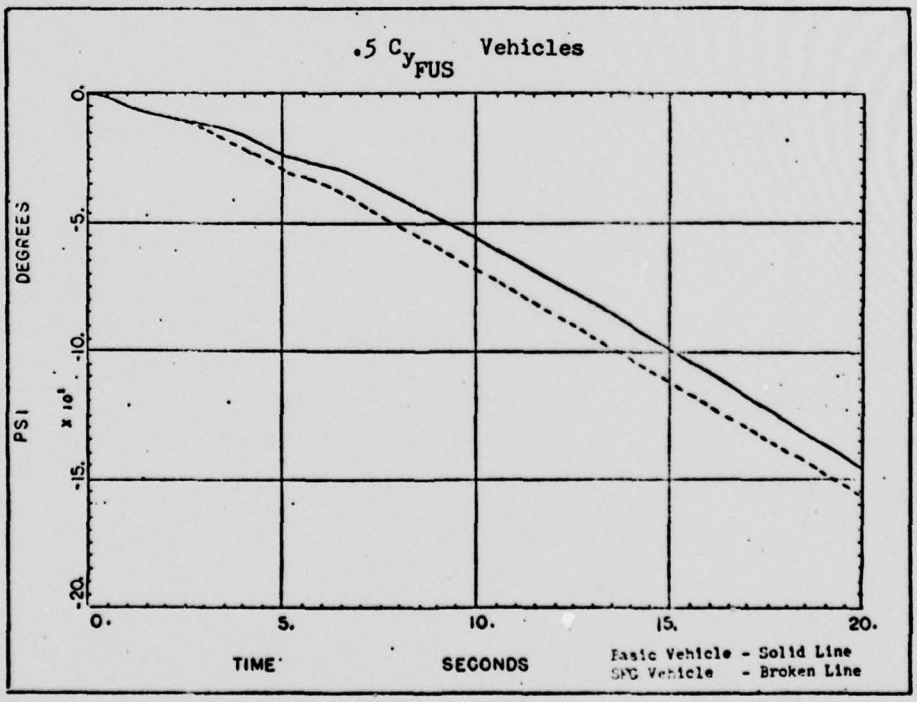

Figure C9. Heading Angle Due to 2° Rudder Step (0 to 5 sec)

BEST AVAILABLE COPY

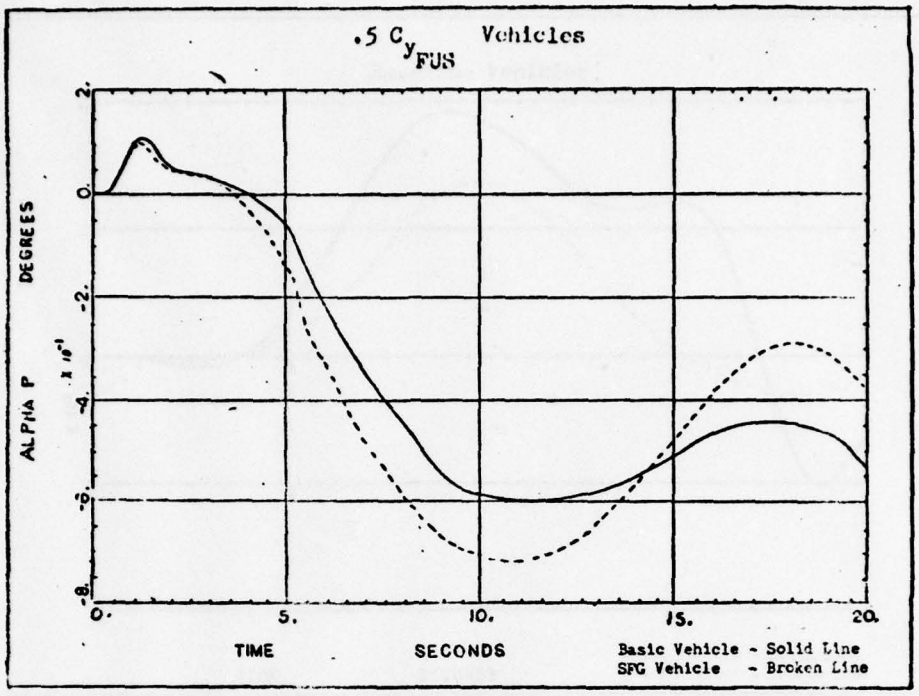

Figure C10. Angle of Attack Due to 2° Rudder Step (0 to 5 sec)

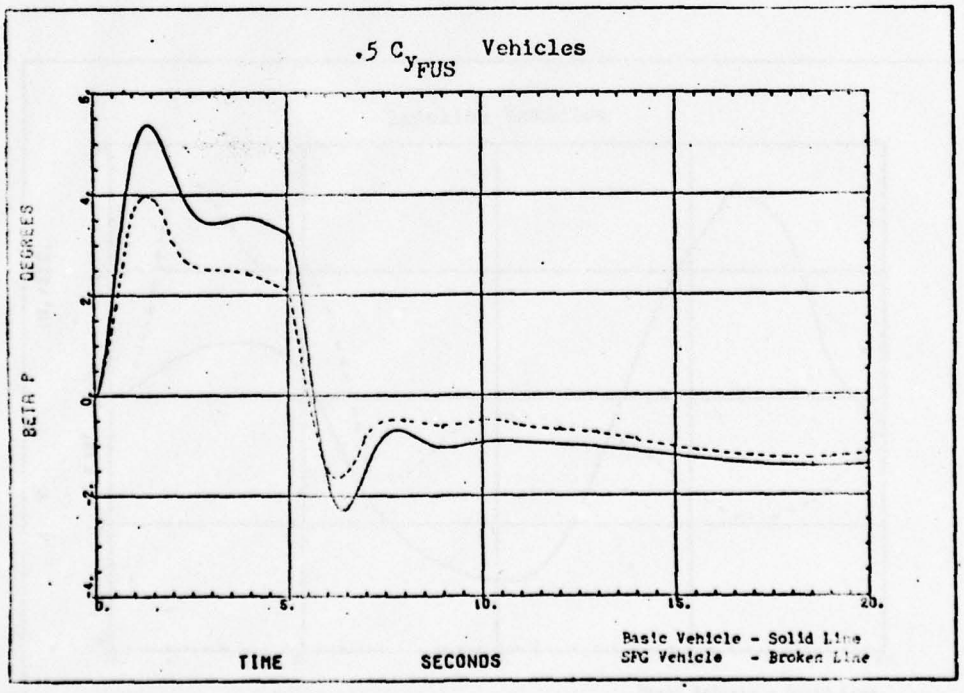

Figure C11. Side Slip Angle Due to 2° Rudder Step (0 to 5 sec)

BEST AVAILABLE COPY

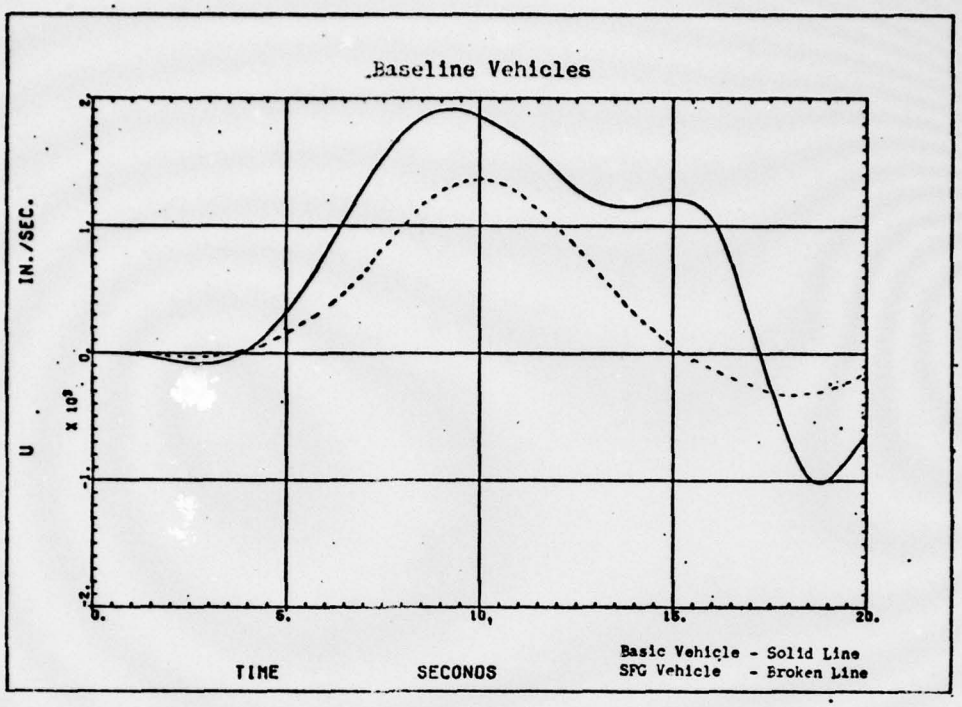

Figure C12. Forward Speed Perturbation Due to 2° Rudder Step (0 to 5 sec)

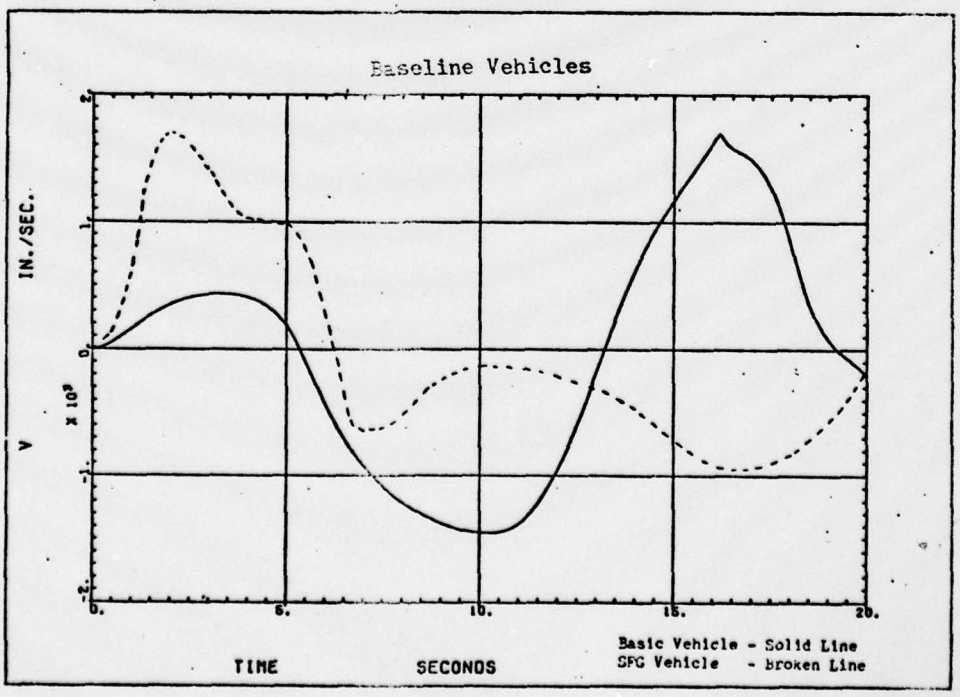

Figure C13. Side Speed Perturbation Due to 2° Rudder Step (0 to 5 sec)

BEST AVAILABLE COPY

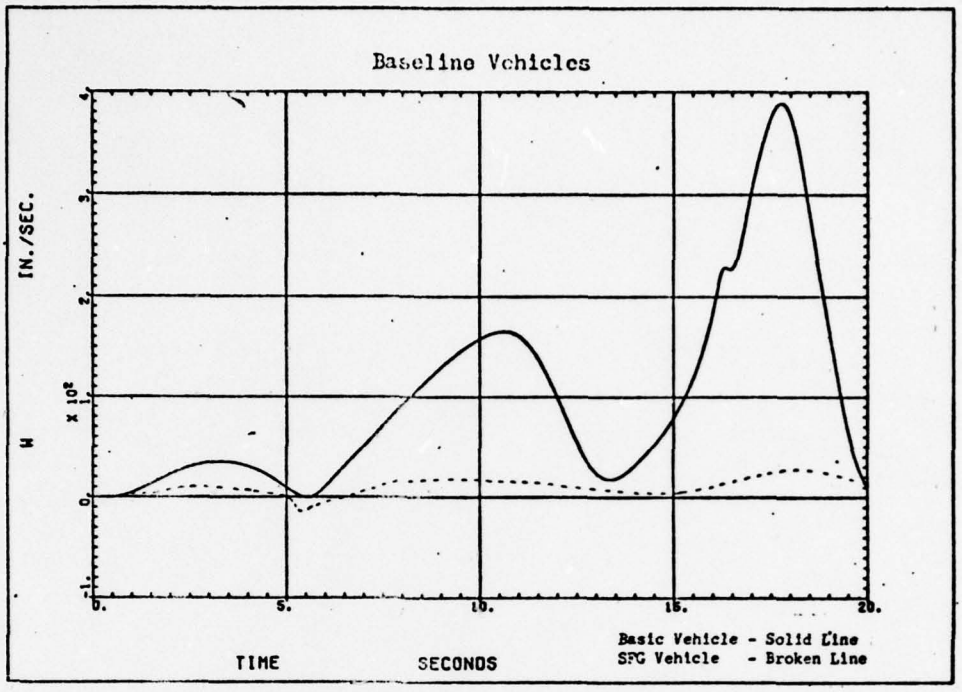

Figure C14. Downward Speed Perturbation Due to 2° Rudder Step (0 to 5 sec)

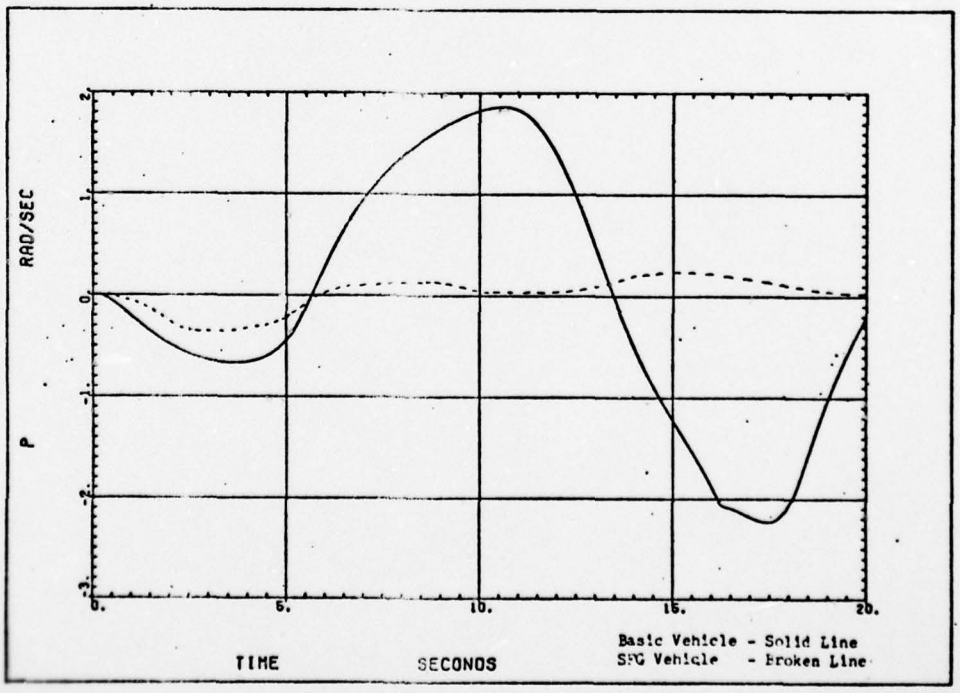

Figure C15. Roll Rate Due to 2° Rudder Step (0 to 5 sec)

BEST AVAILABLE COPY

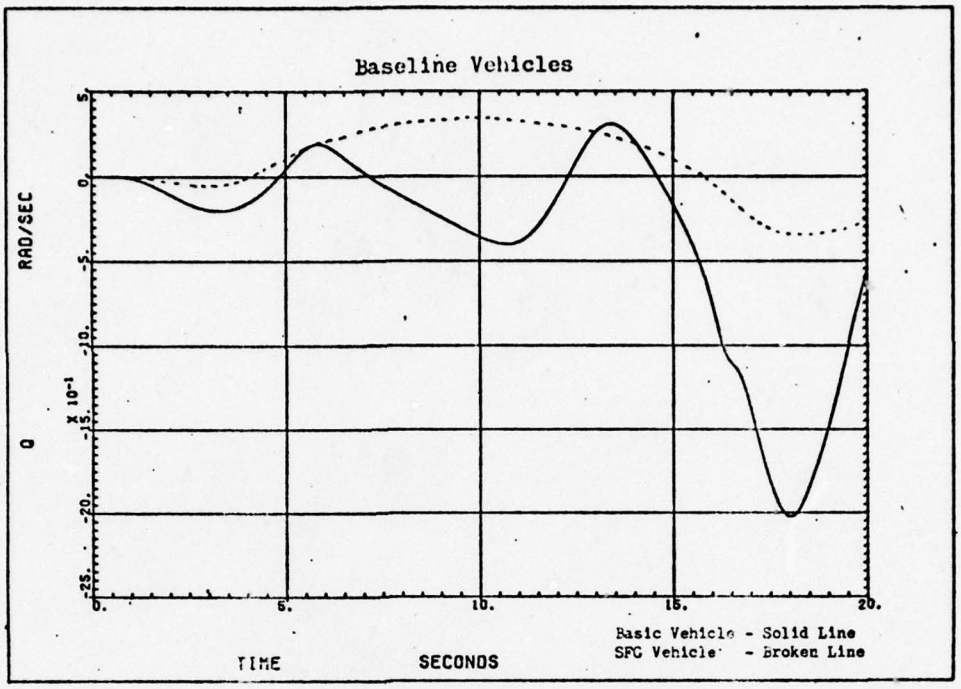

Figure C16. Pitch Rate Due to 2° Rudder Step (0 to 5 sec)

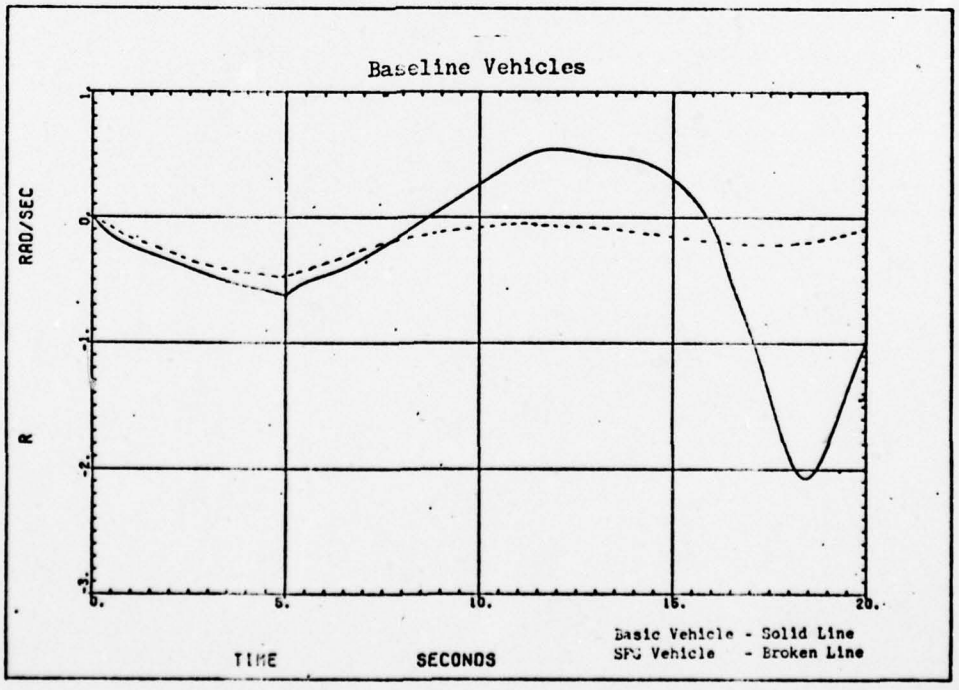

Figure C17. Yaw Rate Due to 2° Rudder Step (0 to 5 sec)

BEST AVAILABLE COPY

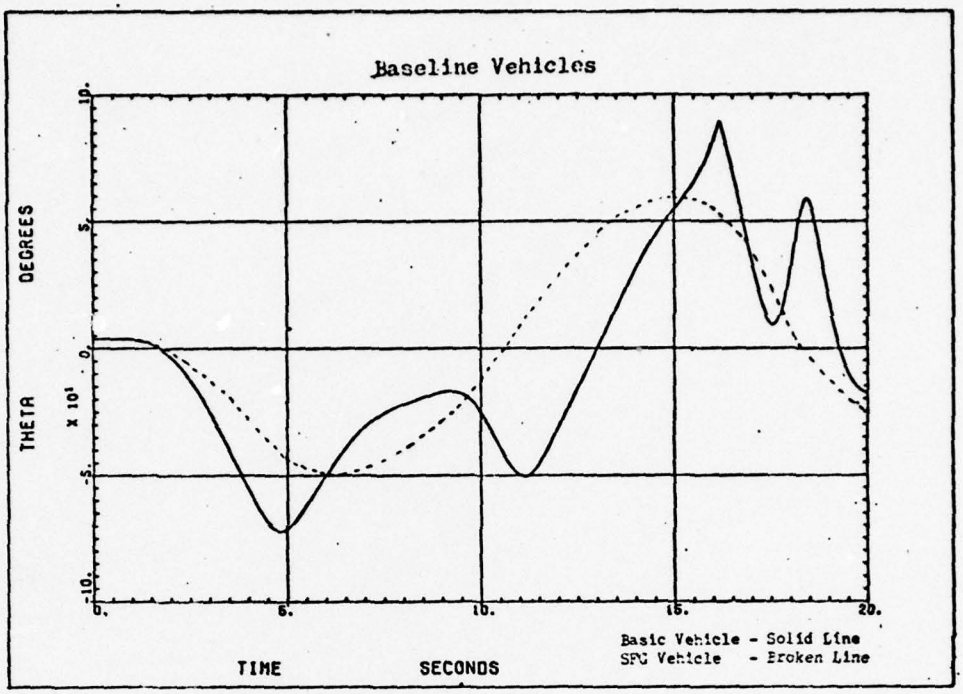

Figure C18. Pitch Angle Due to 2° Rudder Step (0 to 5 sec)

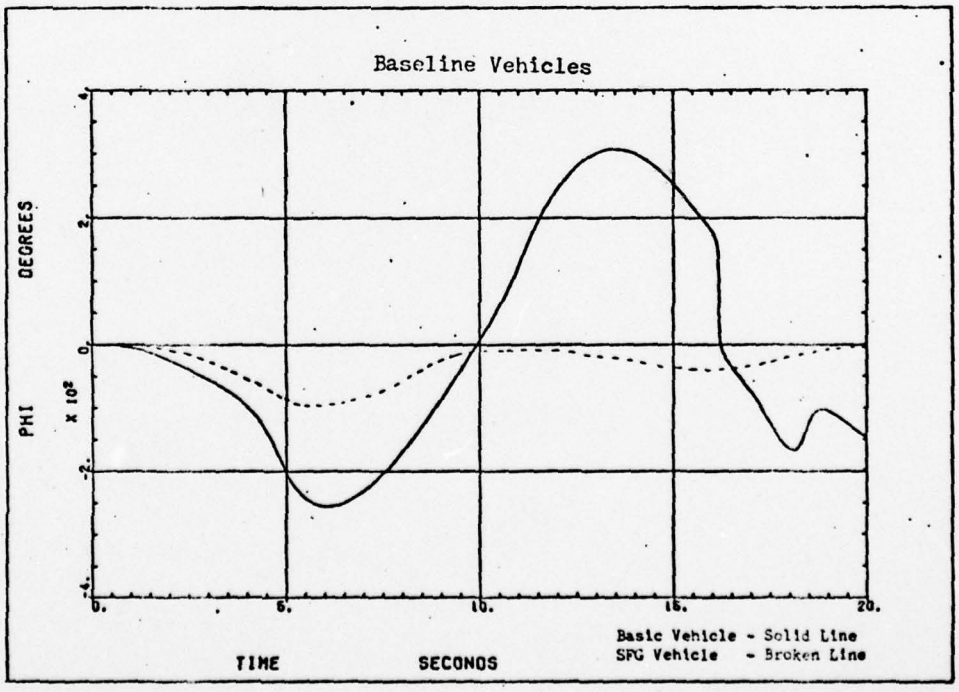

Figure C19. Roll Angle Due to 2° Rudder Step (0 to 5 sec)

BEST AVAILABLE COPY

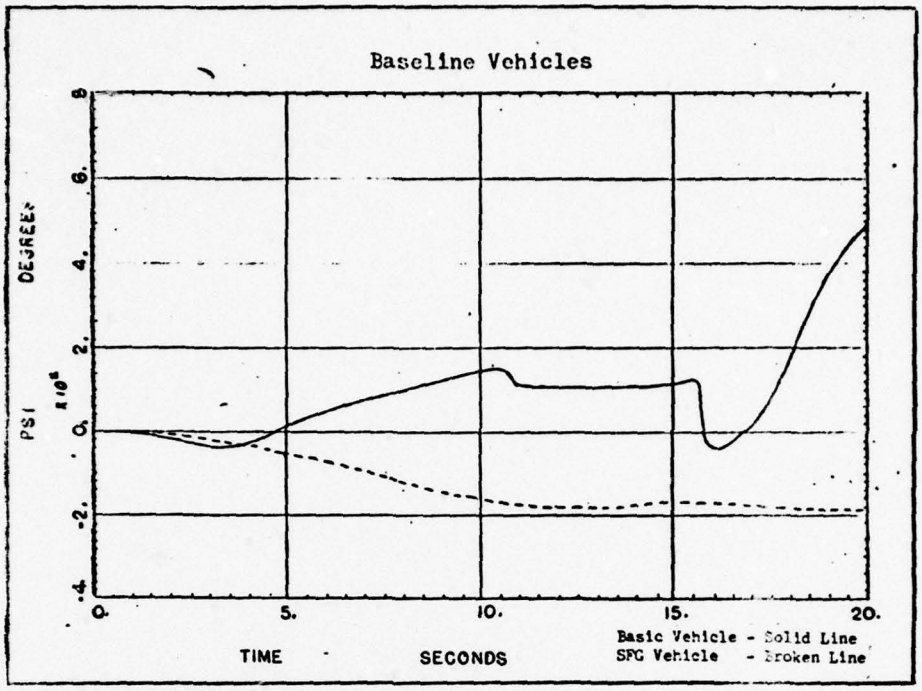

Figure C20. Heading Angle Due to 2° Rudder Step (0 to 5 sec)

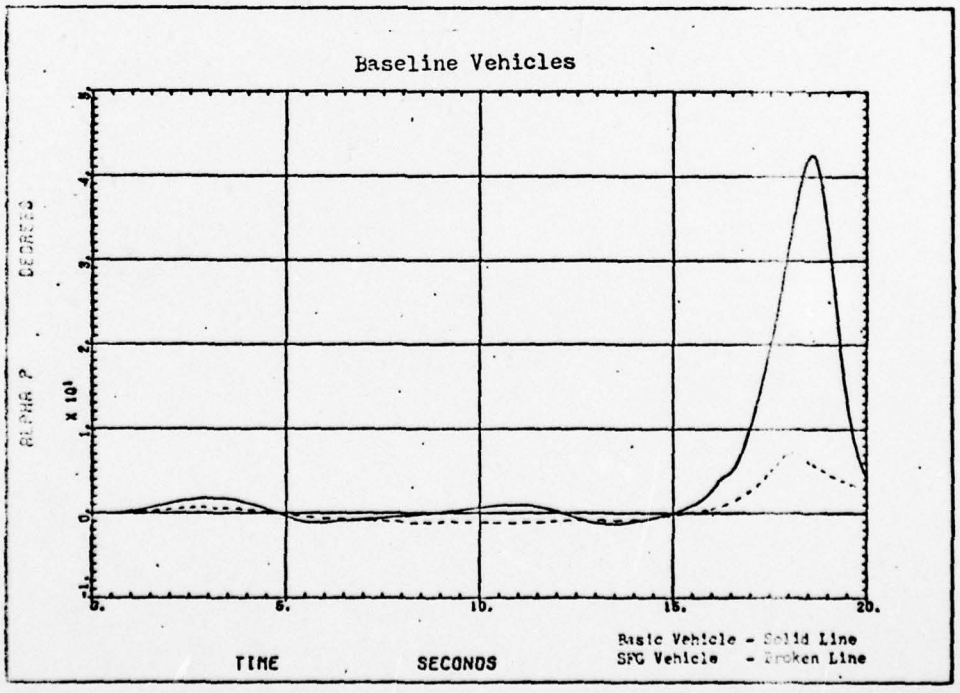

Figure C21. Angle of Attack Due to 2° Rudder Step (0 to 5 sec)

BEST AVAILABLE COPY

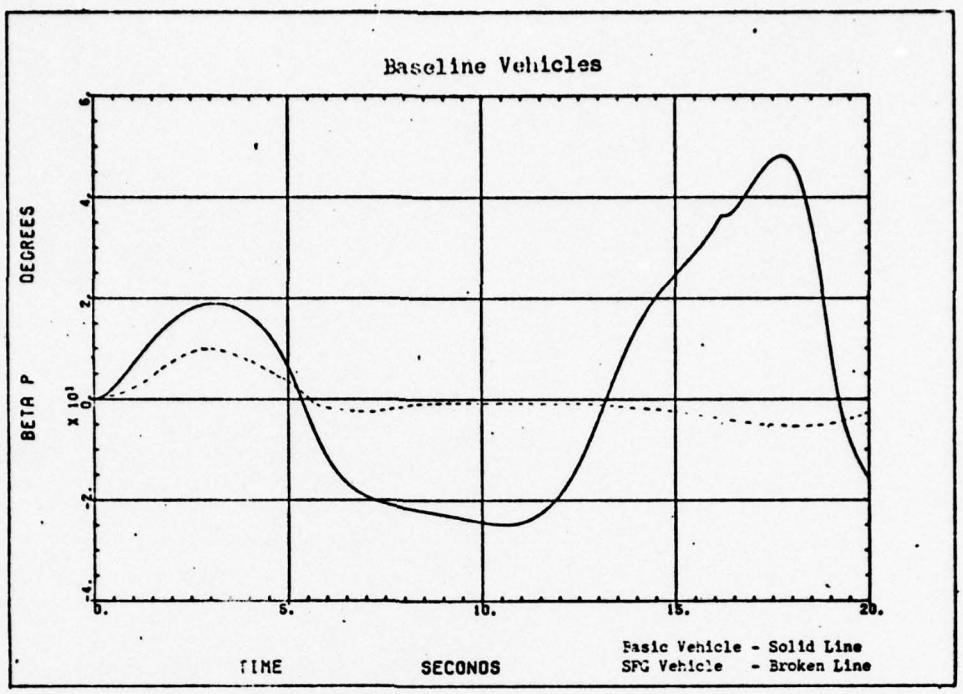

Figure C22. Side Slip Angle Due to 2° Rudder Step (0 to 5 sec)

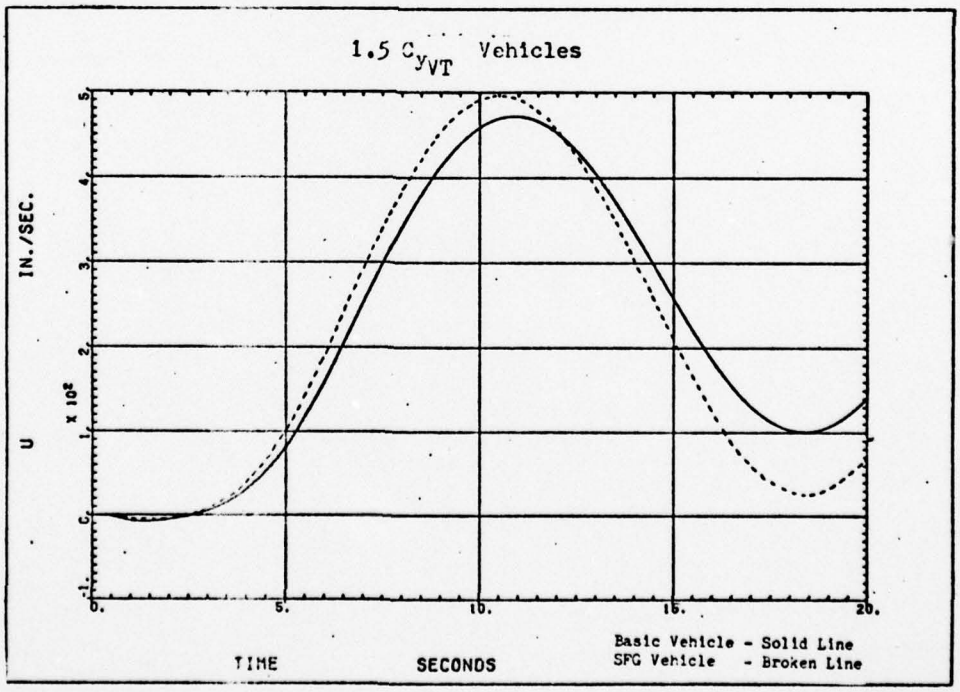

Figure C23. Forward Speed Perturbation Due to 2° Rudder Step (0 to 5 sec)

BEST AVAILABLE COPY

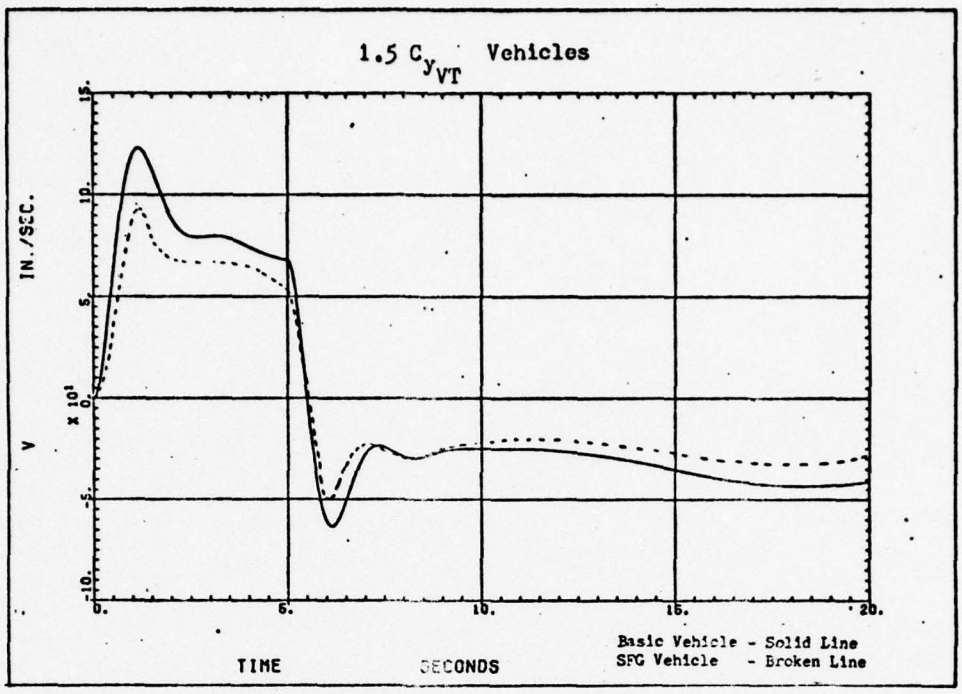

Figure C24. Side Speed Perturbation Due to 2° Rudder Step (0 to 5 sec)

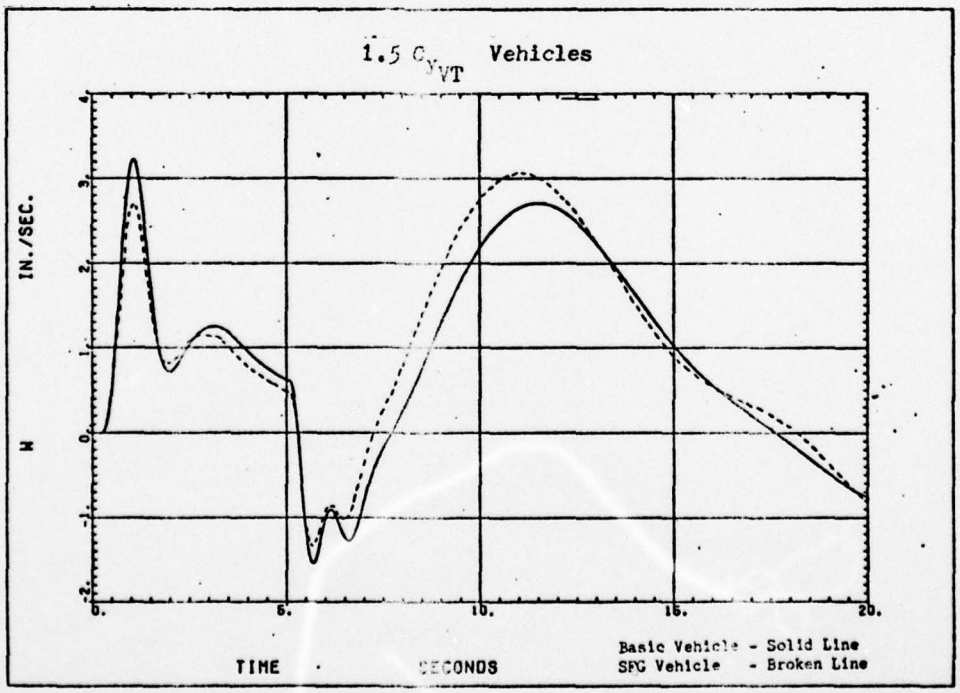

Figure C25. Downward Speed Perturbation Due to 2° Rudder Step (0 to 5 sec)

BEST AVAILABLE COPY

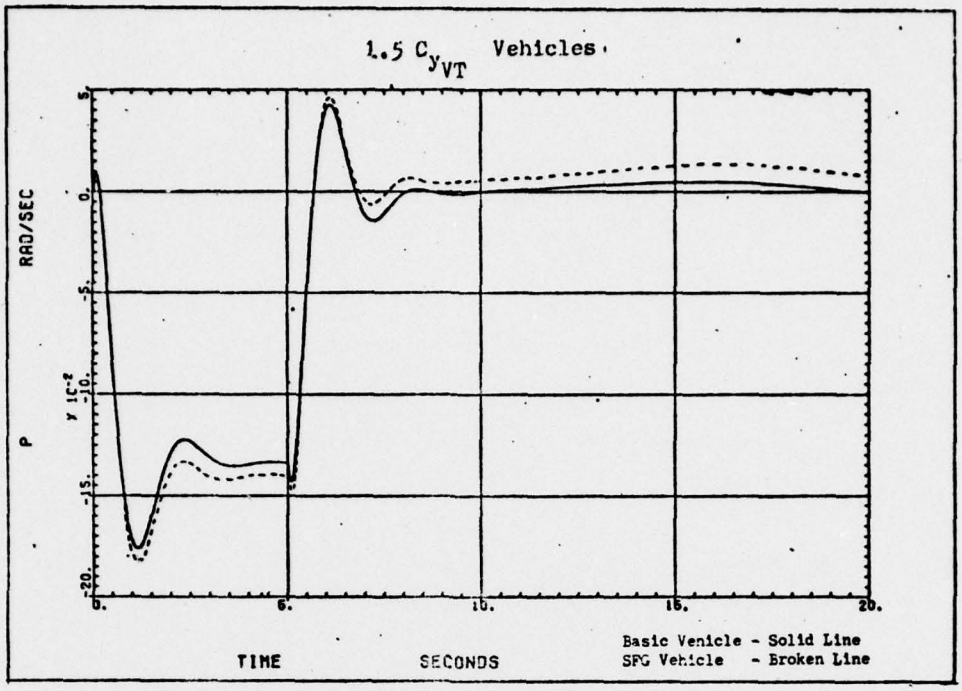

Figure C26. Roll Rate Due to 2° Rudder Step (0 to 5 sec)

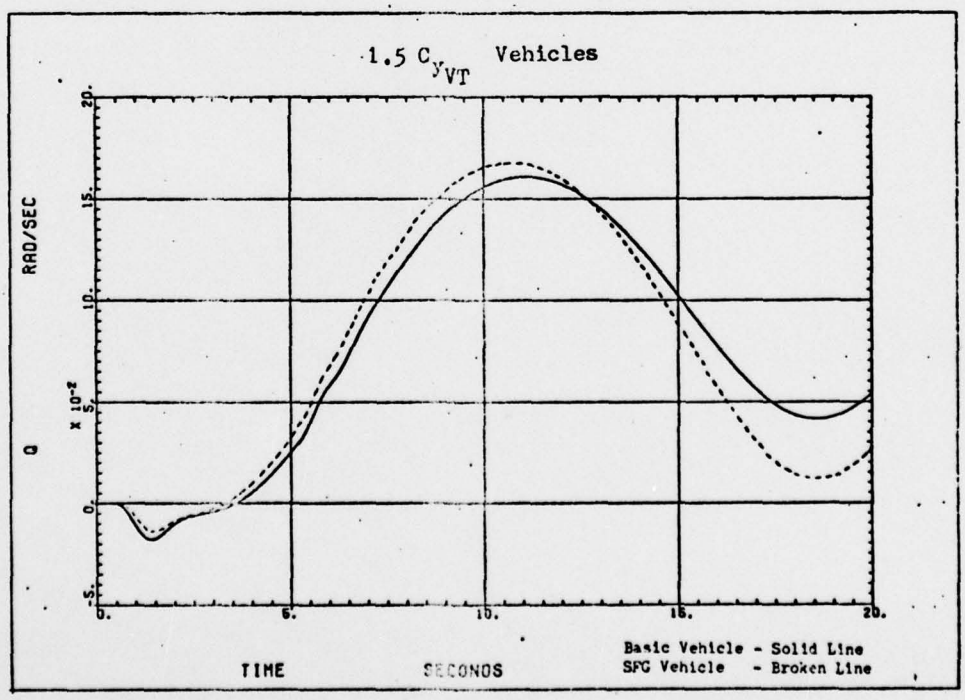

Figure C27. Pitch Rate Due to 2° Rudder Step (0 to 5 sec)

BEST AVAILABLE COPY

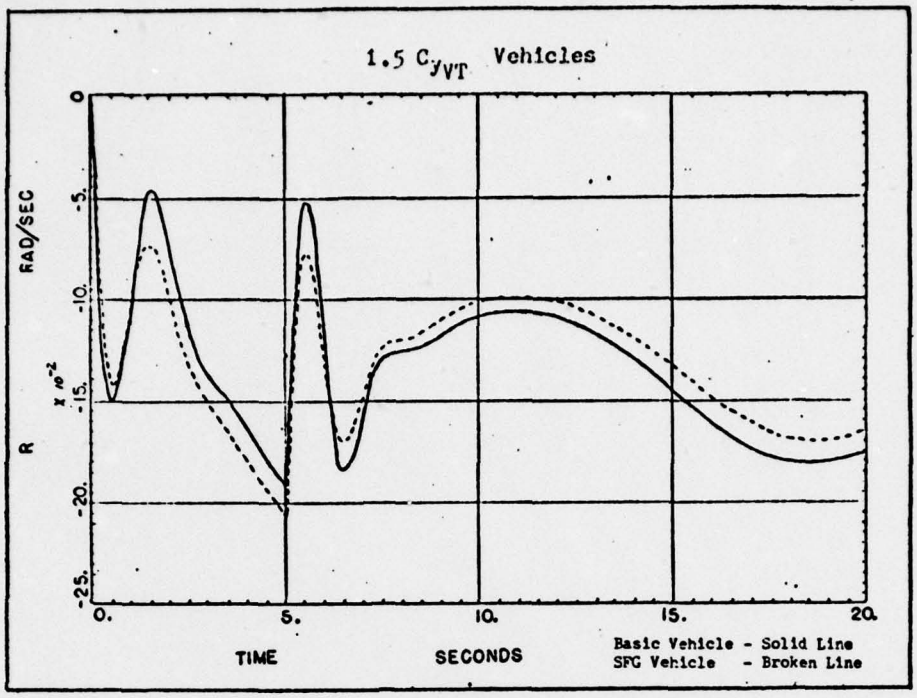

Figure C28. Yaw Rate Due to 2° Rudder Step (0 to 5 sec)

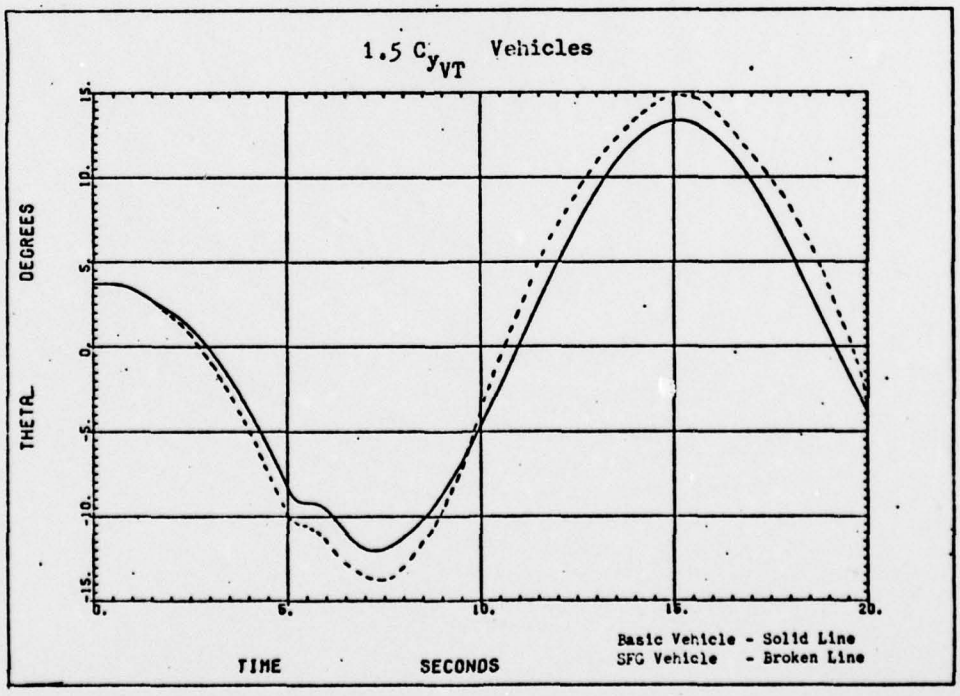

Figure C29. Pitch Angle Due to 2° Rudder Step (0 to 5 sec)

BEST AVAILABLE COPY

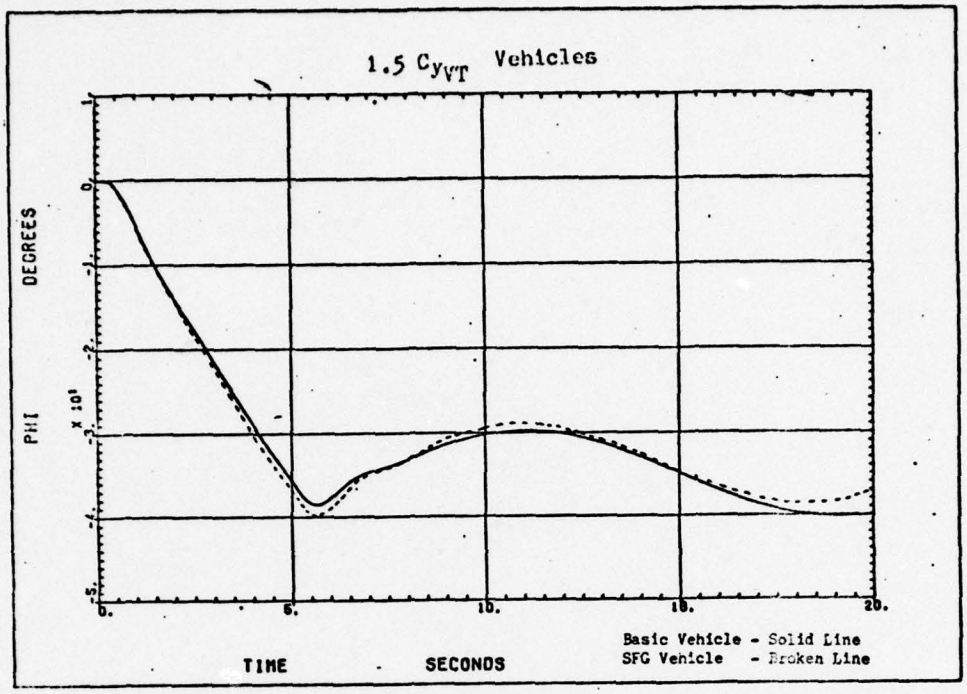

Figure C30. Roll Angle Due to 2° Rudder Step (0 to 5 sec)

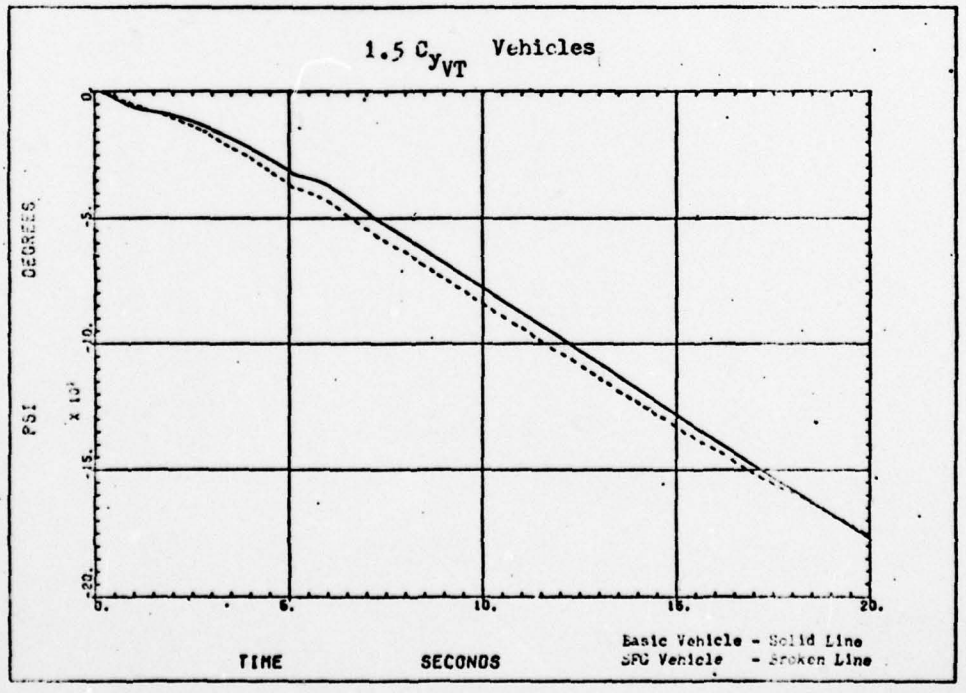

Figure C31. Heading Angle Due to 2° Rudder Step (0 to 5 sec)

BEST AVAILABLE COPY

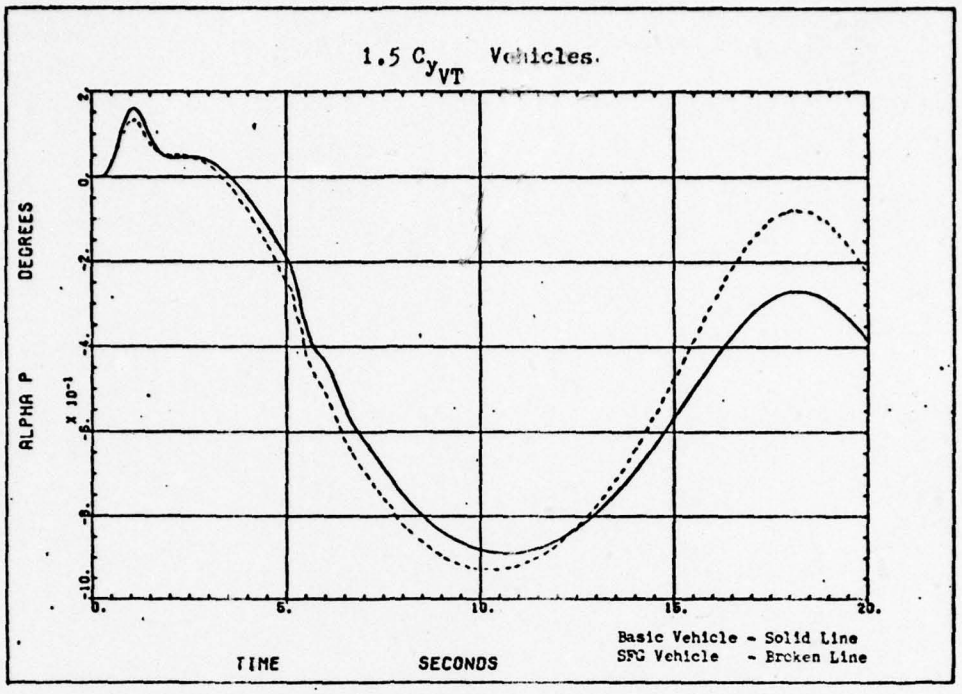

Figure C32. Angle of Attack Due to 2° Rudder Step (0 to 5 sec)

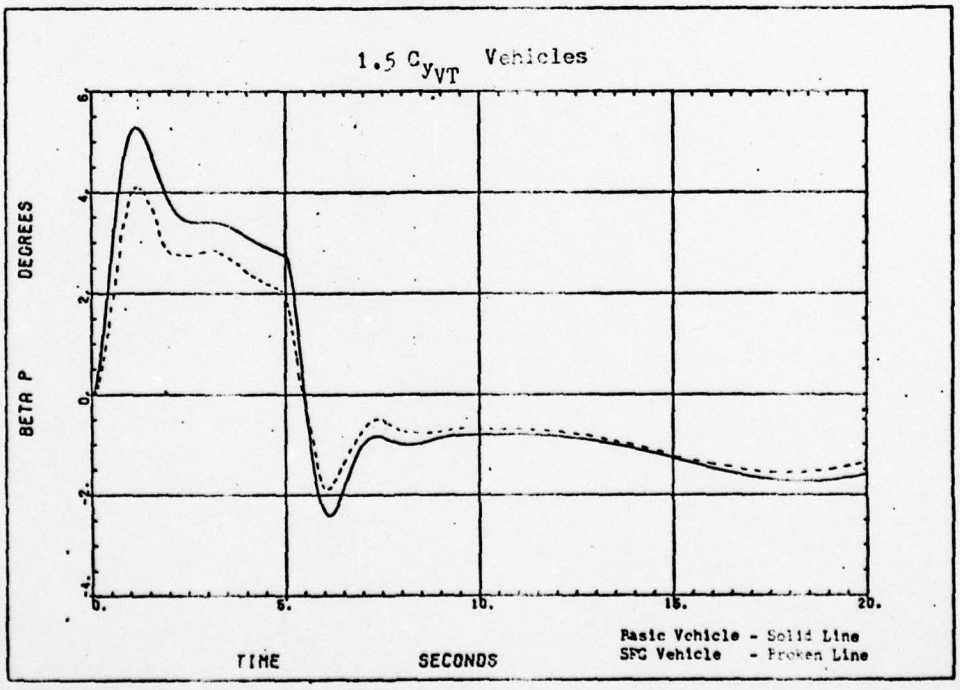

Figure C33. Side Slip Angle Due to 2° Rudder Step (0 to 5 sec)

BEST AVAILABLE COPY

Appendix D.

Time History Plots for Aileron Step Input

This section contains the complete set of time history plots for the baseline and modified vehicles. The 2° aileron step input was initiated at time zero and held for 5 seconds. The following variables are plotted in this order: u, v, w, p, q, r, θ, ϕ, ψ, α, β.

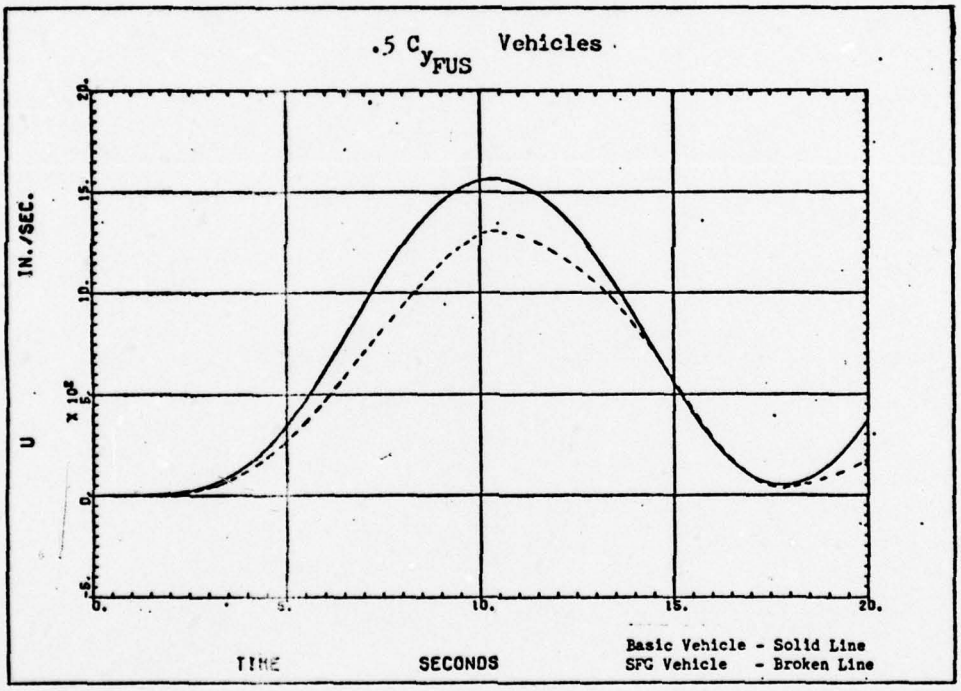

Figure D1. Forward Speed Perturbation Due to 2° Aileron Step (0 to 5 sec).

BEST AVAILABLE COPY

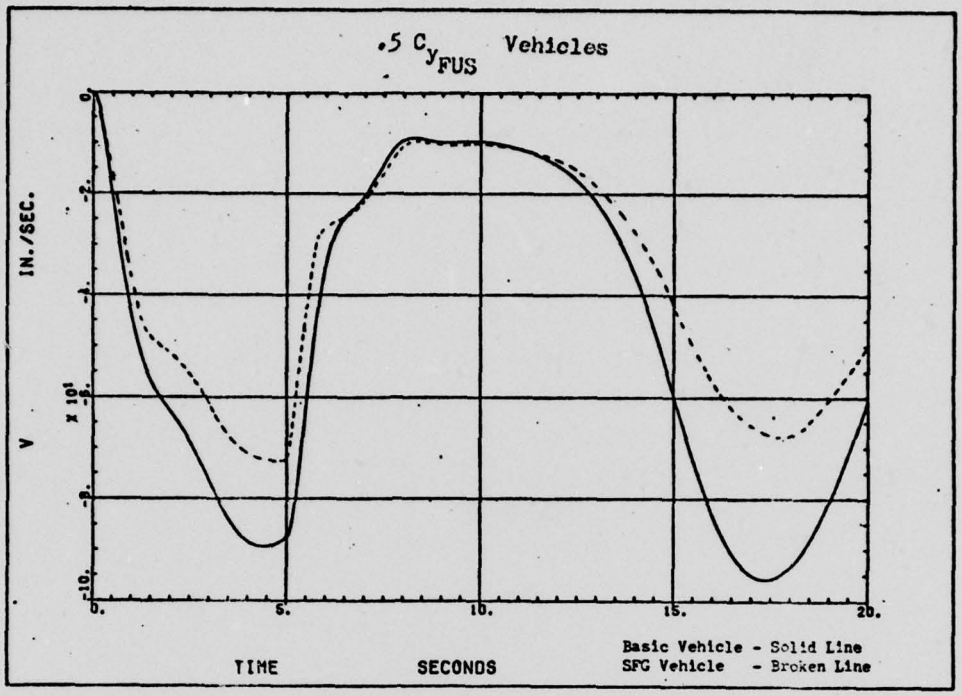

Figure D2. Side Speed Perturbation Due to 2° Aileron Step (0 to 5 sec)

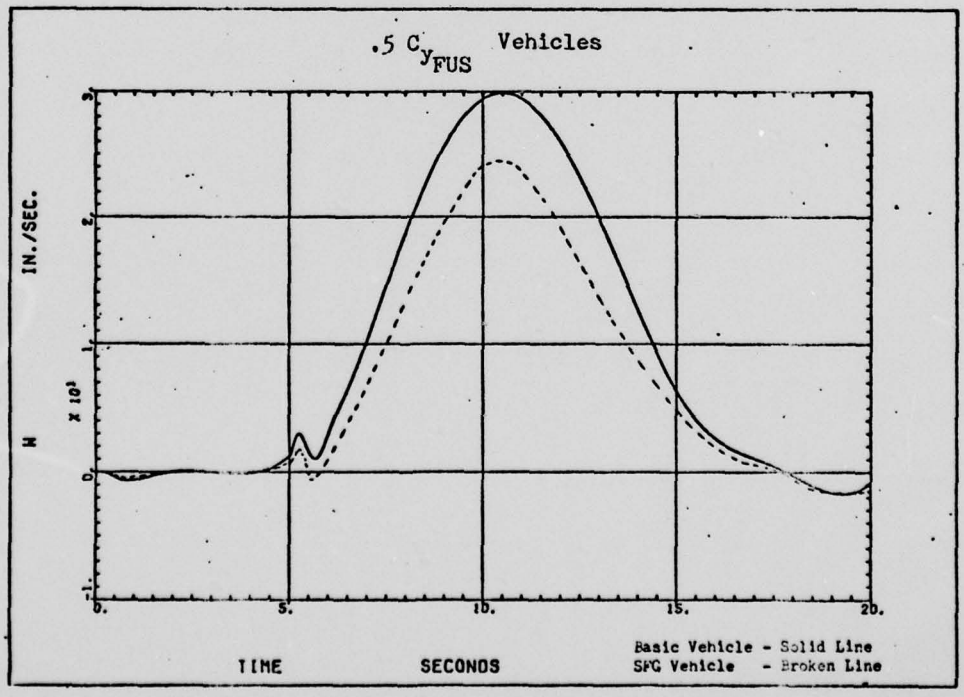

Figure D3. Downward Speed Perturbation Due to 2° Aileron Step (0 to 5 sec)

BEST AVAILABLE COPY

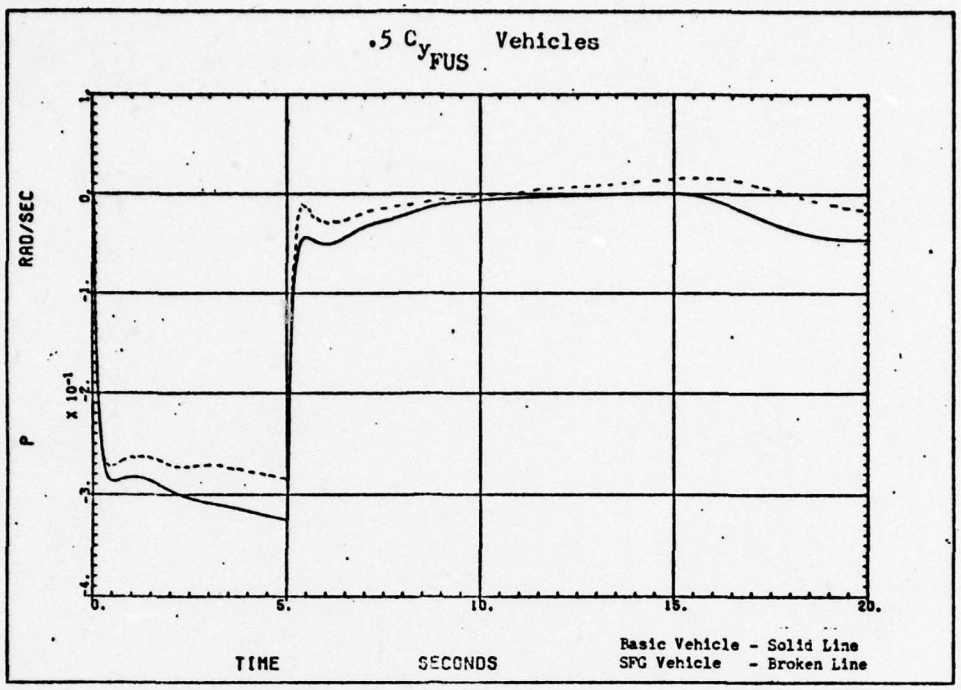

Figure D4. Roll Rate Due to 2° Aileron Step (0 to 5 Sec)

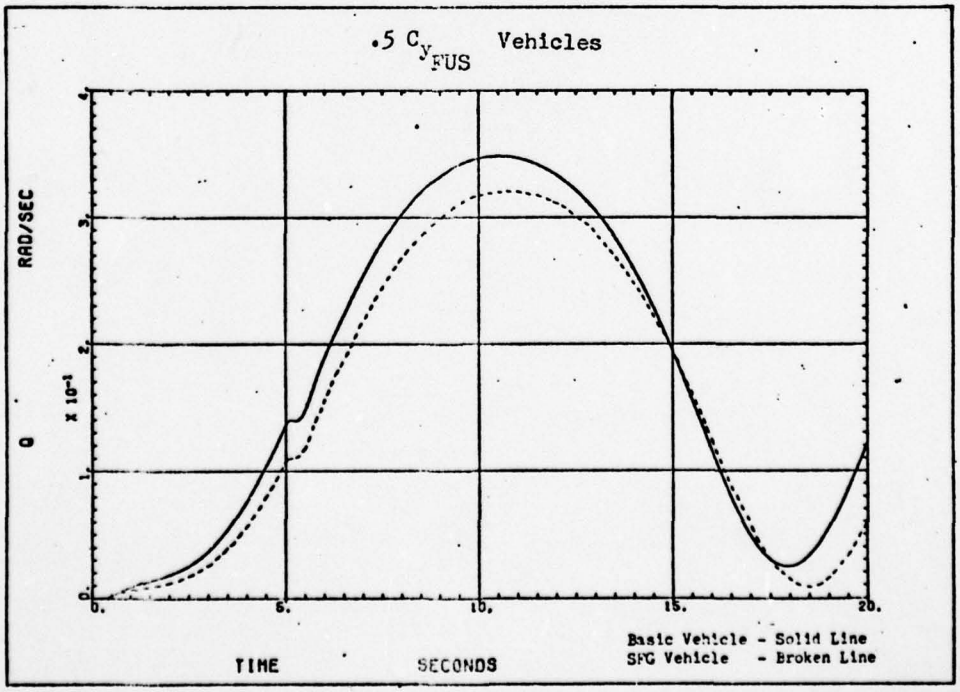

Figure D5. Pitch Rate Due to 2° Aileron Step (0 to 5 sec)

BEST AVAILABLE COPY

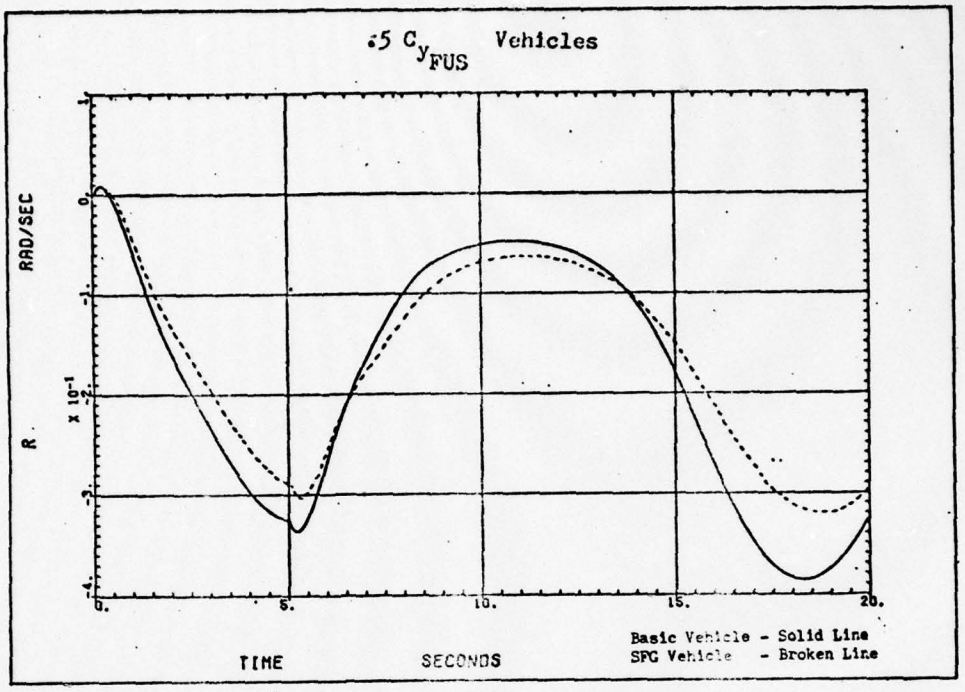

Figure D6. Yaw Rate Due to 2° Aileron Step (0 to 5 sec)

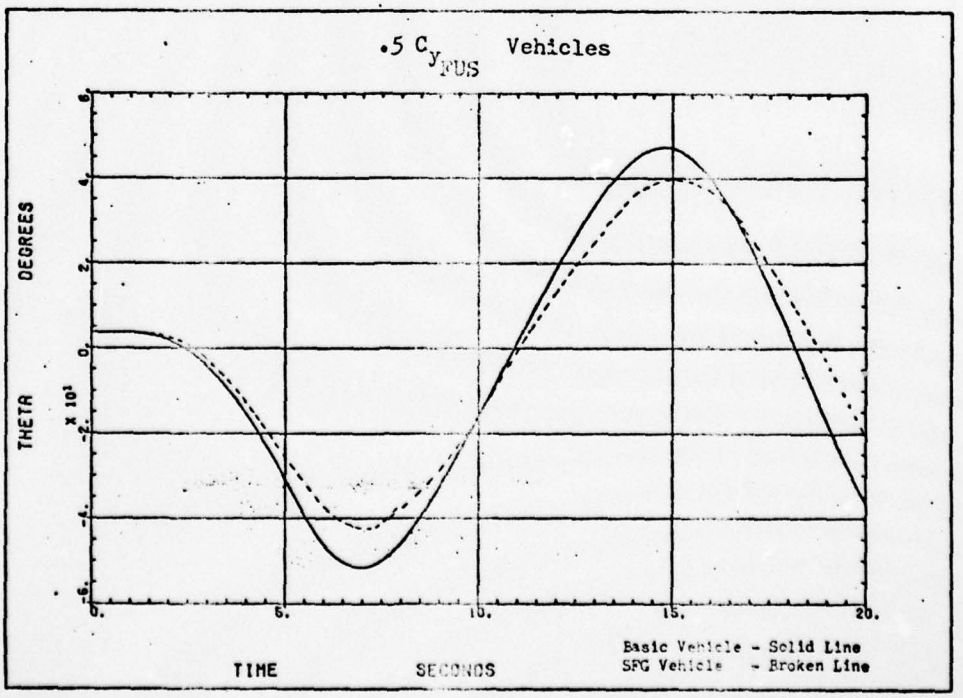

Figure D7. Pitch Angle Due to 2° Aileron Step (0 to 5 sec)

BEST AVAILABLE COPY

AD-A048 901 AIR FORCE INST OF TECH WRIGHT-PATTERSON AFB OHIO SCH--ETC F/G 1/3
DESIGN AND EVALUATION OF A SIDE FORCE GENERATOR MODIFICATION FO--ETC(U)
DEC 77 G R LEIMBACH

UNCLASSIFIED AFIT/GAE/AA/77D-7 NL

2 OF 2
AD A048901

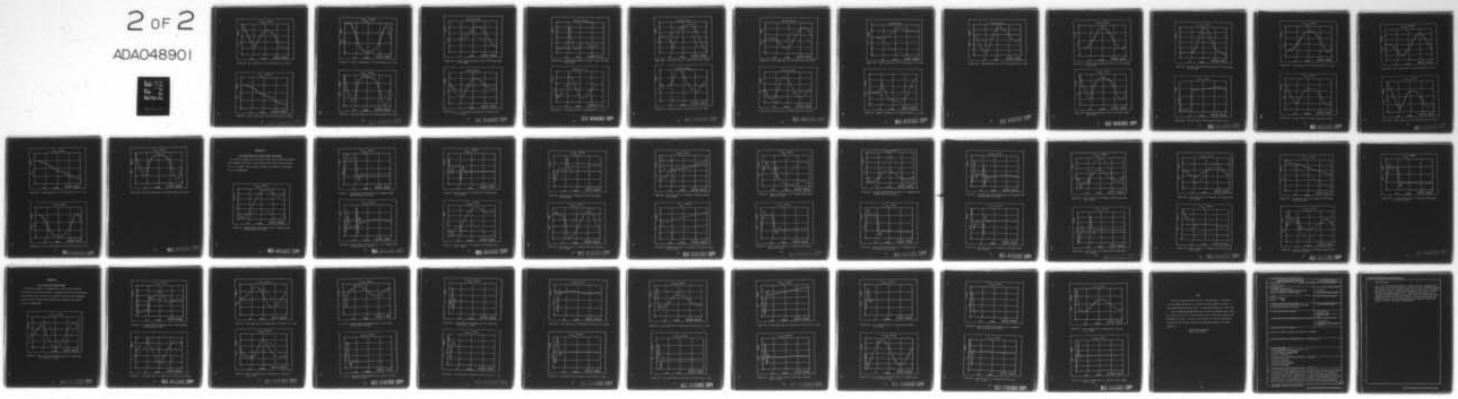

END
DATE FILMED
2-78
DDC

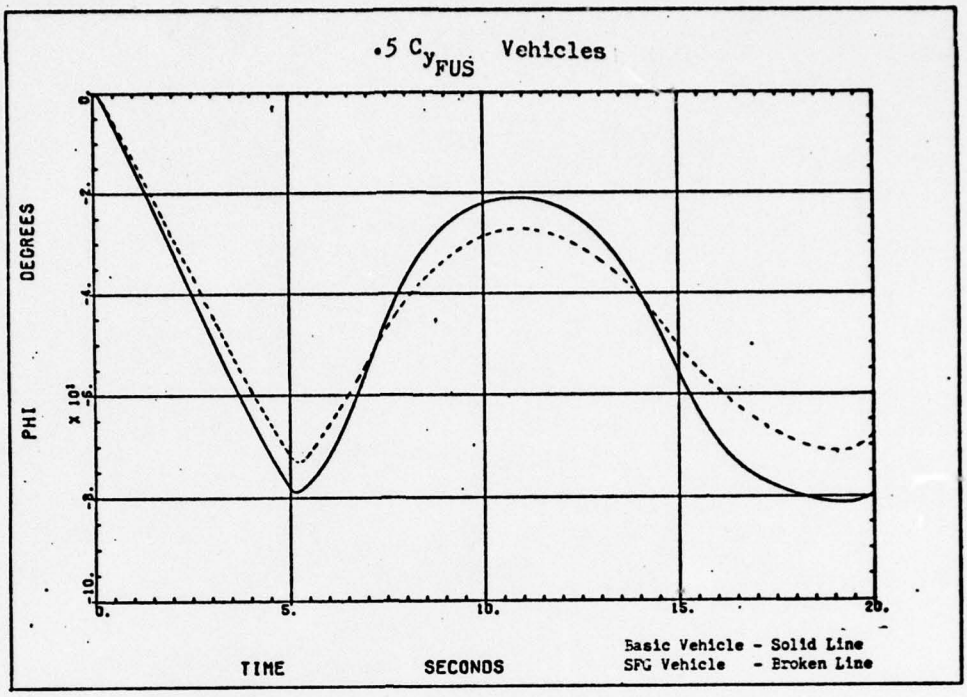

Figure D8. Roll Angle Due to 2° Aileron Step (0 to 5 sec)

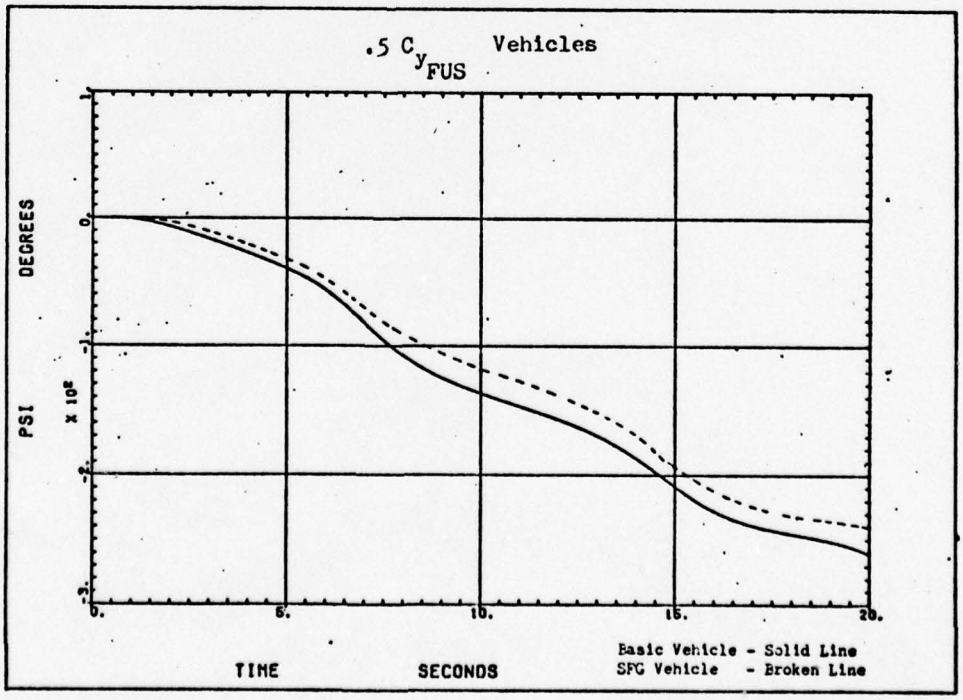

Figure D9. Heading Angle Due to 2° Aileron Step (0 to 5 sec)

BEST AVAILABLE COPY

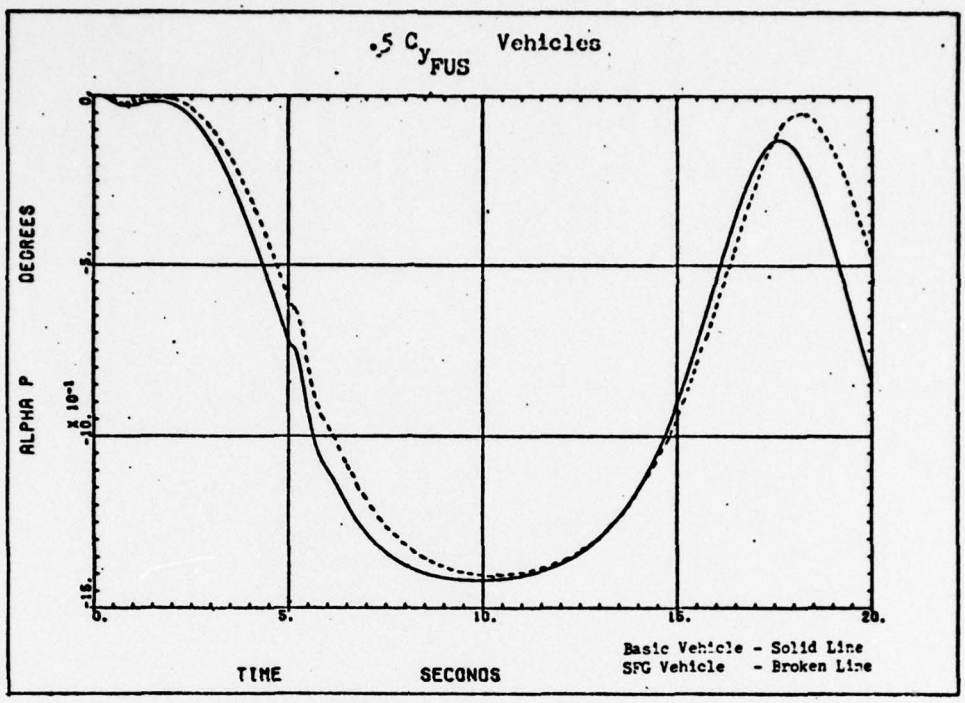

Figure D10. Angle of Attack Due to 2° Aileron Step (0 to 5 sec)

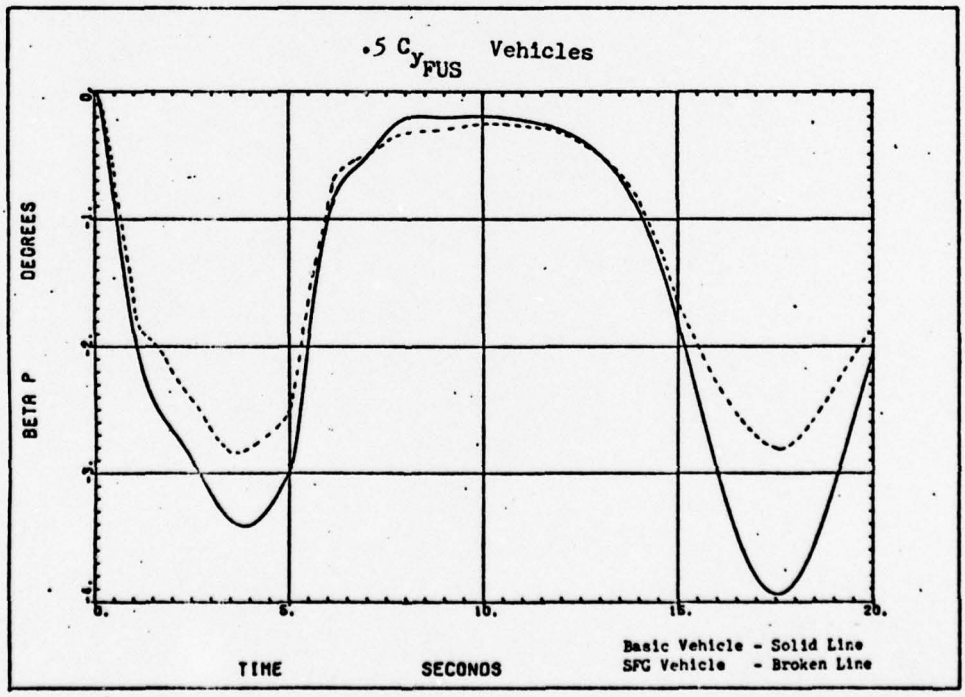

Figure D11. Side Slip Angle Due to 2° Aileron Step (0 to 5 sec)

BEST AVAILABLE COPY

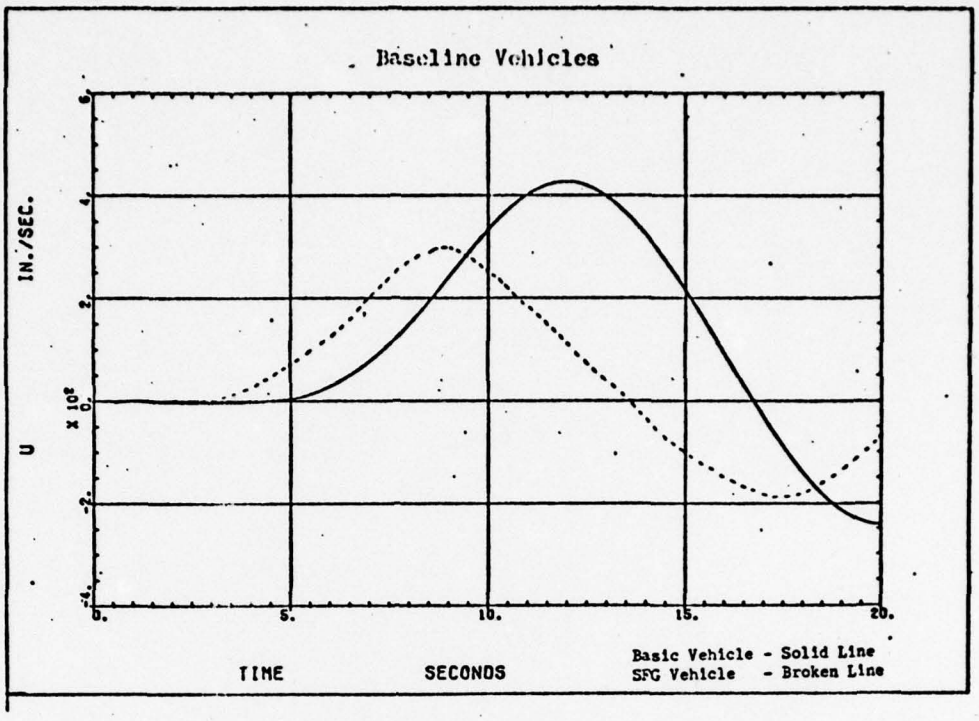

Figure D12. Forward Speed Perturbation Due to 2°Aileron Step (0 to 5 sec)

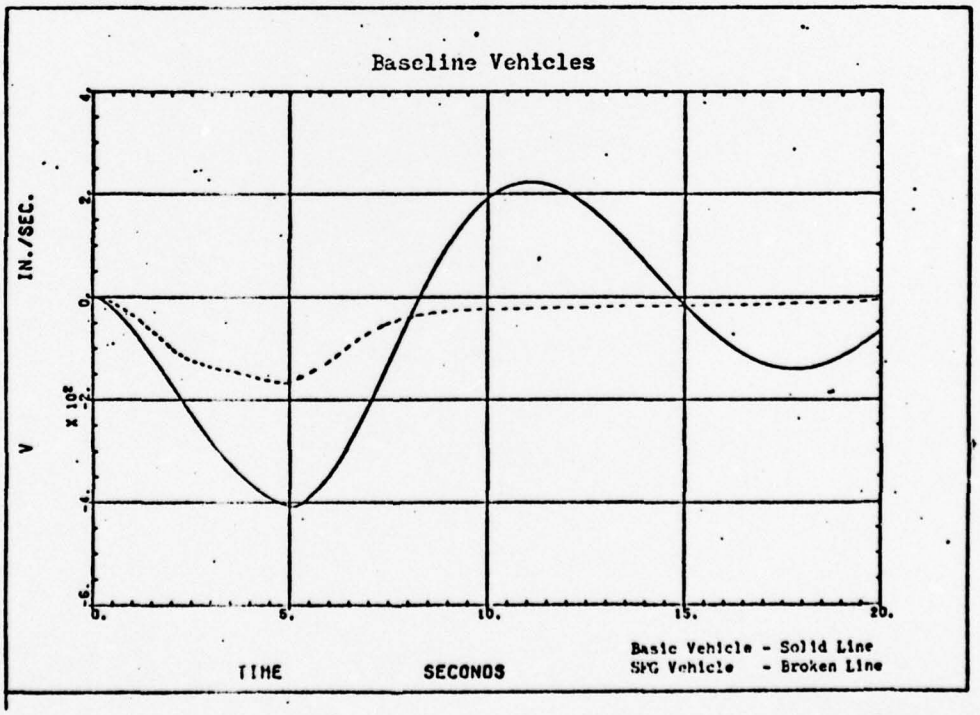

Figure D13. Side Speed Perturbation Due to 2° Aileron Step (0 to 5 sec)

BEST AVAILABLE COPY

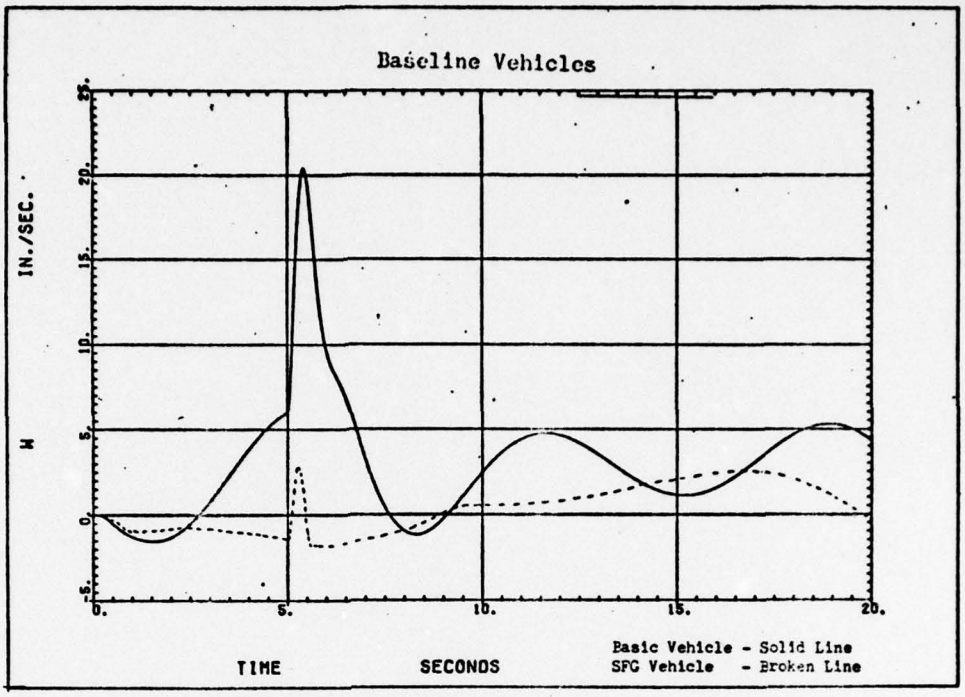

Figure D14. Downward Speed Perturbation Due to 2° Aileron Step (0 to 5 sec)

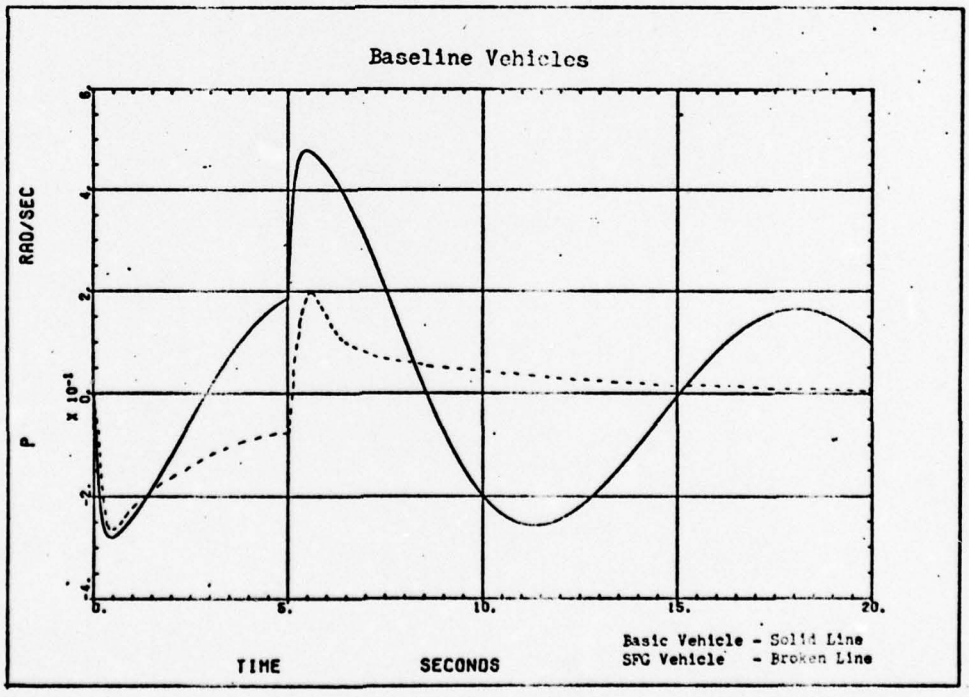

Figure D15. Roll Rate Due to 2° Aileron Step (0 to 5 sec)

BEST AVAILABLE COPY

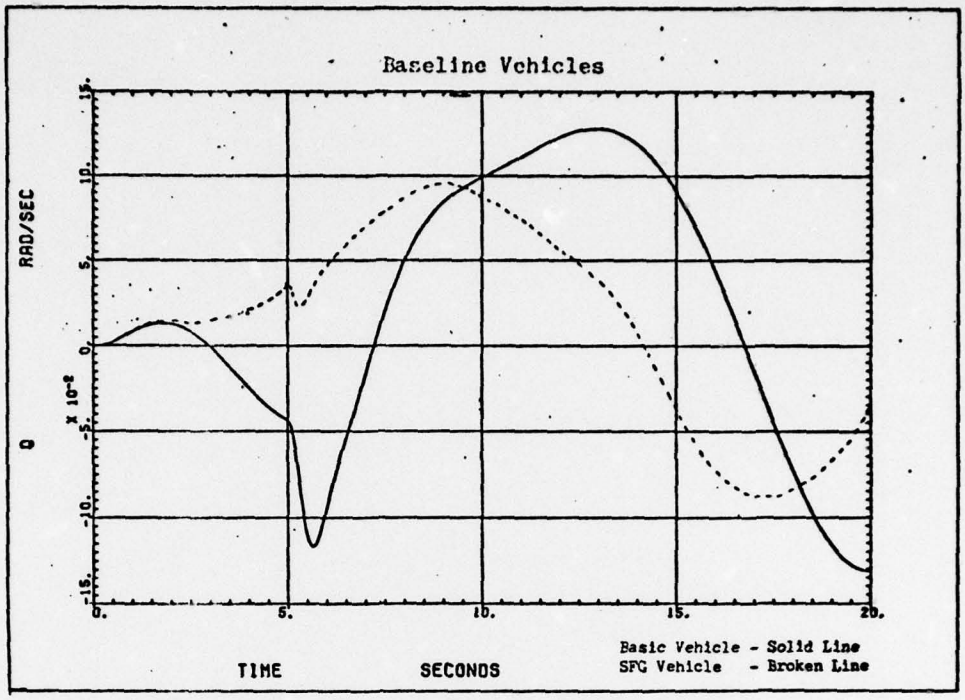

Figure D16. Pitch Rate Due to 2° Aileron Step (0 to 5 sec)

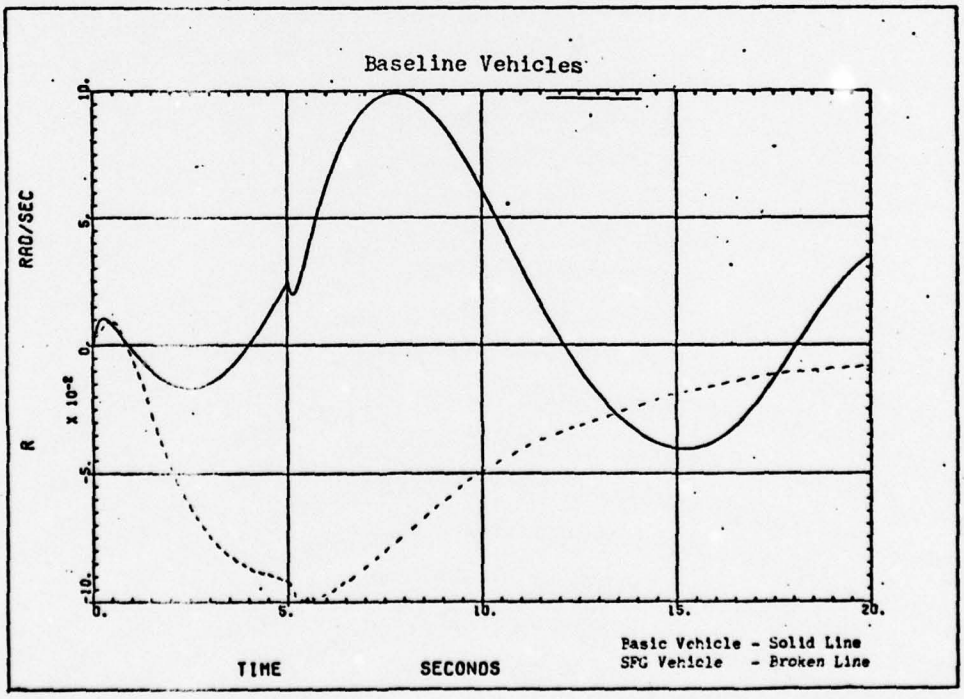

Figure D17, Yaw Rate Due to 2° Aileron Step (0 to 5 sec)

BEST AVAILABLE COPY

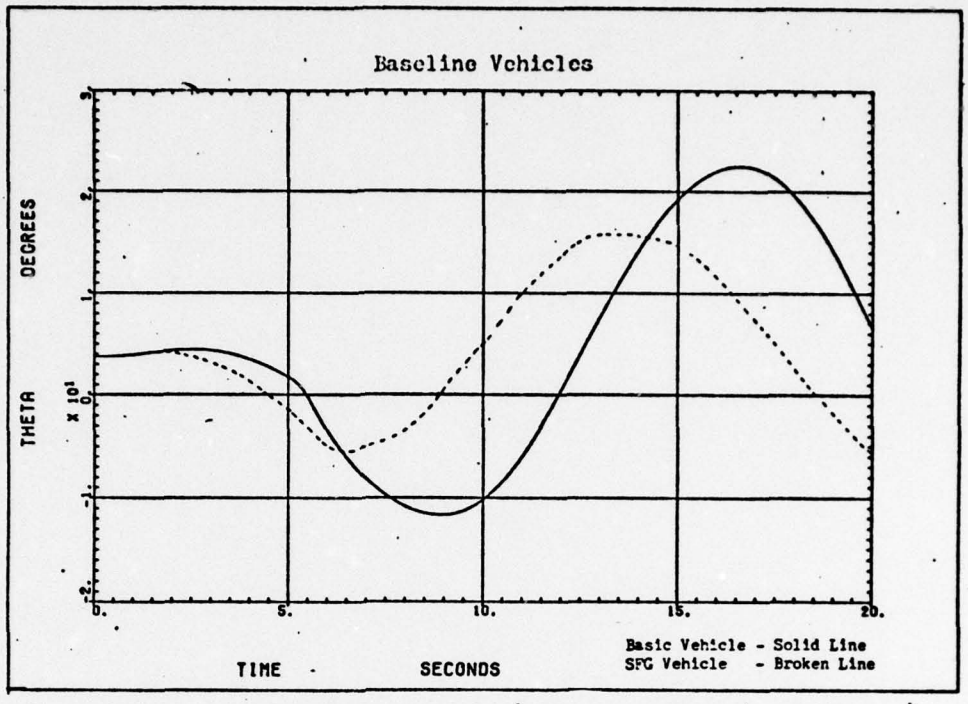

Figure D18. Pitch Angle Due to 2° Aileron Step (0 to 5 sec)

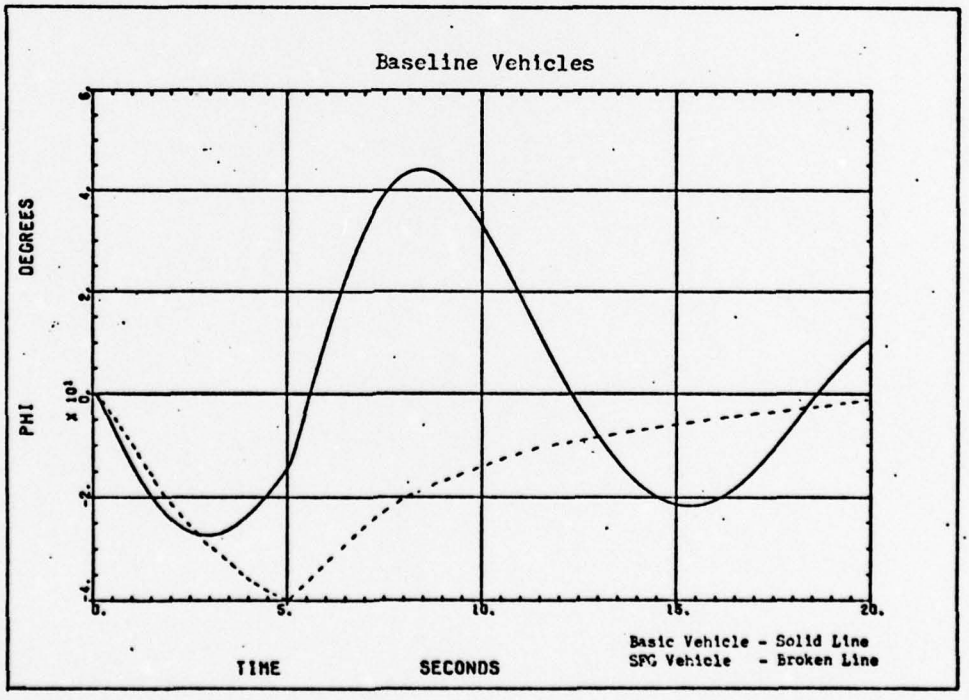

Figure D19. Roll Angle Due to 2°Aileron Step (0 to 5 sec)

BEST AVAILABLE COPY

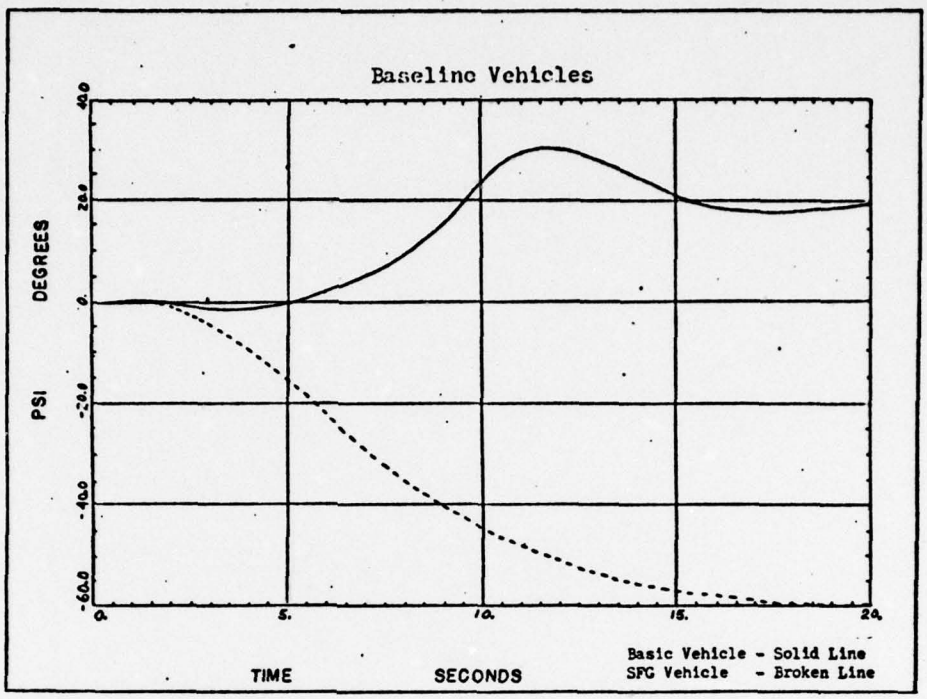

Figure D20. Heading Angle Due to 2° Aileron Step (0 to 5 sec)

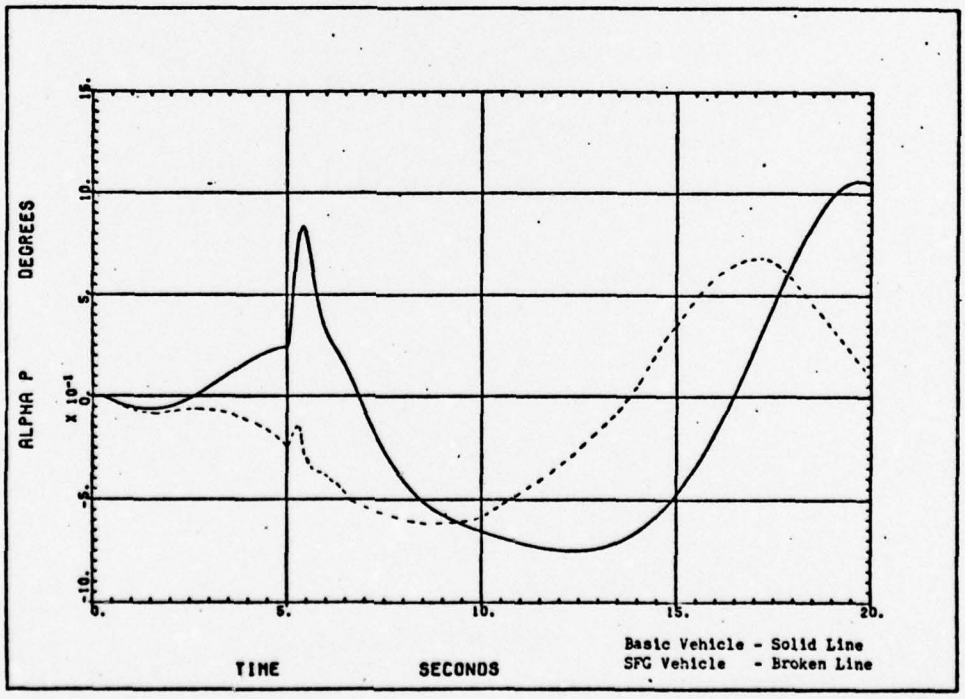

Figure D21. Angle of Attack Due to 2° Aileron Step (0 to 5 sec)

BEST AVAILABLE COPY

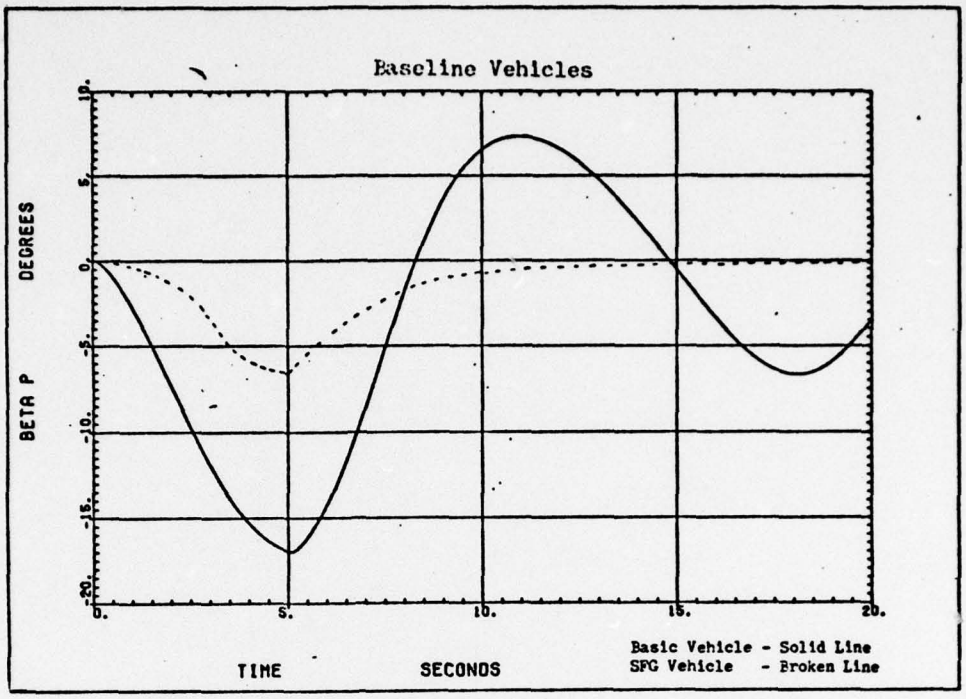

Figure D22. Side Slip Angle Due to 2^{o} Aileron Step (0 to 5 sec)

BEST AVAILABLE COPY

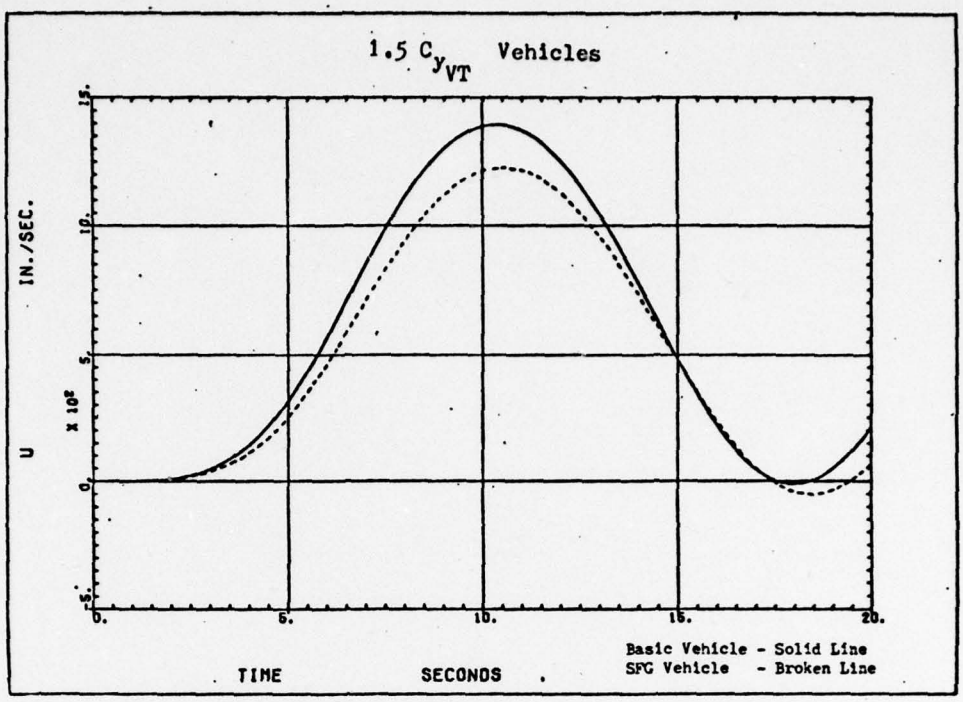

Figure D23. Forward Speed Perturbation Due to 2° Aileron Step (0 to 5 sec)

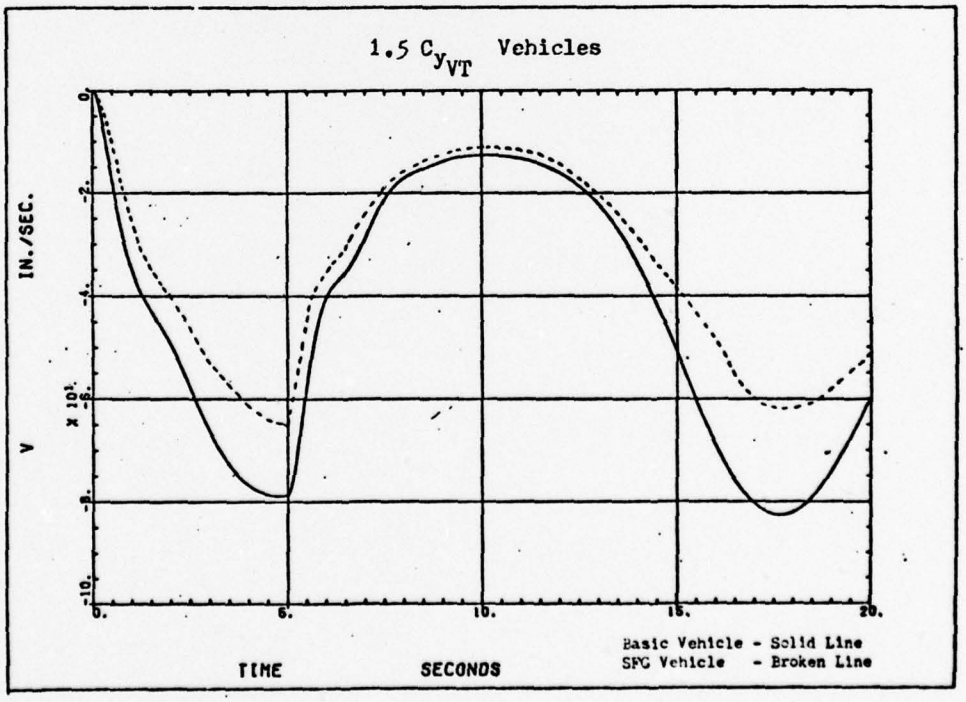

Figure D24. Side Speed Perturbation Due to 2° Aileron Step (0 to 5 sec)

BEST AVAILABLE COPY

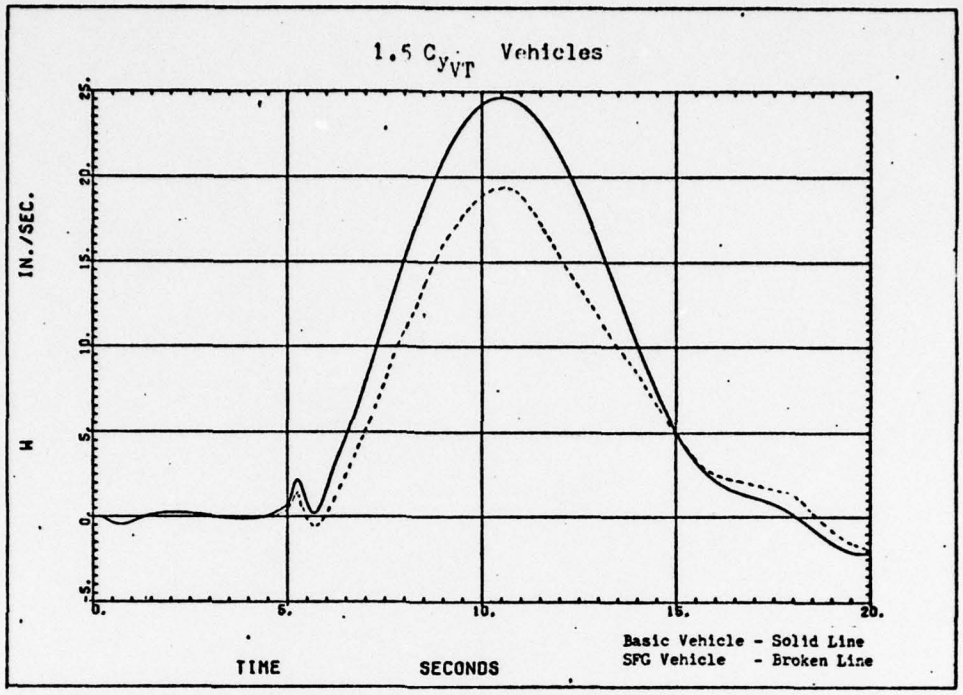

Figure D25. Downward Speed Perturbation Due to 2° Aileron Step (0 to 5 sec)

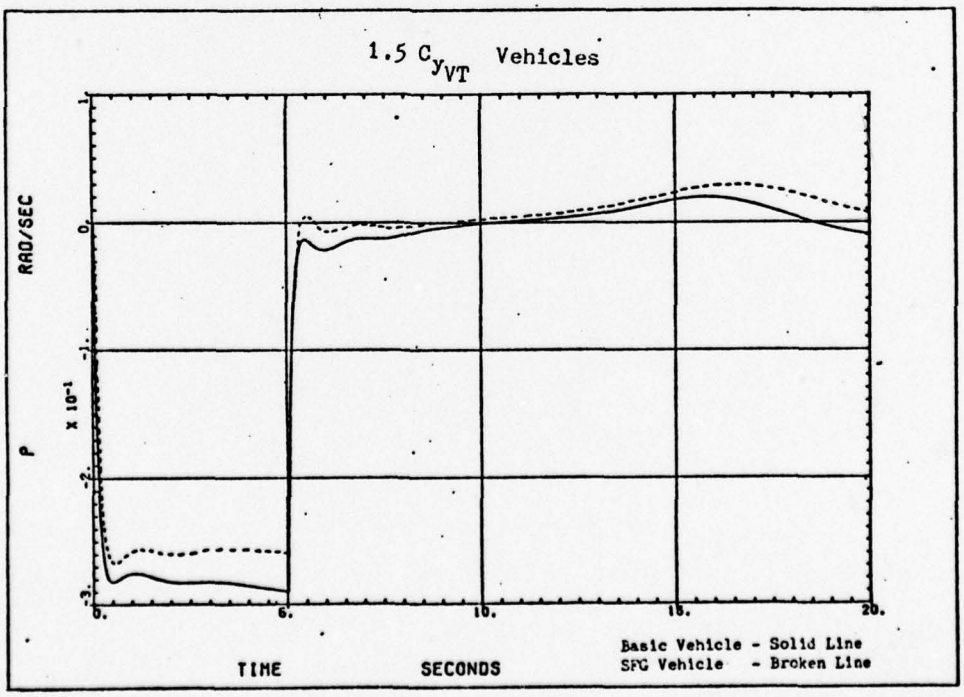

Figure D26, Roll Rate Due to 2° Aileron Step (0 to 5 sec)

BEST AVAILABLE COPY

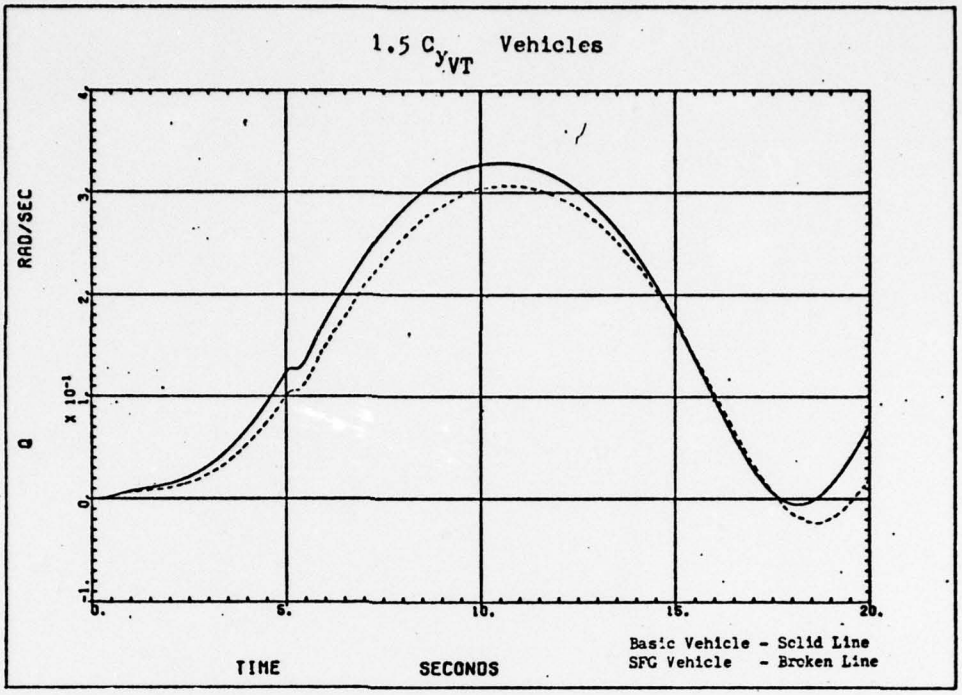

Figure D27. Pitch Rate Due to 2° Aileron Step (0 to 5 sec)

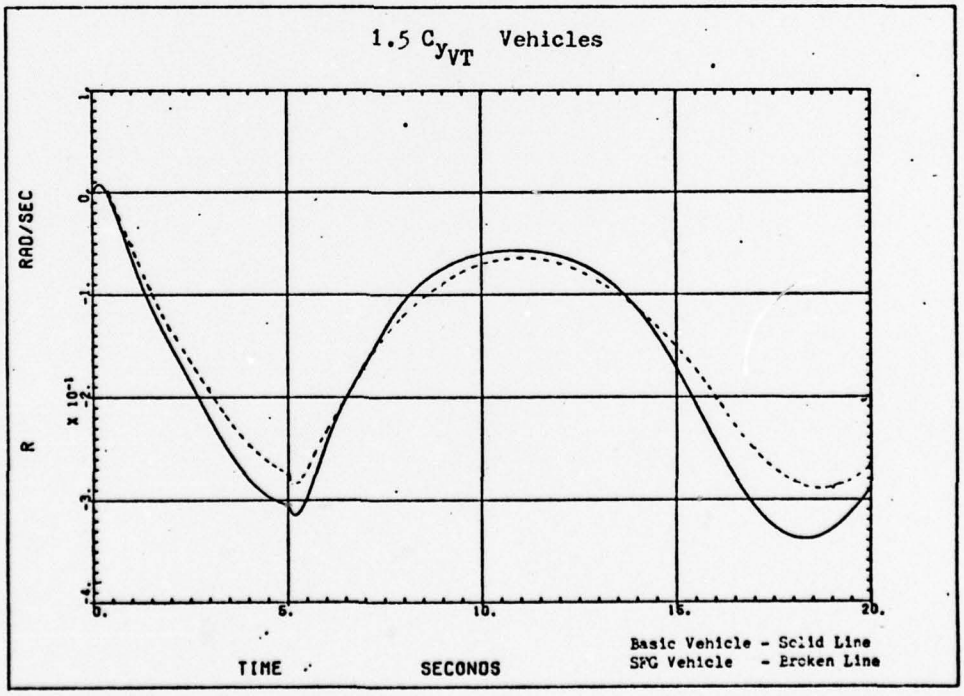

Figure D28. Yaw Rate Due to 2° Aileron Step (0 to 5 sec)

BEST AVAILABLE COPY

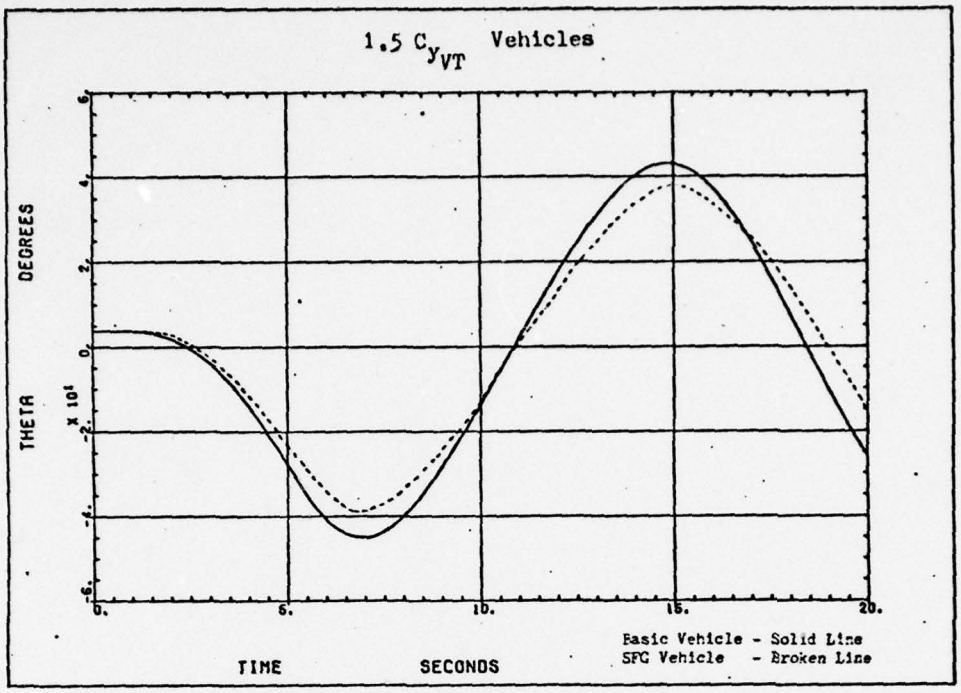

Figure D29. Pitch Angle Due to 2° Aileron Step (0 to 5 sec)

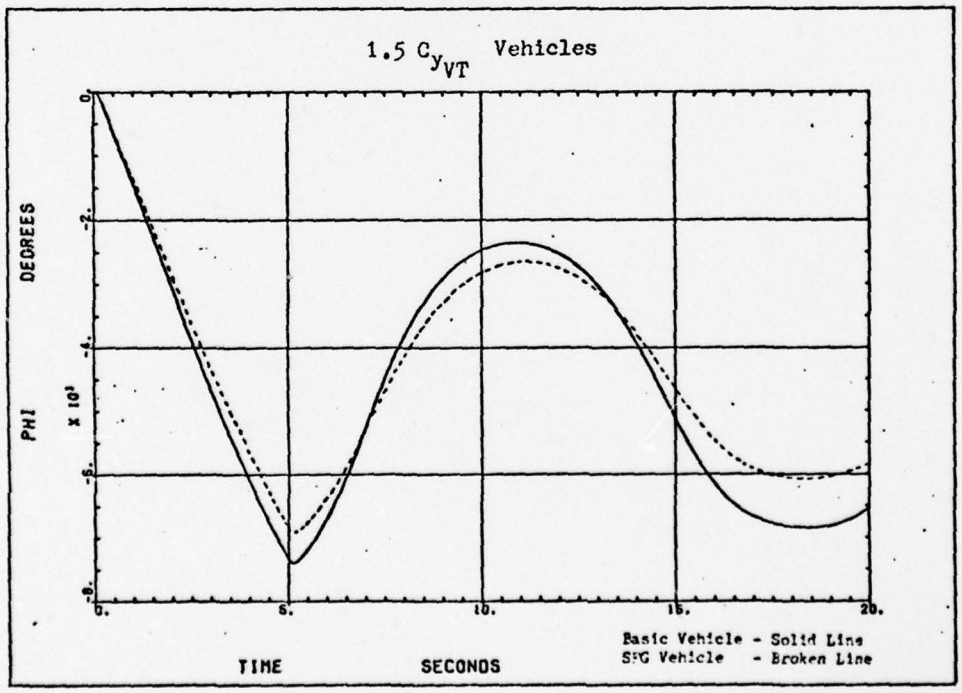

Figure D30. Roll Angle Due to 2° Aileron Step (0 to 5 sec)

BEST AVAILABLE COPY

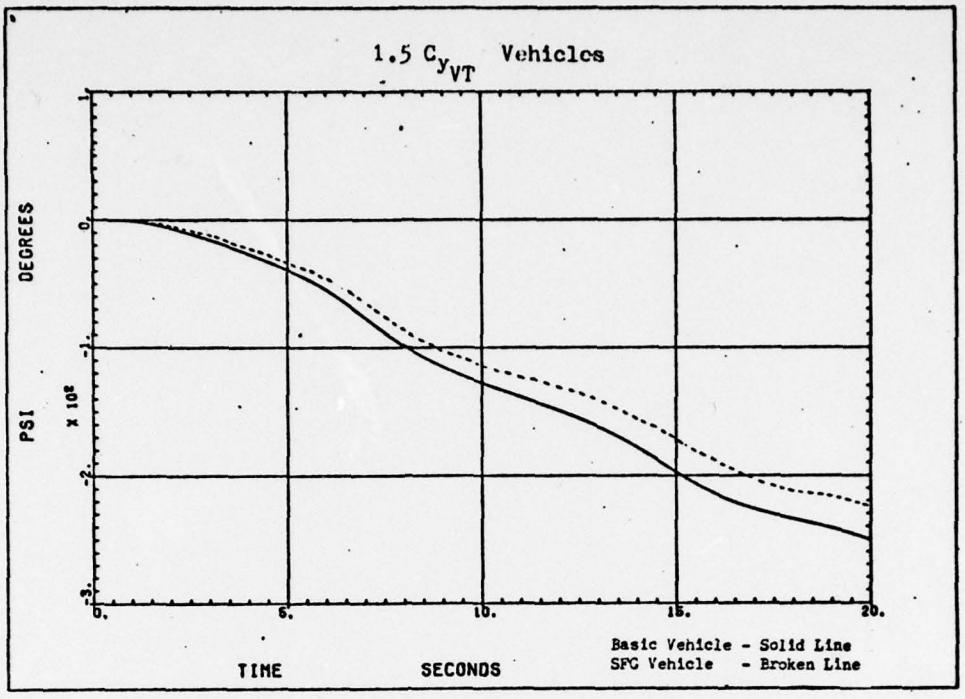

Figure D31. Heading Angle Due to 2° Aileron Step (0 to 5 sec)

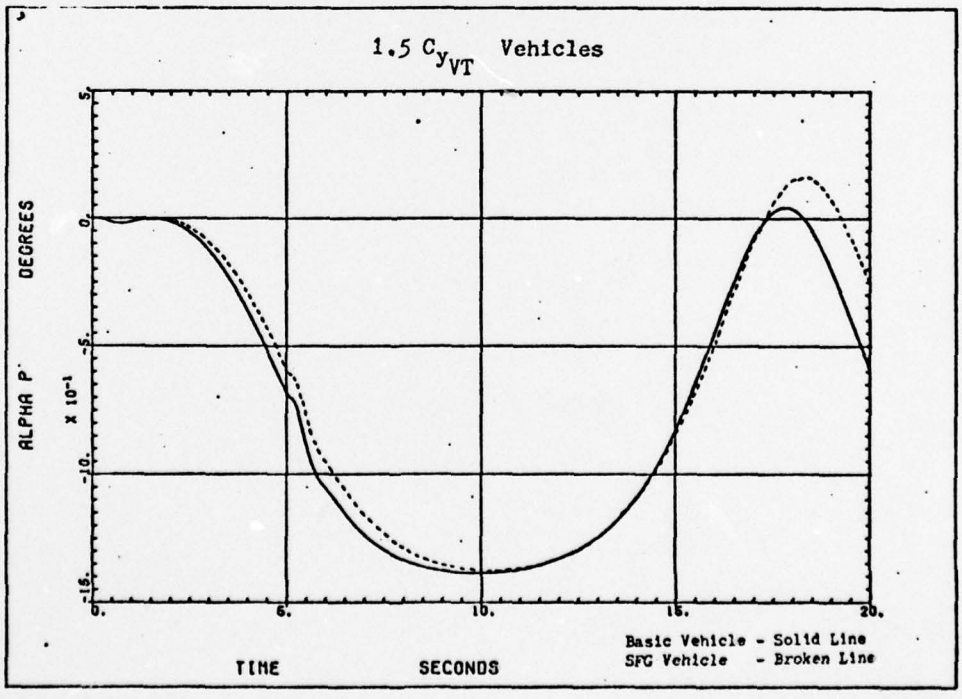

Figure D32. Angle of Attack Due to 2° Aileron Step (0 to 5 sec)

BEST AVAILABLE COPY

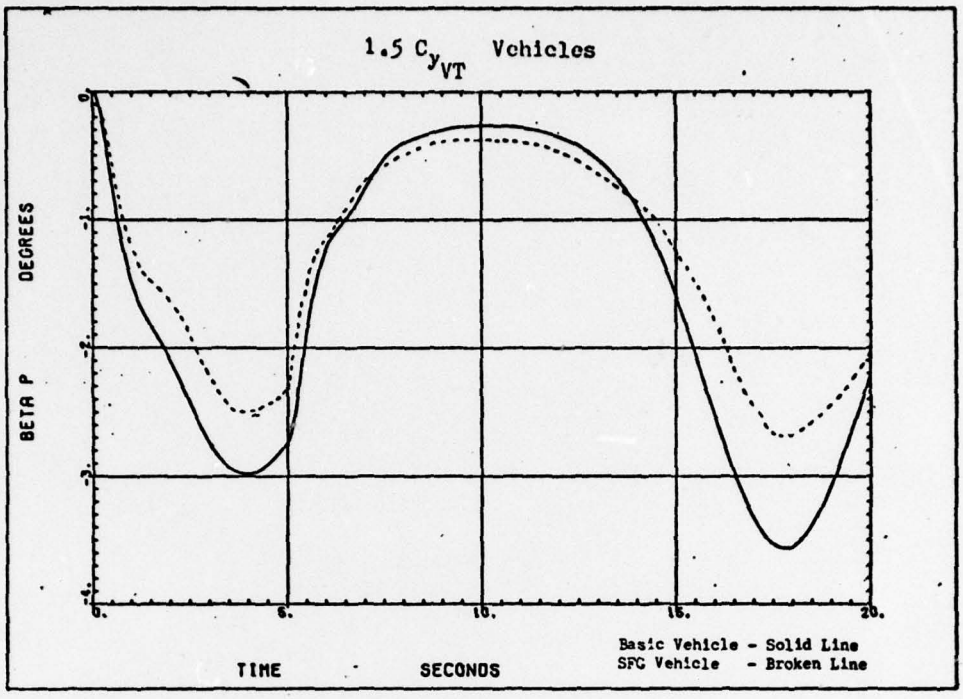

Figure D33. Side Slip Angle Due to 2° Aileron Step (0 to 5 sec)

BEST AVAILABLE COPY

Appendix E

Time History Plots for Cross Control Step Input

This section contains the time history plots for the modified vehicles. The 4° Rudder/-1.68° Aileron step input was initiated at time zero and held for 5 seconds. The following variables are plotted in this order: $u, v, w, p, q, r, \theta, \phi, \psi, \alpha, \beta$.

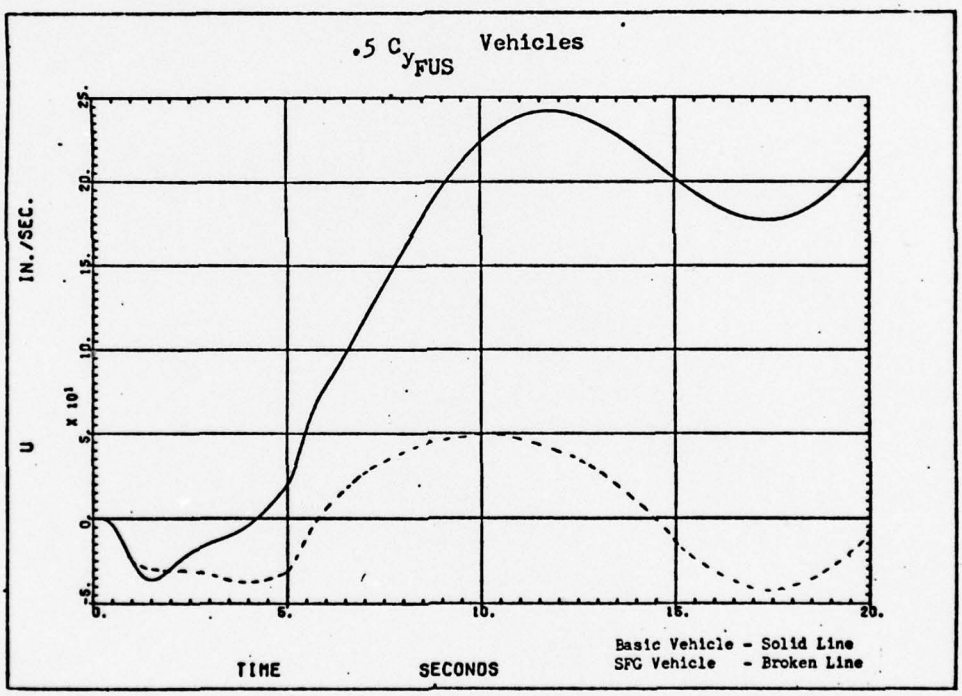

Figure E1. Forward Speed Perturbation Due to 4° Rudder/-1.68° Aileron Step (0 to 5 sec)

BEST AVAILABLE COPY

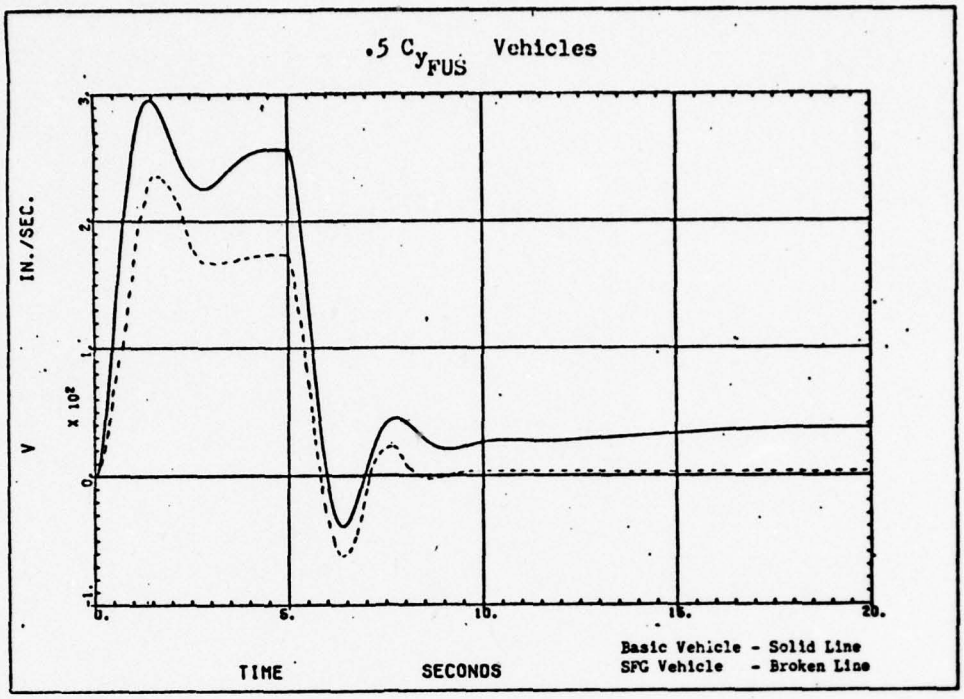

Figure E2. Side Speed Perturbation Due to 4° Rudder/-1.68° Aileron Step (0 to 5 sec)

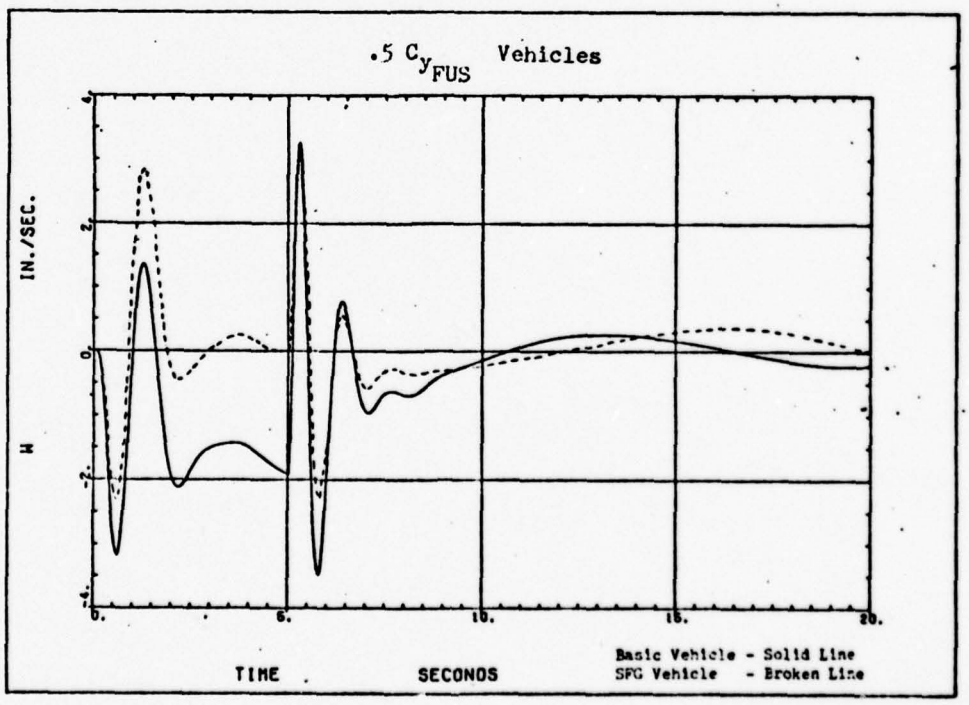

Figure E3. Downward Speed Perturbation Due to 4° Rudder/-1.68° Aileron Step (0 to 5 sec)

BEST AVAILABLE COPY

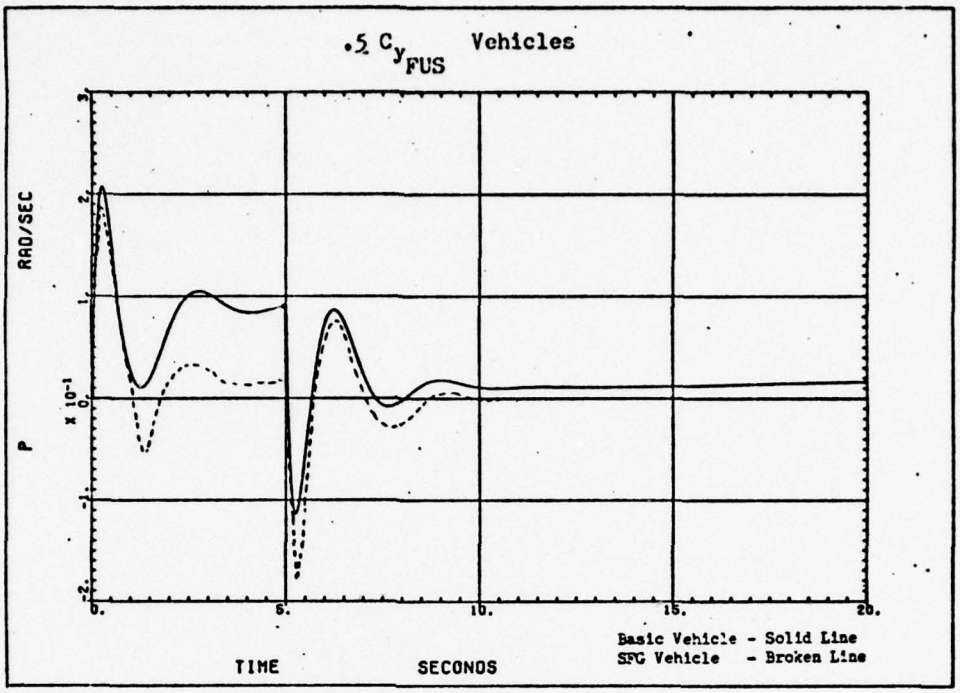

Figure E4. Roll Rate Due to 4° Rudder/-1.68° Aileron Step (0 to 5 sec)

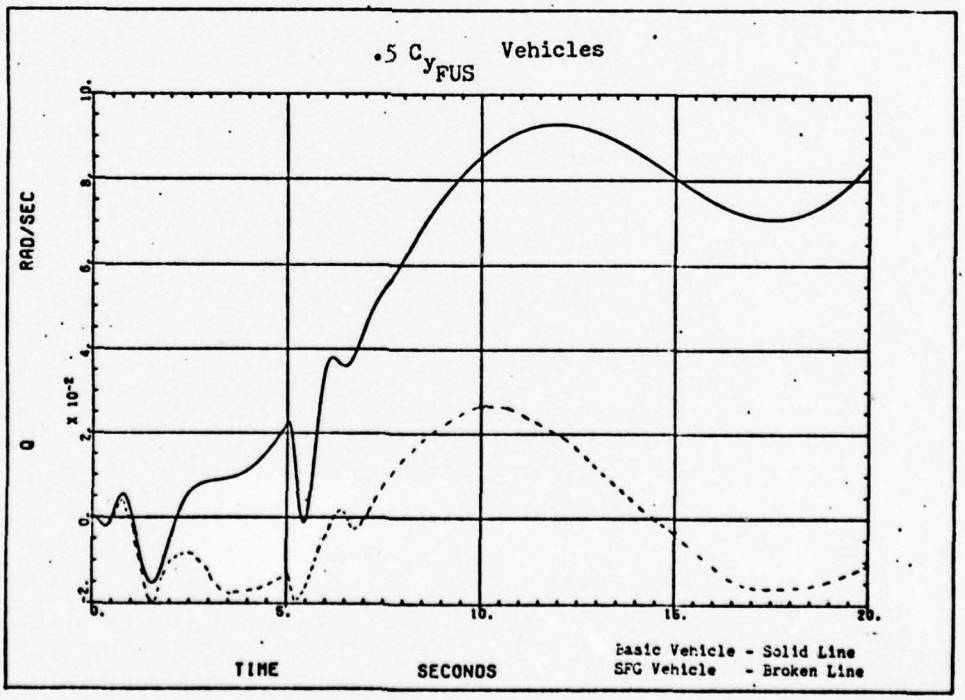

Figure E5. Pitch Rate Due to 4° Rudder/-1.68° Aileron Step (0 to 5 sec)

BEST AVAILABLE COPY

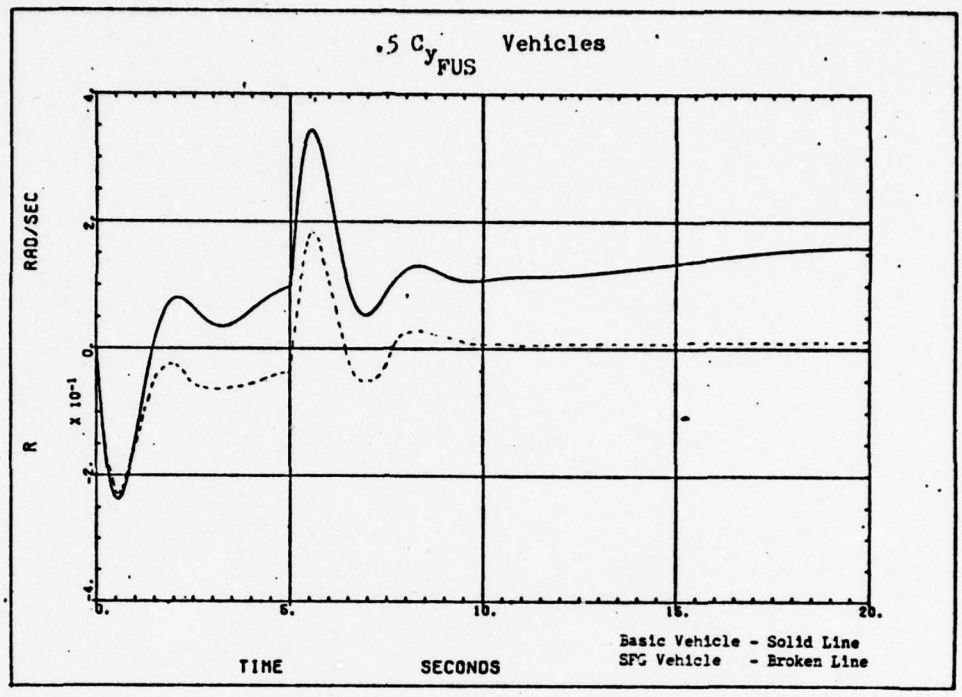

Figure E6. Yaw Rate Due to 4° Rudder/-1.68° Aileron Step (0 to 5 sec)

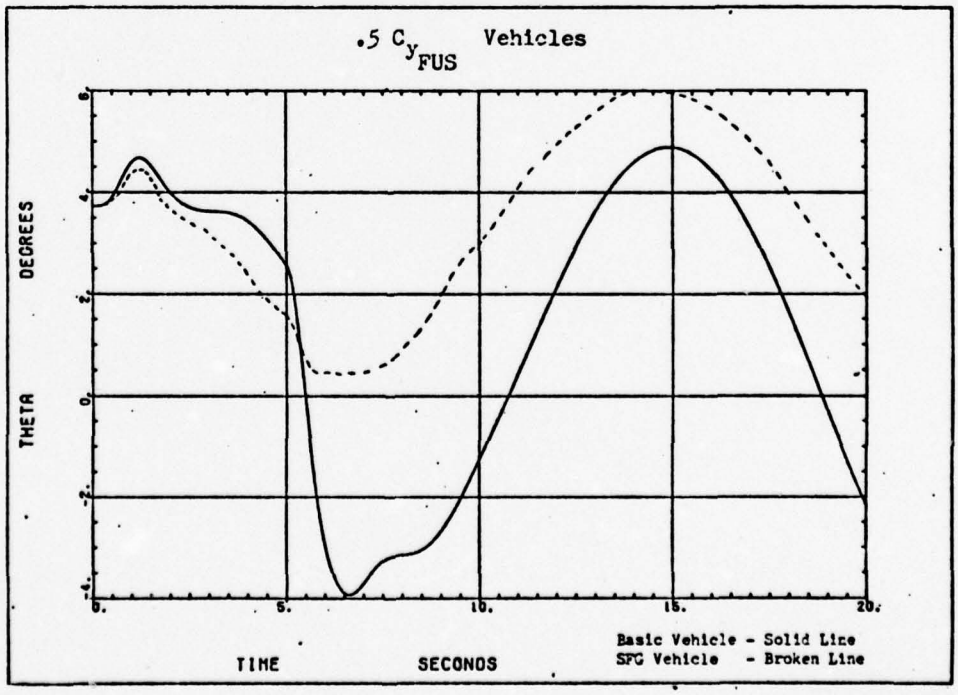

Figure E7. Pitch Angle Due to 4° Rudder/-1.68° Aileron Step (0 to 5 sec)

BEST AVAILABLE COPY

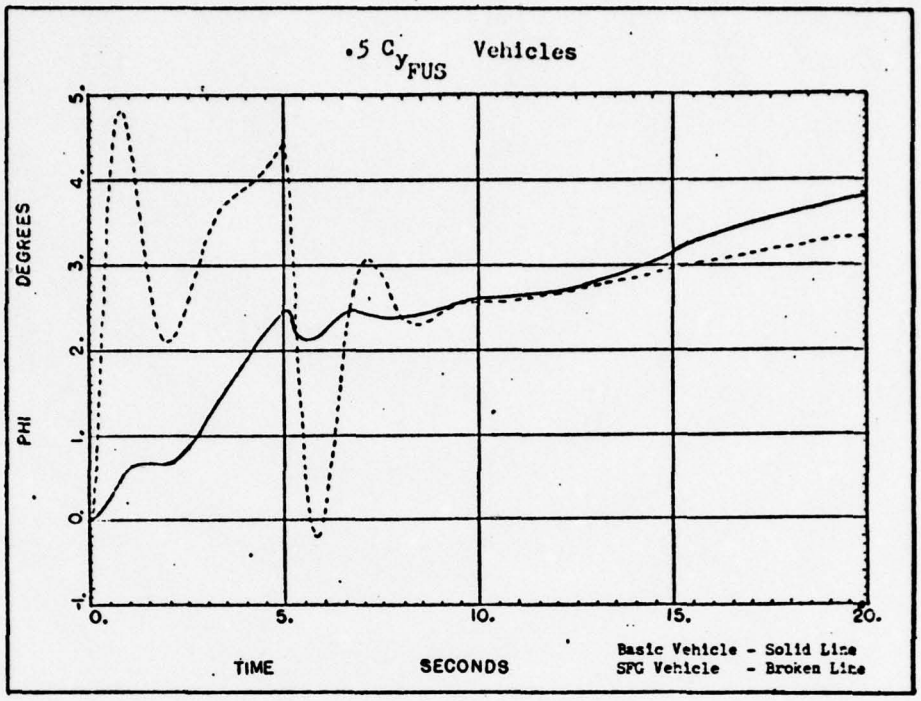

Figure E8. Roll Angle Due to 4° Rudder/-1.68° Aileron Step (0 to 5 sec)

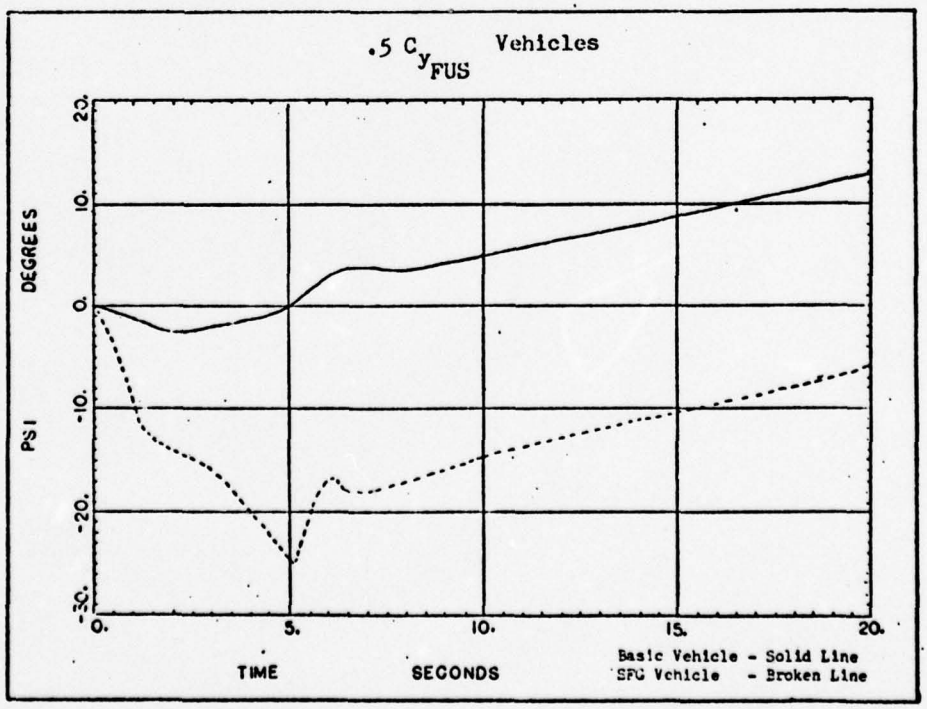

Figure E9. Heading Angle Due to 4° Rudder/-1.68° Aileron Step (0 to 5 sec)

BEST AVAILABLE COPY

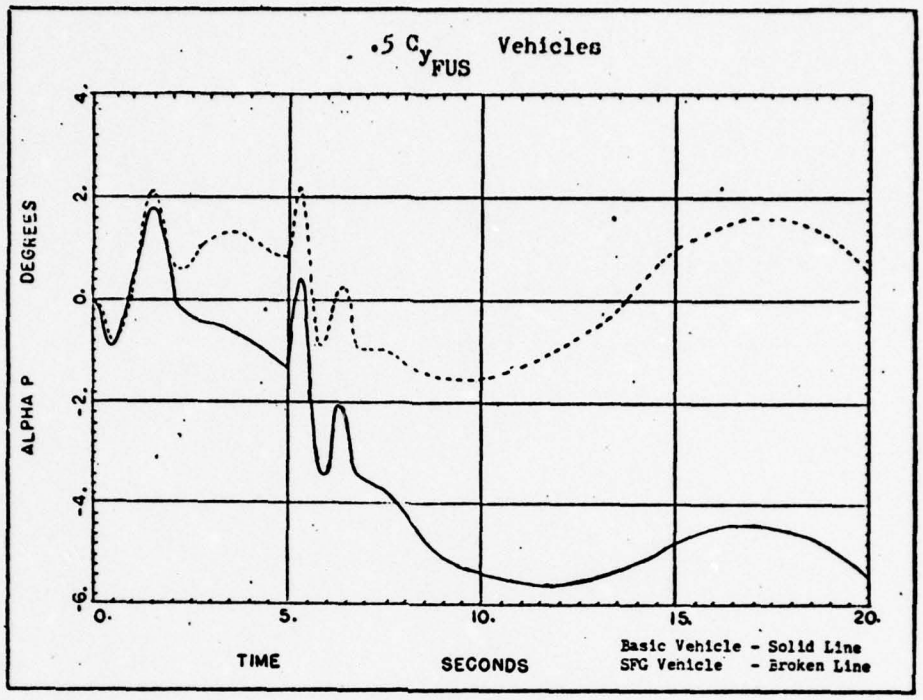

Figure E10. Angle of Attack Due to 4° Rudder/-1.68° Aileron Ste (0 to 5 sec)

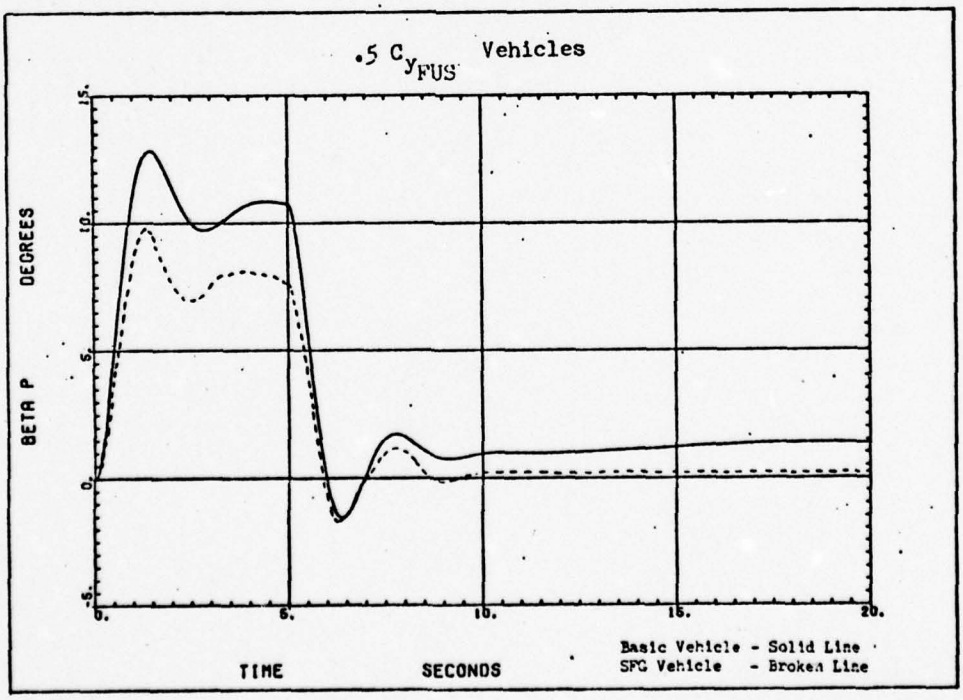

Figure E11. Side Slip Angle Due to 4° Rudder/-1.68° Aileron Step (0 to 5 sec)

BEST AVAILABLE COPY

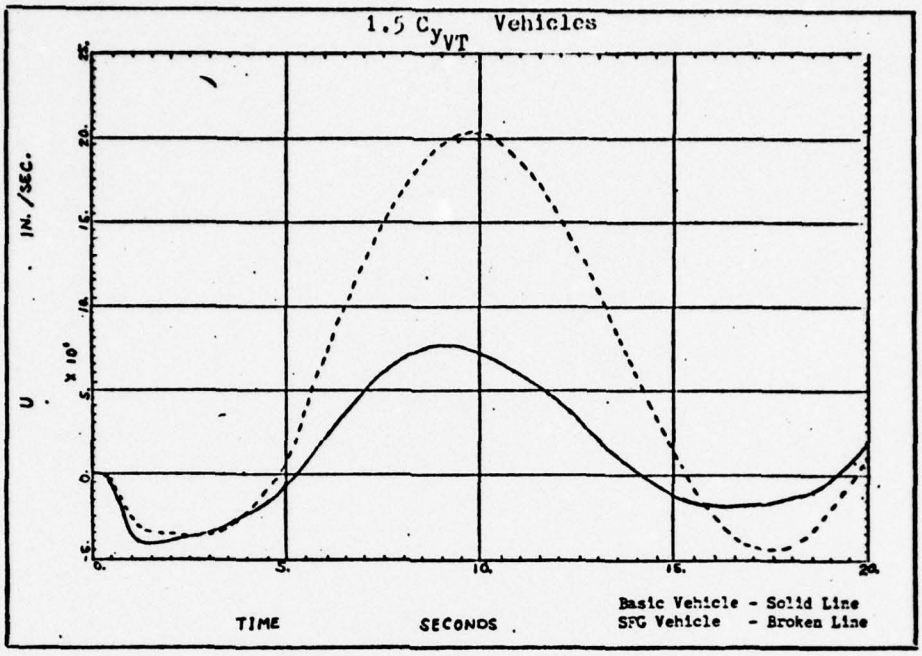

Figure E12. Forward Speed Perturbation Due to 4° Rudder/-1.68° Aileron Step (0 to 5 sec)

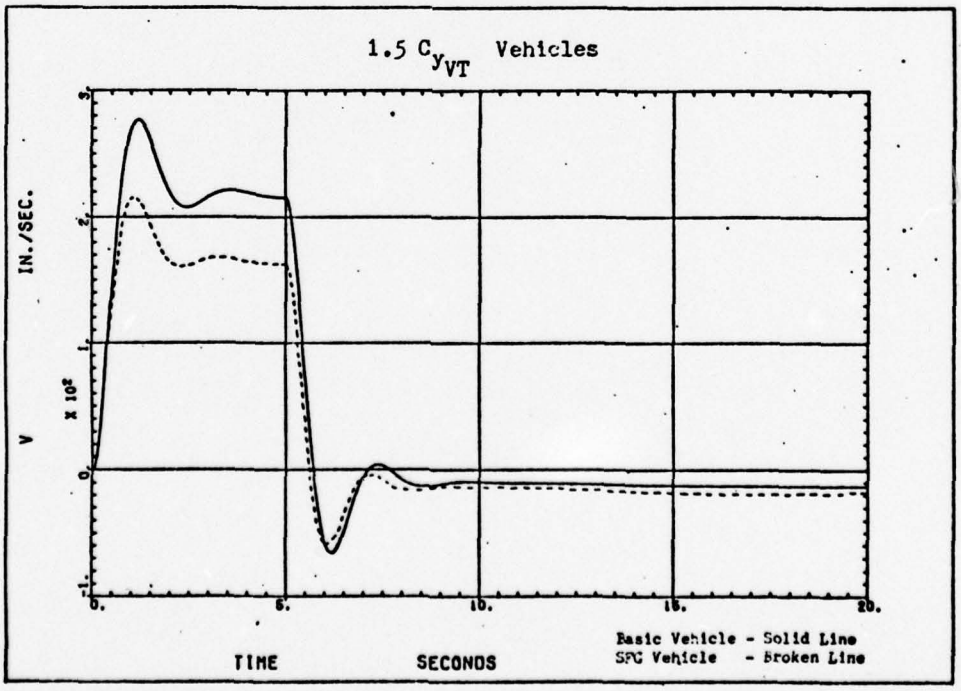

Figure E13. Side Speed Perturbation Due to 4° Rudder/-1.68° Aileron Step (0 to 5 sec)

BEST AVAILABLE COPY

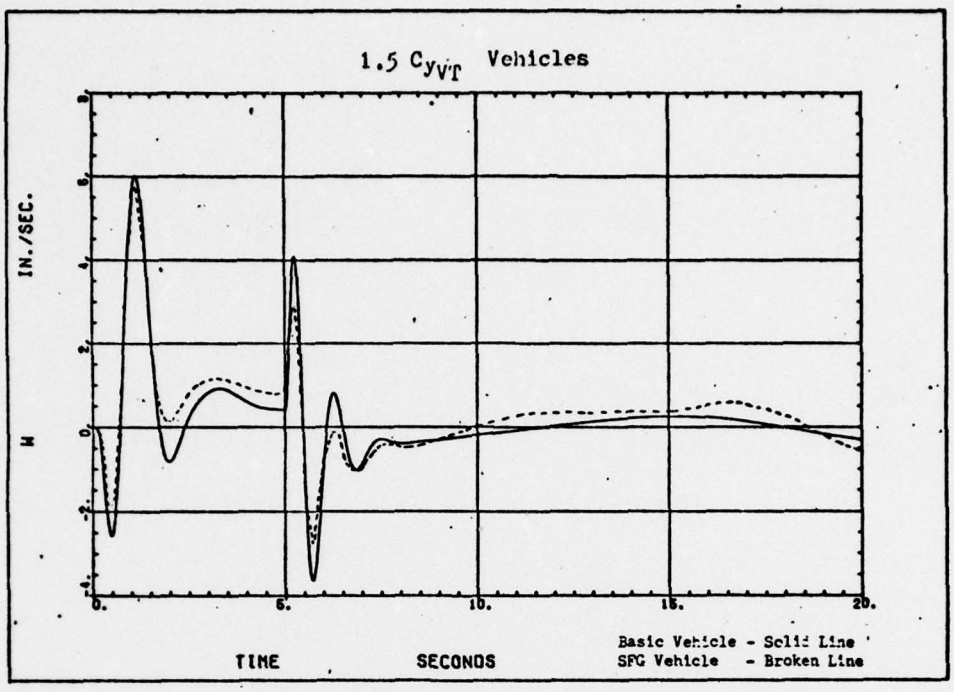

Figure E14. Downward Speed Perturbation Due to 4° Rudder/-1.68° Aileron Step (0 to 5 sec)

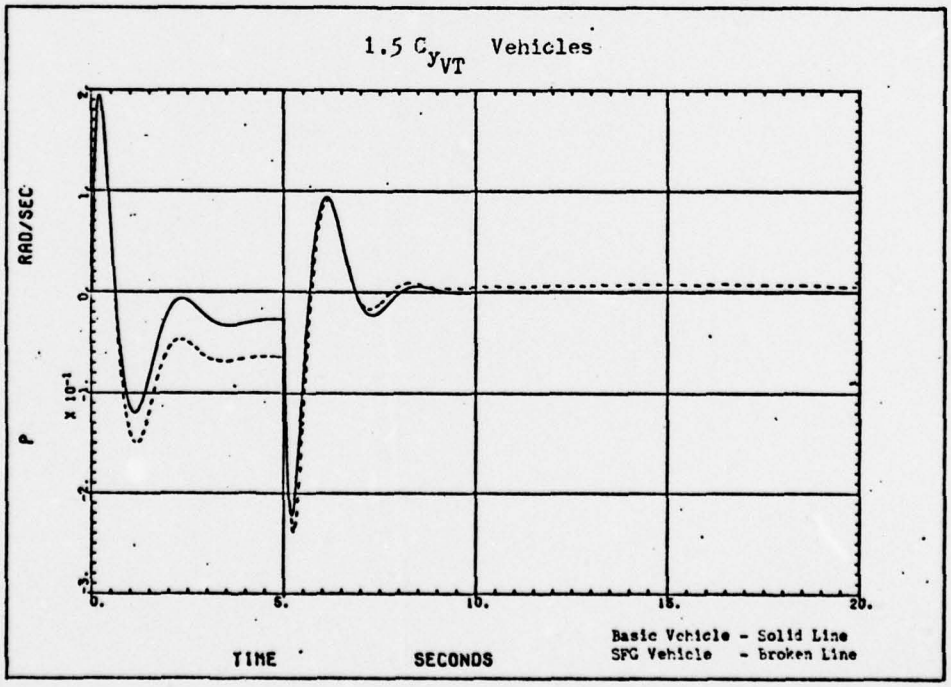

Figure E15. Roll Angle Due to 4° Rudder/-1.68° Aileron Step (0 to 5 sec)

BEST AVAILABLE COPY

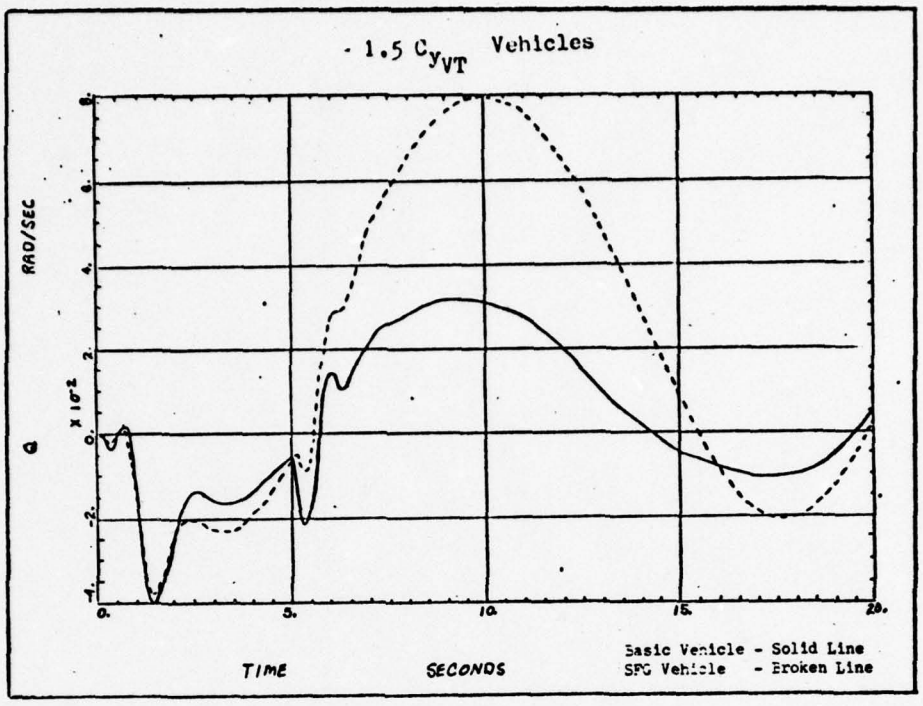

Figure E16. Pitch Rate Due to 4° Rudder/-1.68° Aileron Step (0 to 5 sec)

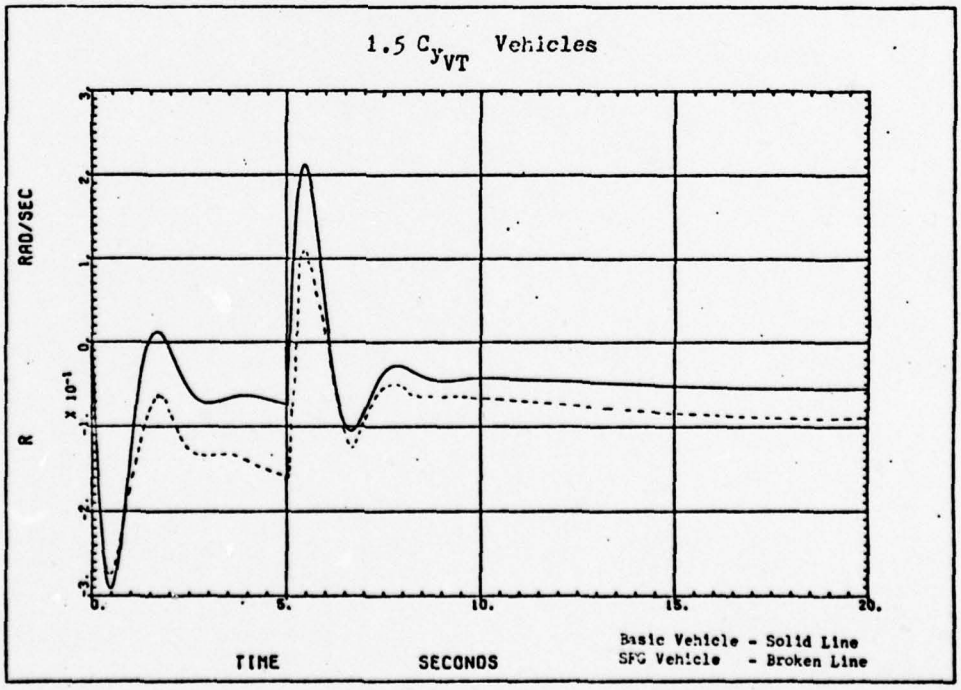

Figure E17. Yaw Rate Due to 4° Rudder/-1.68° Aileron Step (0 to 5 sec)

BEST AVAILABLE COPY

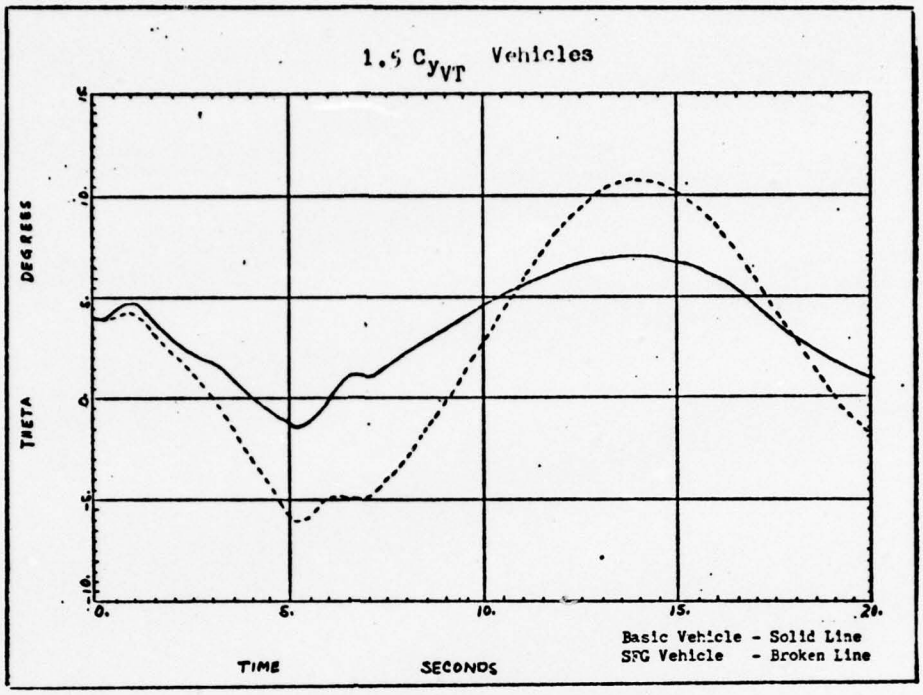

Figure E18. Pitch Angle Due to 4^{o} Rudder/-1.68^{o} Aileron Step (0 to 5 sec)

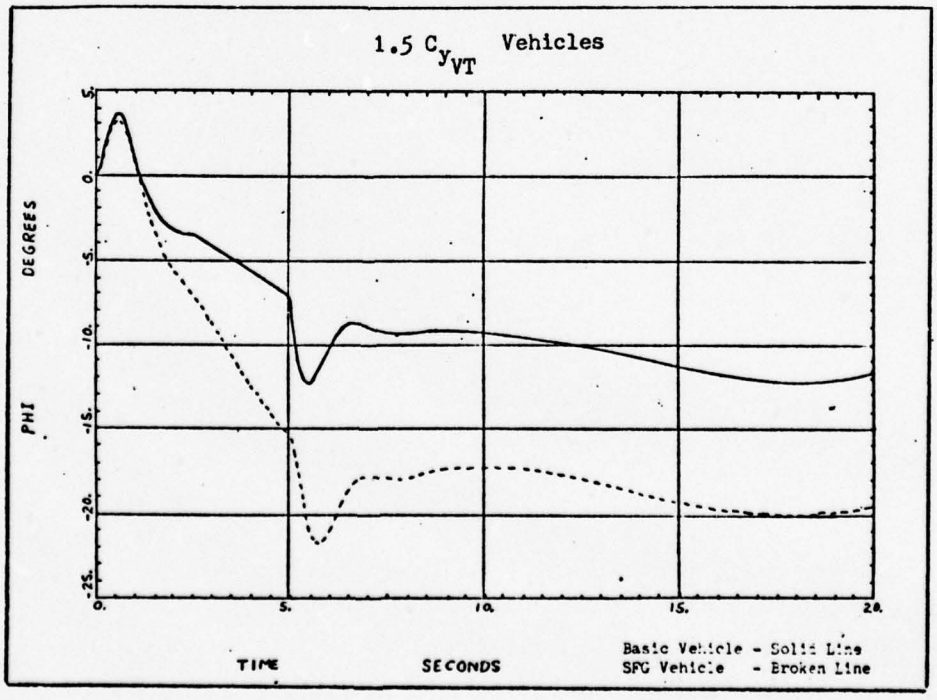

Figure E19. Roll Angle Due to 4^{o} Rudder/-1.68^{o} Aileron Step (0 to 5 sec)

BEST AVAILABLE COPY

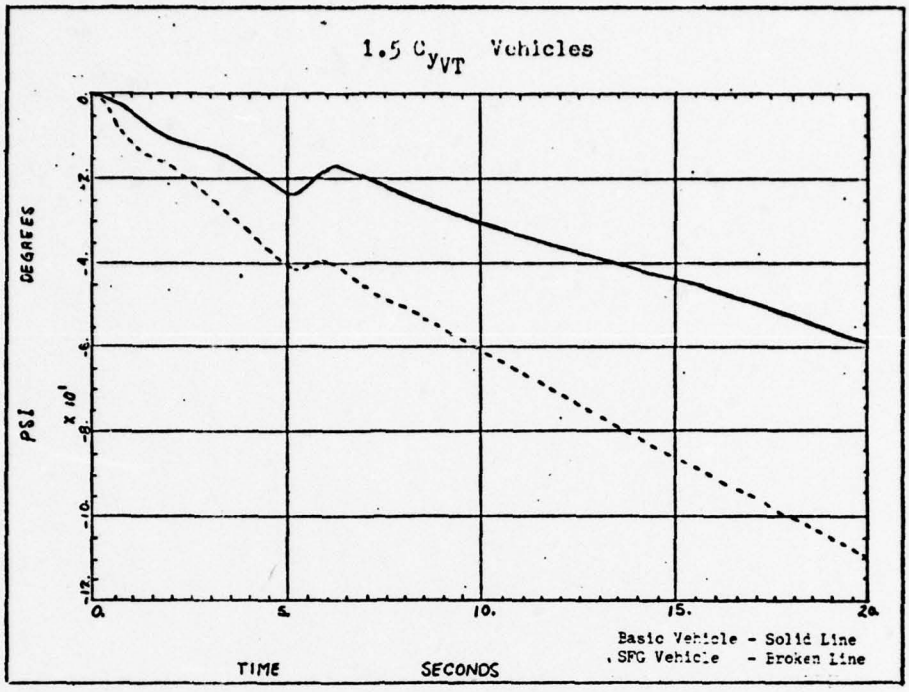

Figure E20. Heading Angle Due to 4^{o} Rudder/-1.68^{o} Aileron Step (0 to 5 sec)

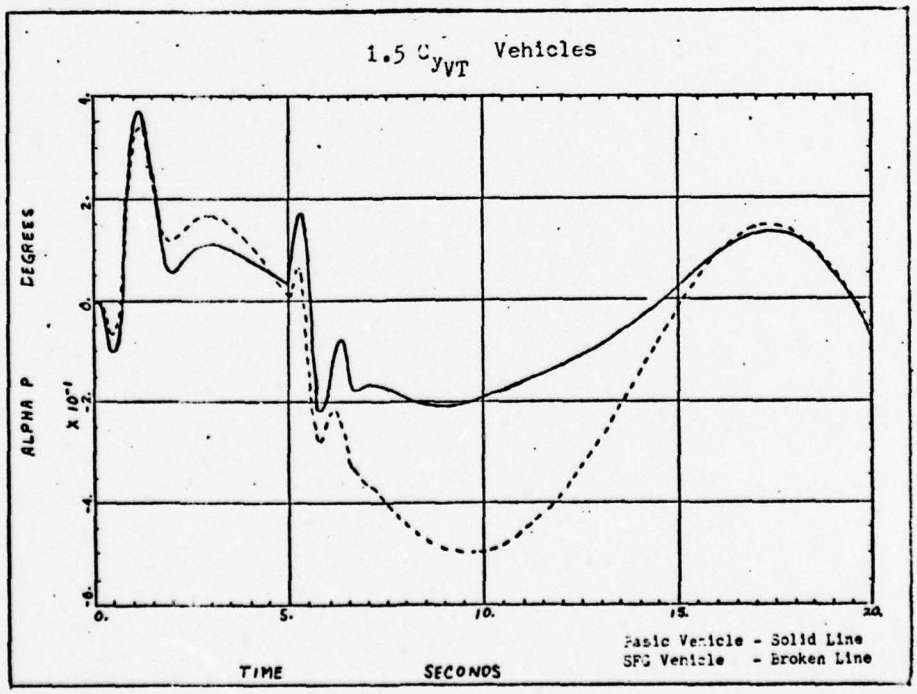

Figure E21. Angle of Attack Due to 4^{o} Rudder/-1.68^{o} Aileron Step (0 to 5 sec)

BEST AVAILABLE COPY

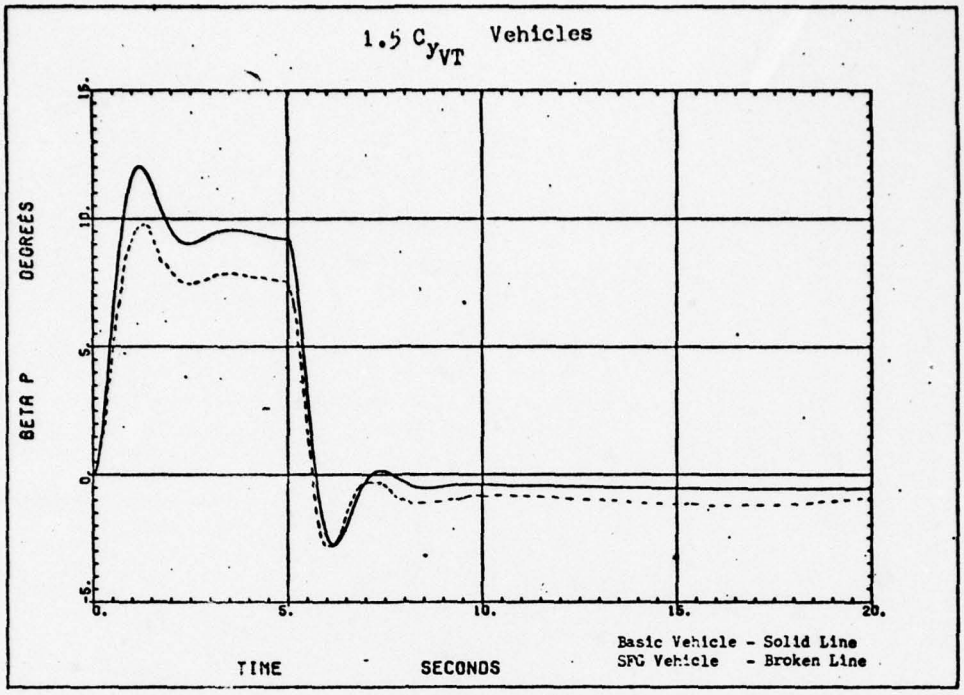

Figure E22. Side Slip Angle Due to 4^{o} Rudder/-1.68^{o} Aileron Step (0 to 5 sec)

BEST AVAILABLE COPY

Appendix F

Gust Input Time Response Plots

This section contains the complete set of time history plots for the baseline and modified vehicles. Wind gusts from the u,v,w directions with a magnitude of 11.09 fps were applied at time zero and maintained for one second. The following variables are plotted in this order: u,v,w,p,q,r,θ,ϕ,ψ,α,β.

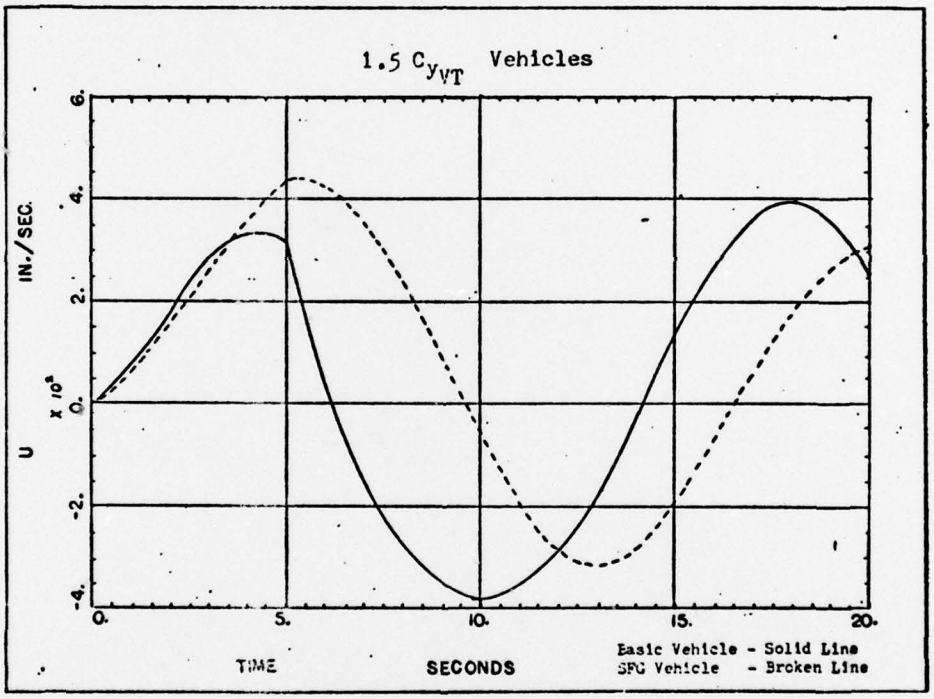

Figure F1. Forward Speed Perturbation Due to a Forward Gust 11.09 fps (0 to 1 sec)

BEST AVAILABLE COPY

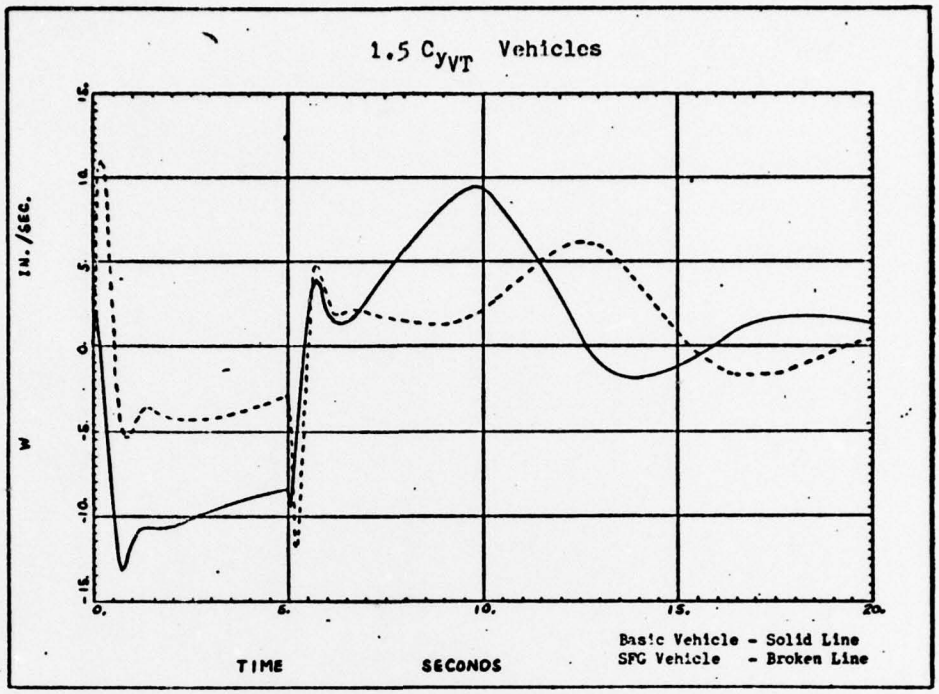

Figure F2. Downward Speed Perturbation Due to a Forward Gust 11.09 fps (0 to 1 sec)

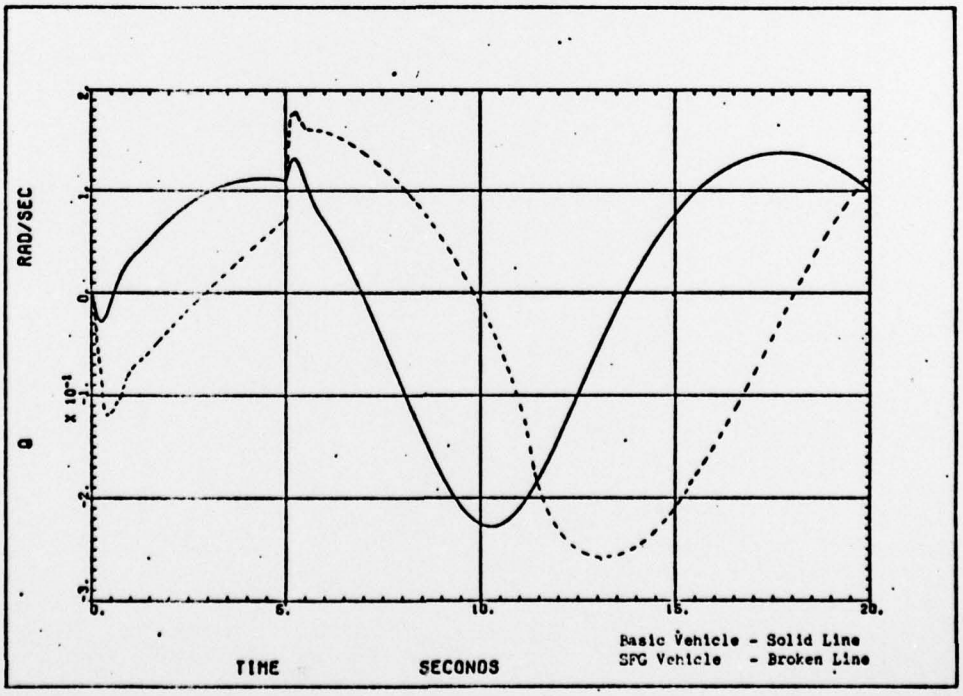

Figure F3. Pitch Rate Due to a Forward Gust 11.09 fps (0 tol sec)

BEST AVAILABLE COPY

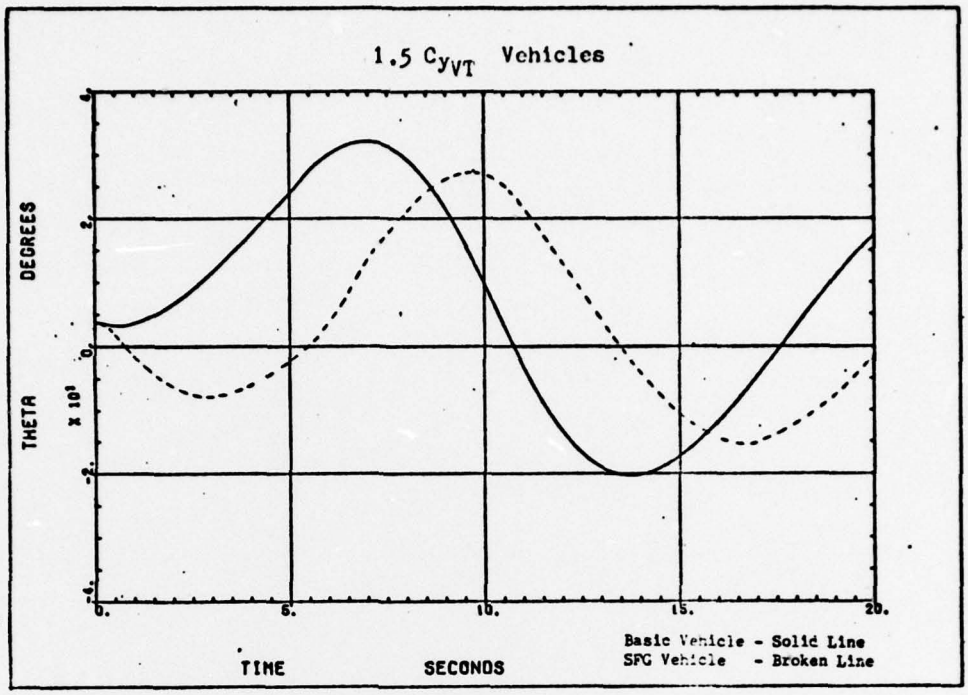

Figure F4. Pitch Angle Due to a Forward Gust 11.09 fps (0 to 1 sec)

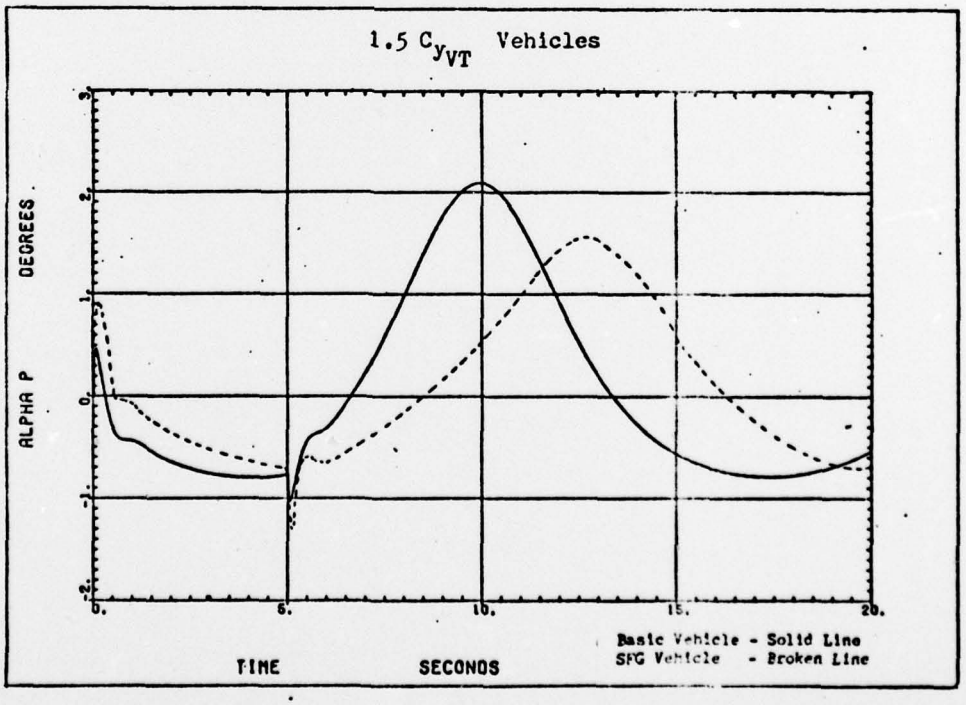

Figure F5. Angle of Attack Due to a Forward Gust 11.09 fps (0 to 1 sec)

BEST AVAILABLE COPY

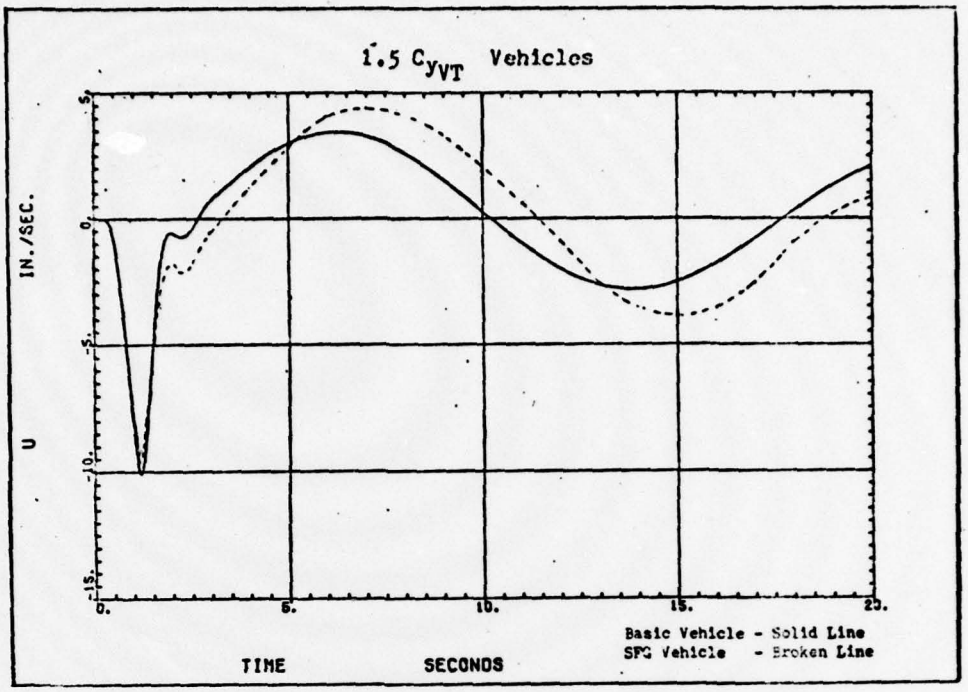

Figure F6. Forward Speed Perturbation Due to a Side Gust 11.09 fps (0 to 1 sec)

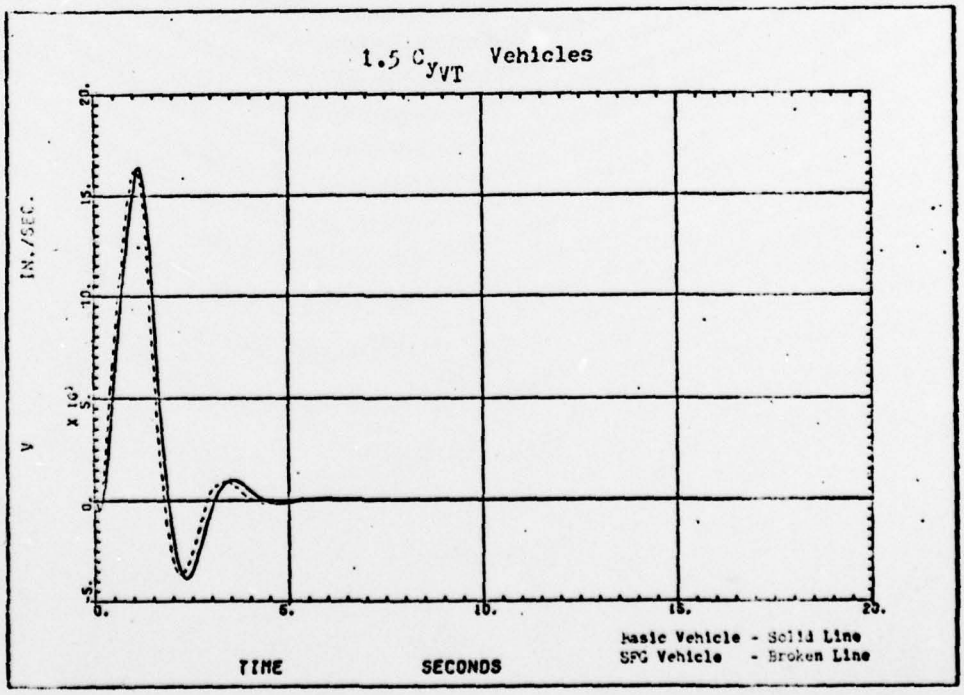

Figure F7. Side Speed Perturbation Due to a Side Gust 11.09 fps (0 to 1 sec)

BEST AVAILABLE COPY

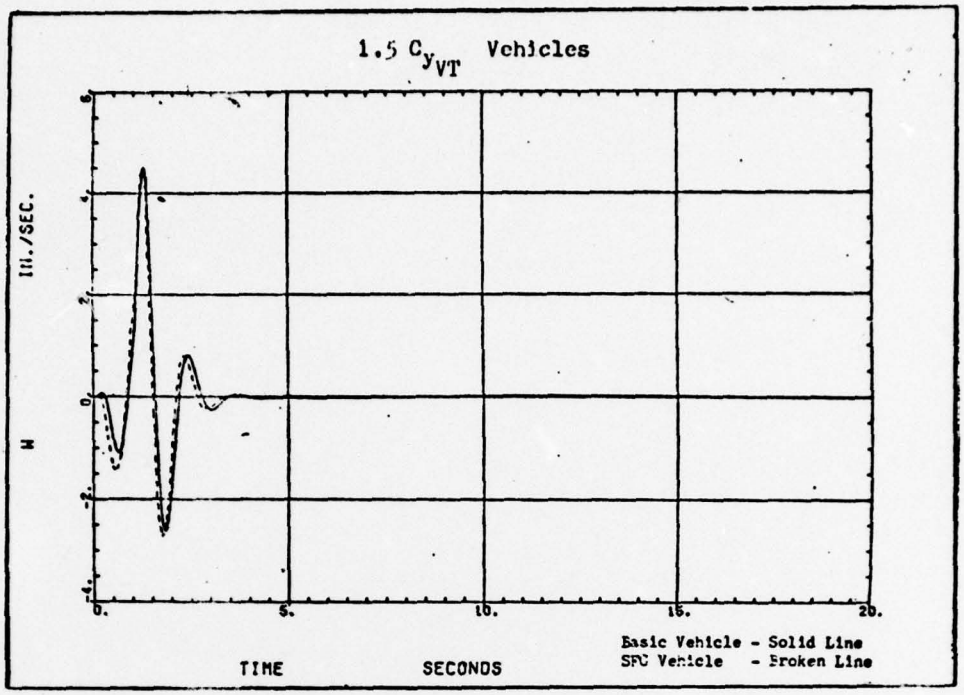

Figure F8. Downward Speed Perturbation Due to a Side Gust 11.09 fps (0 to 1 sec)

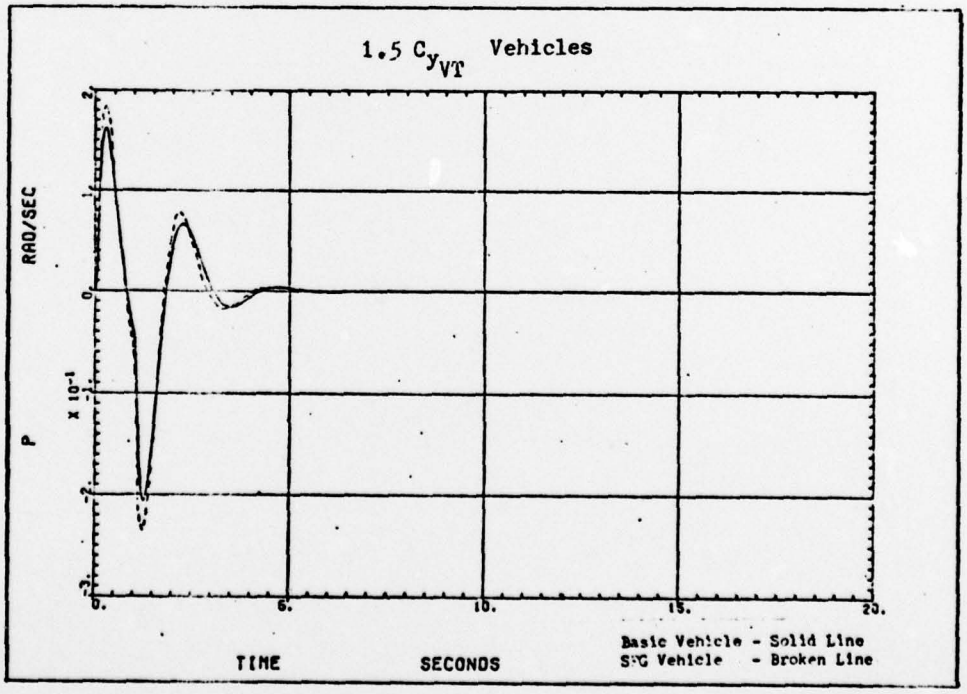

Figure F9. Roll Rate Due to a Side Gust 11.09 fps (0 to 1 sec)

BEST AVAILABLE COPY

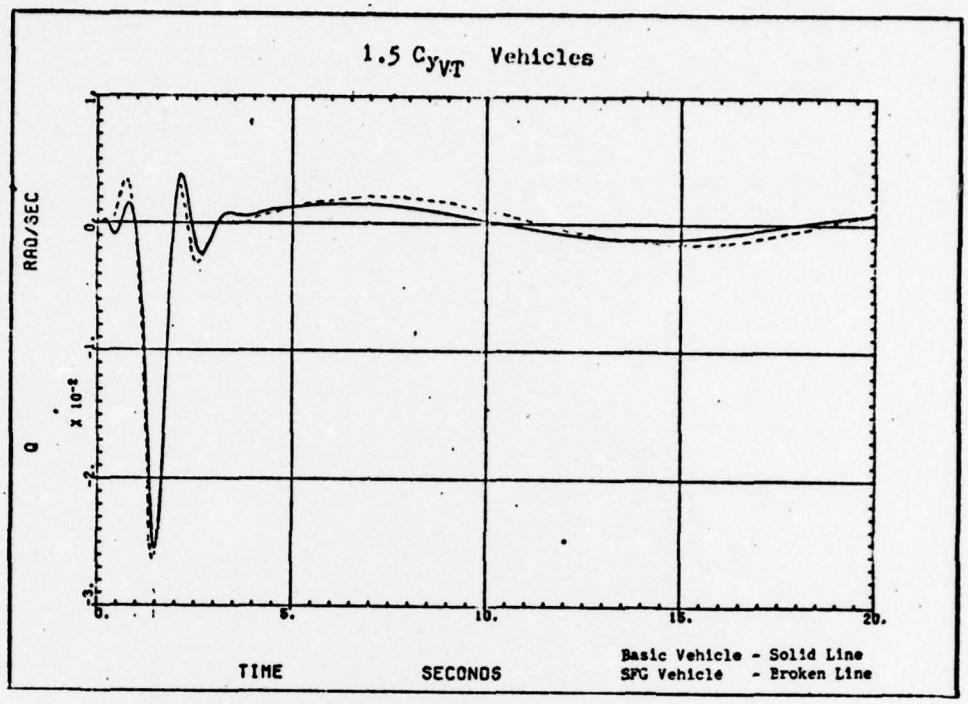

Figure F10. Pitch Rate Due to a Side Gust 11.09 fps (0 to 1 sec)

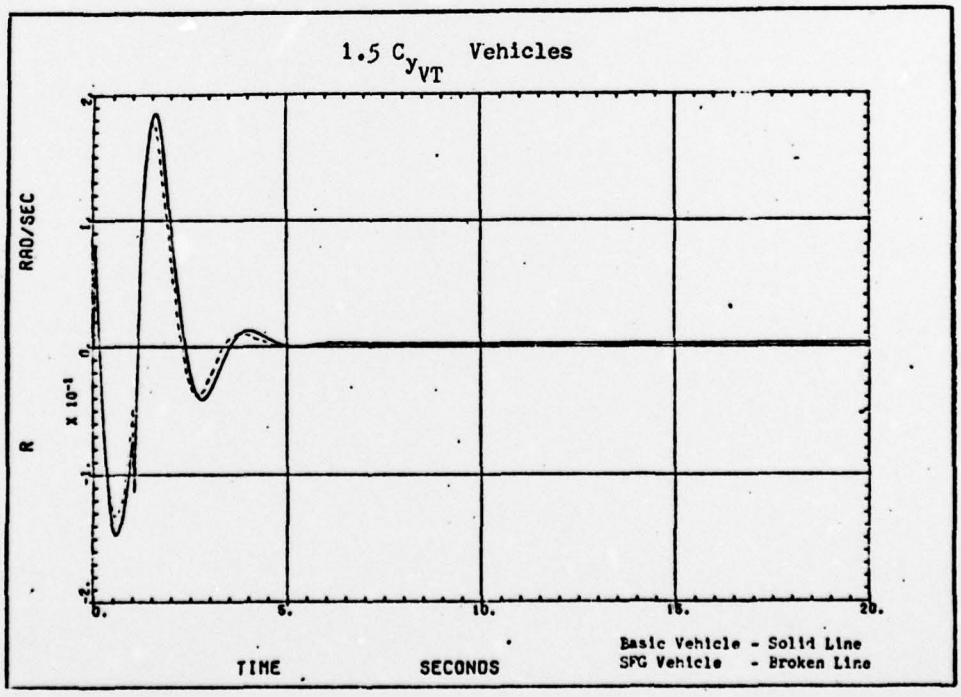

Figure F11. Yaw Rate Due to a Side Gust 11.09 fps (0 to 1 sec)

BEST AVAILABLE COPY

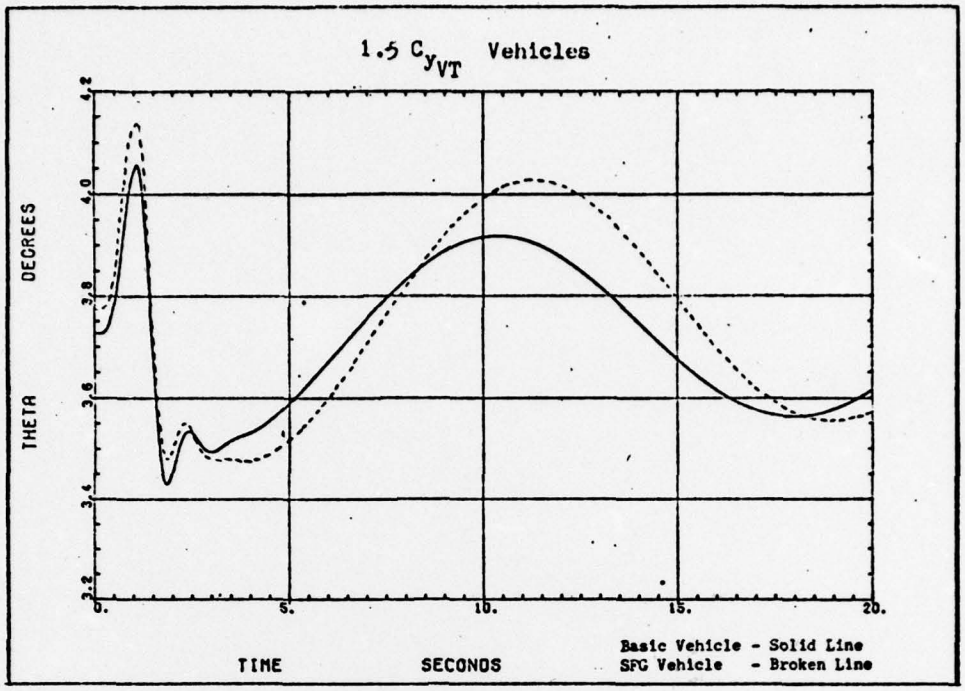

Figure F12. Pitch Angle Due to a Side Gust 11.09 fps (0 to 1 sec)

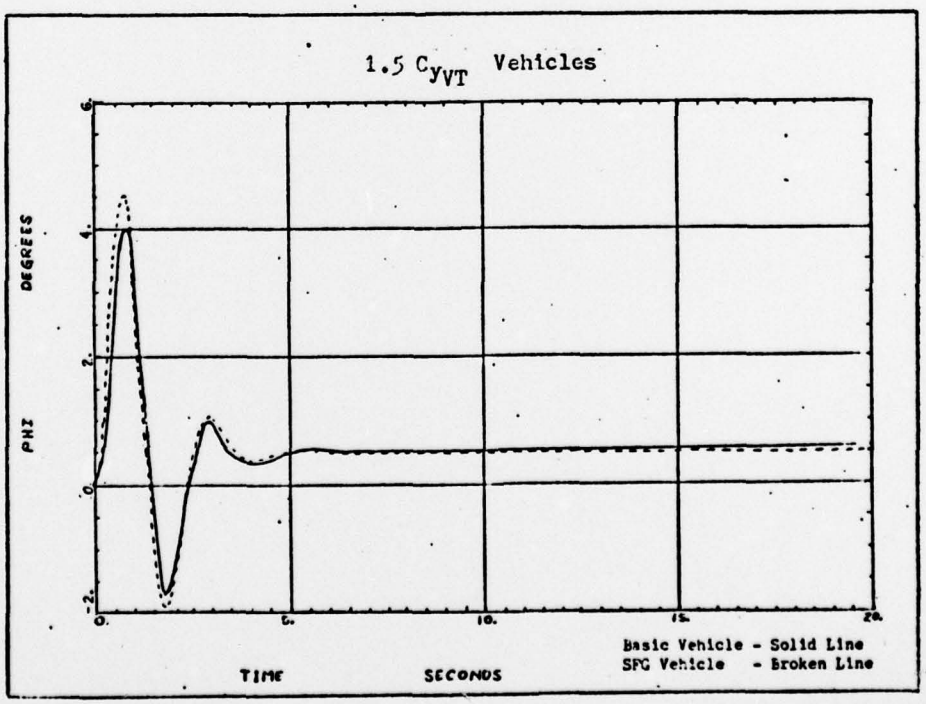

Figure F13. Roll Angle Due to a Side Gust 11.09 fps (0 to 1 sec)

BEST AVAILABLE COPY

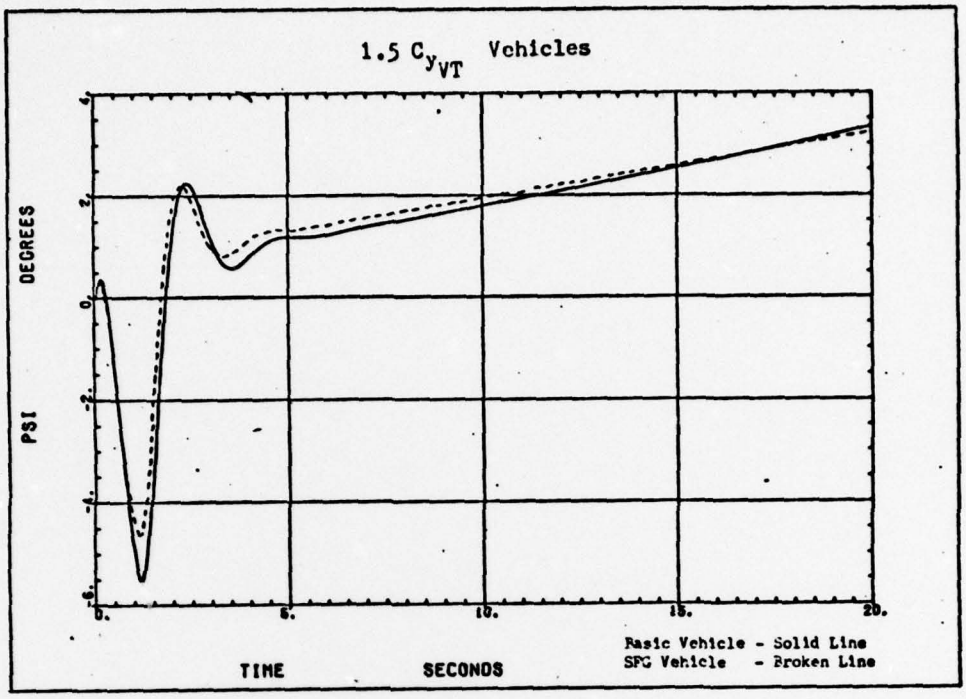

Figure F14. Heading Angle Due to a Side Gust 11.09 fps (0 to 1 sec)

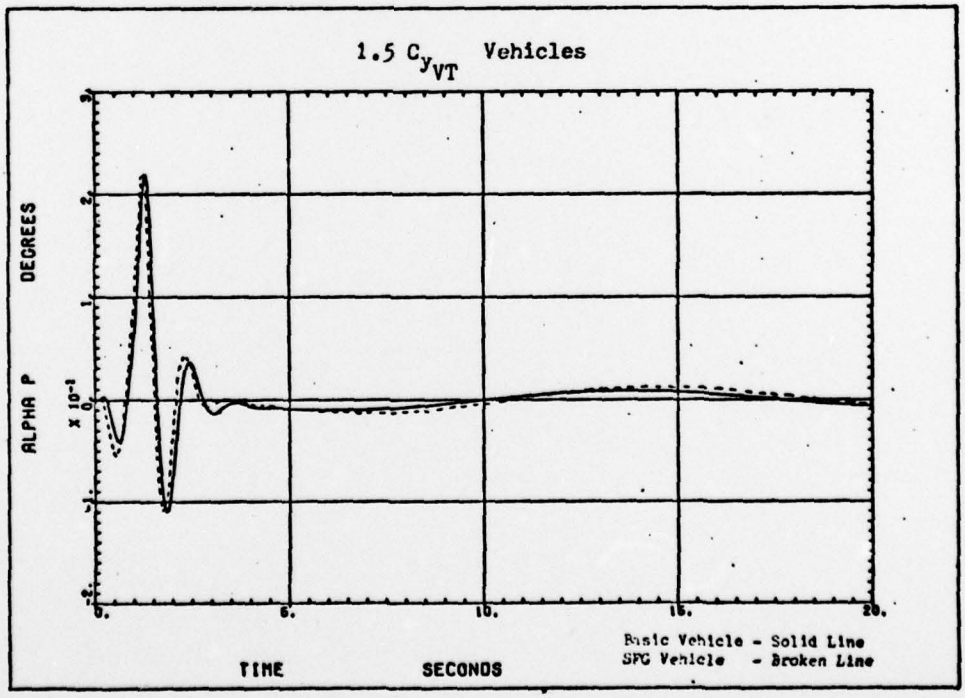

Figure F15. Angle of Attack Due to a Side Gust 11.09 fps (0 to 1 sec)

BEST AVAILABLE COPY

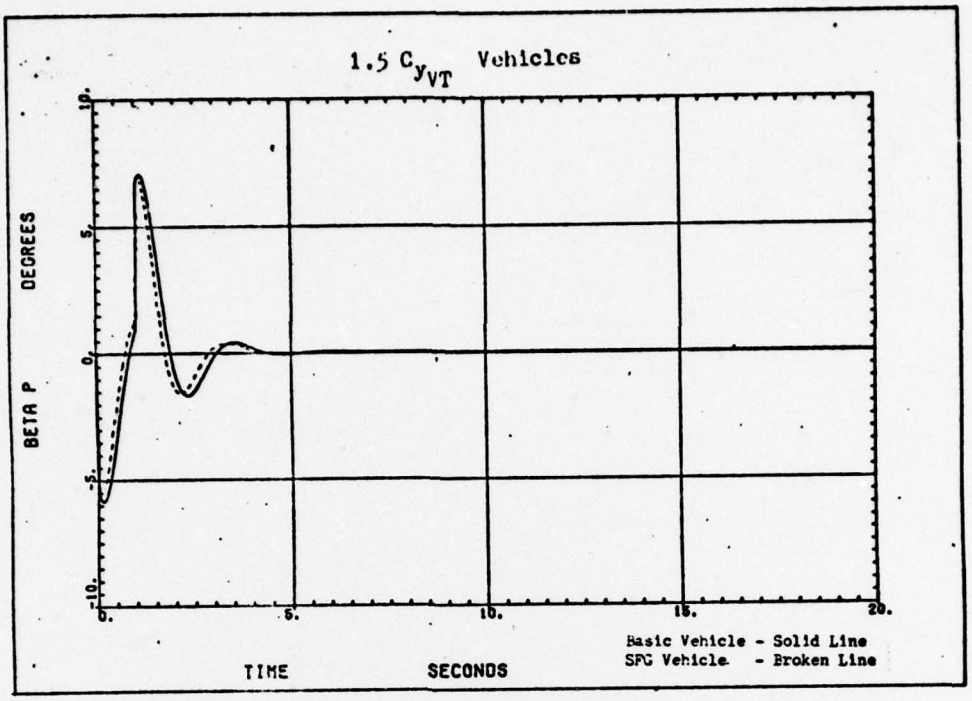

Figure F16. Side Slip Angle Due to a Side Gust 11.09 fps (0 to 1 sec)

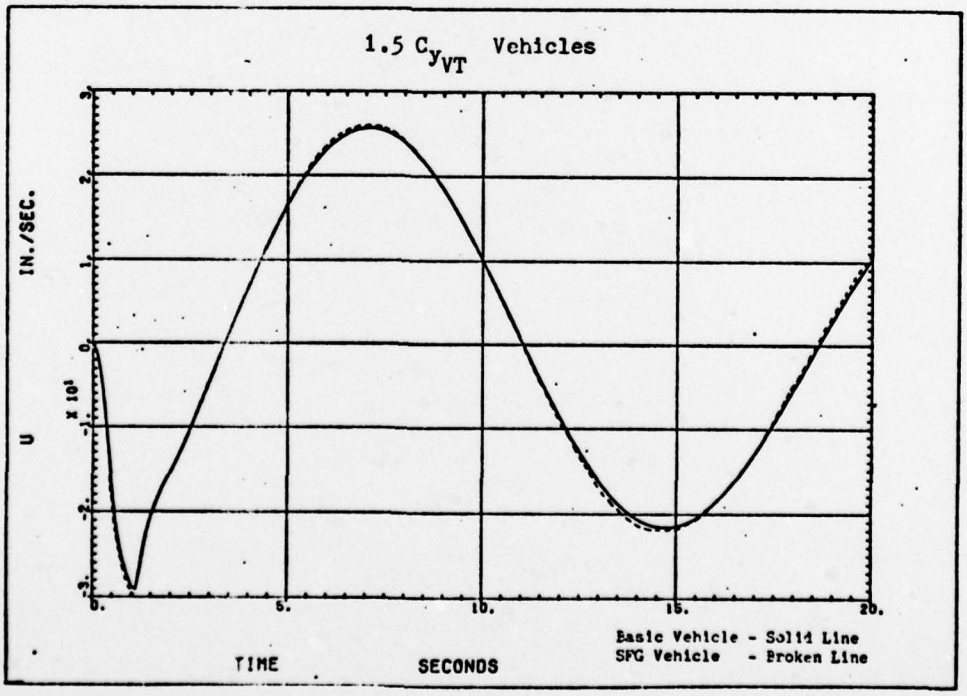

Figure F17. Forward Speed Perturbation Due to a Downward Gust 11.09 fps (0 to 1 sec)

BEST AVAILABLE COPY

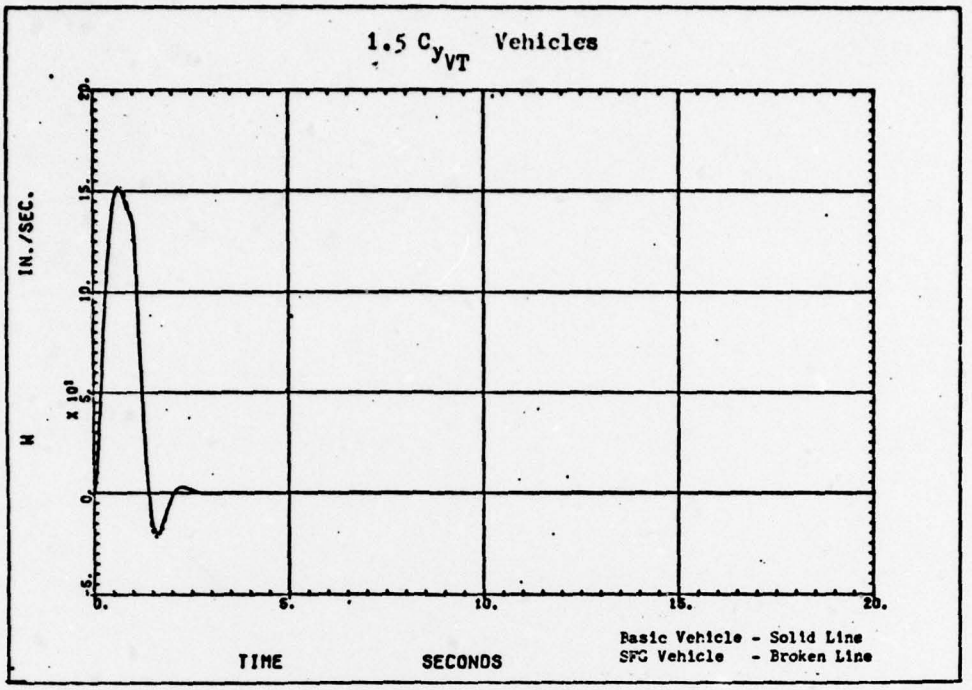

Figure F18. Downward Speed Perturbation Due to a Downward Gust 11.09 fps (0 to 1 sec)

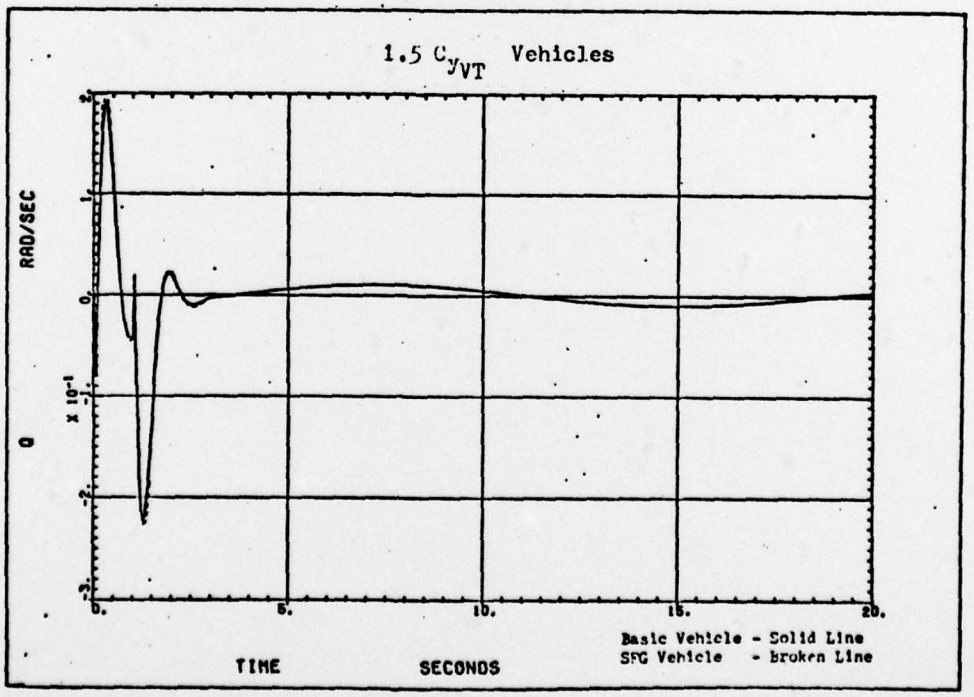

Figure F19. Pitch Rate Due to a Downward Gust 11.09 fps (0 to 1 sec)

BEST AVAILABLE COPY

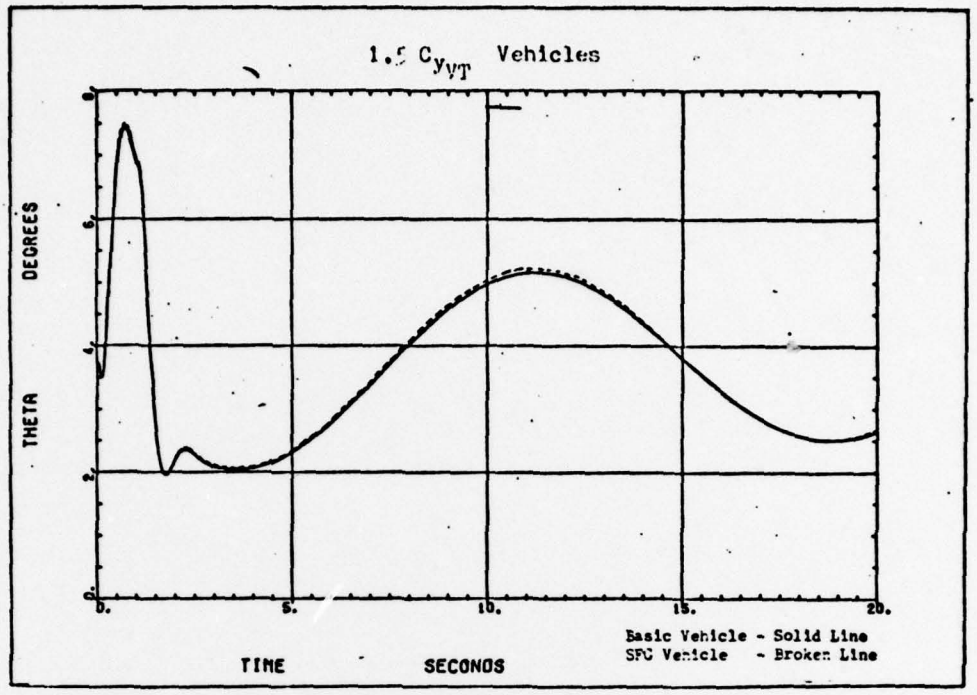

Figure F20. Pitch Angle Due to a Downward Gust 11.09 fps (0 to 1 sec)

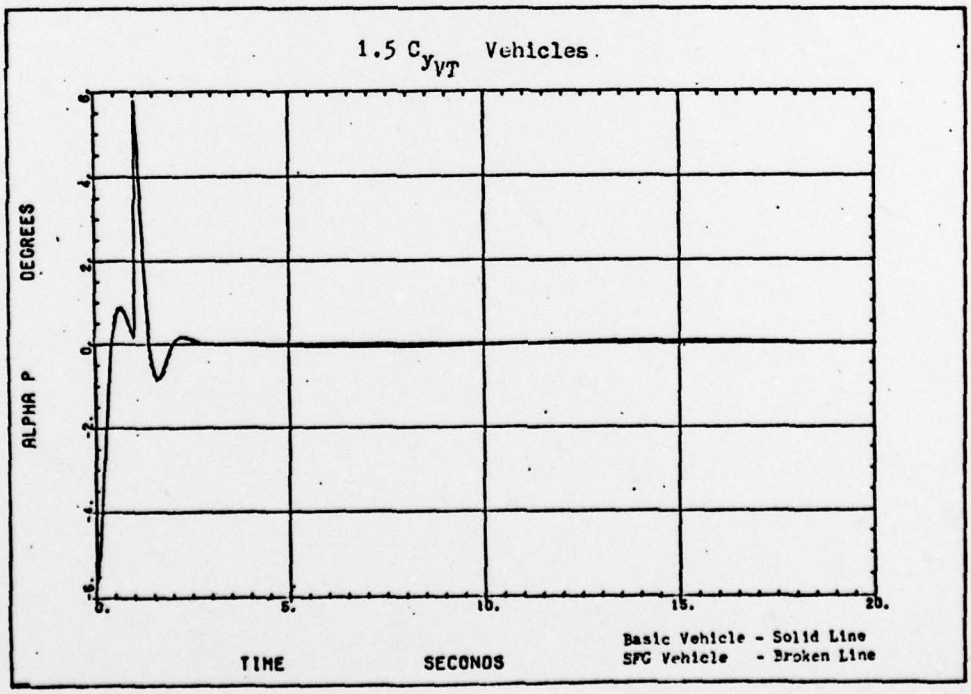

Figure F21. Angle of Attack Due to a Downward Gust 11.09fps (0 to 1 sec)

BEST AVAILABLE COPY

Vita

Glenn R. Leimbach was born June 30, 1948 and grew up in the small town of Jackson, Minnesota. He entered the USAF Academy, Colorado, in June 1966 and graduated with a B.S. in Engineering Mechanics in June 1970.

After completing undergraduate pilot training at Randolph AFB, Texas, he served two tours as a T-38 Instructor Pilot at Moody AFB, Georgia, and Randolph AFB, Texas. In June of 1976 he left Air Training Command and entered the AFIT Graduate Aeronautical Engineering program. His home address is:

4028 Slipperwood Place
Dayton, Ohio 45424

SECURITY CLASSIFICATION OF THIS PAGE (When Data Entered)

REPORT DOCUMENTATION PAGE		READ INSTRUCTIONS BEFORE COMPLETING FORM
1. REPORT NUMBER AFIT/GAE/AA/77D-7	2. GOVT ACCESSION NO.	3. RECIPIENT'S CATALOG NUMBER
4. TITLE (and Subtitle) DESIGN AND EVALUATION OF A SIDE FORCE GENERATOR MODIFICATION FOR THE XBQM-106, REMOTELY PILOTED VEHICLE		5. TYPE OF REPORT & PERIOD COVERED MS Thesis 6. PERFORMING ORG. REPORT NUMBER
7. AUTHOR(s) Glenn R. Leimbach Captain USAF		8. CONTRACT OR GRANT NUMBER(s)
9. PERFORMING ORGANIZATION NAME AND ADDRESS Air Force Institute of Technology (AFIT/EN) Wright-Patterson AFB, Ohio 45433		10. PROGRAM ELEMENT, PROJECT, TASK AREA & WORK UNIT NUMBERS
11. CONTROLLING OFFICE NAME AND ADDRESS		12. REPORT DATE December 1977 13. NUMBER OF PAGES 122
14. MONITORING AGENCY NAME & ADDRESS(if different from Controlling Office)		15. SECURITY CLASS. (of this report) Unclassified 15a. DECLASSIFICATION/DOWNGRADING SCHEDULE

16. DISTRIBUTION STATEMENT (of this Report)

Approved for public release; distribution unlimited

17. DISTRIBUTION STATEMENT (of the abstract entered in Block 20, if different from Report)

18. SUPPLEMENTARY NOTES

Approved for public release; IAW AFR 190-17

Jerral F. Guess, Captain, USAF
Director of Information

19. KEY WORDS (Continue on reverse side if necessary and identify by block number)

Side Force Generator
Remotely Piloted Vehicle
Longitudinal Time Response
Lateral Time Response

20. ABSTRACT (Continue on reverse side if necessary and identify by block number)

Wingtip and fuselage mounted side force generator (SFG) surfaces were designed and installed on the XBQM-106 remotely piloted vehicle (RPV) to enhance its lateral terminal response characteristics. These surfaces were sized and positioned in an attempt to keep the net rolling and yawing moments about the CG unchanged when the aircraft was side slipping. The FLEXSTAB digital computer system in conjunction with traditional hand calculated methods were used to evaluate the RPV's stability, control, and time response characteris-

over

DD FORM 1 JAN 73 1473 EDITION OF 1 NOV 65 IS OBSOLETE

SECURITY CLASSIFICATION OF THIS PAGE (When Data Entered)

Block 20 cont'd.

tics. The time history responses to rudder, aileron, rudder/aileron, and wind gust inputs were generated and plotted by the FLEXSTAB program. From these plots it was determined that the SFG modification increased the yaw rate response 10.6% while decreasing the roll rate 10.7% and the side slip angle response 25.1%. The dutch roll damping was increased 4% and the DR period decreased 8%. The roll mode time to half amplitude increased 16.7% and the spiral stability increased for the modified vehicle. The longitudinal stability suffered a slight decrease due to the addition of the SFG.